Intervalence Charge Transfer (IVCT) in Trinuclear and Tetranuclear Complexes of Iron, Ruthenium, and Osmium

Deanna M. D'Alessandro and F. Richard Keene*

School of Pharmacy & Molecular Sciences, James Cook University, Townsville, Queensland 4811, Australia

Received August 24, 2005

Contents

1. Introduction

Electron and energy transfer are ubiquitous in biological, chemical, and physical processes, which has led to extensive multidisciplinary research efforts to elucidate the factors influencing mechanistic pathways. Of considerable importance in these studies have been investigations of intramolecular electron and energy transfer within polymetallic assemblies as a result of the diversity (coordination number, ligand environment, stereochemistry, and redox characteristics) provided by the metal centers in such structures.

Because of their multicomponent nature, these structures have considerable design potential to exploit the cooperation between the metals and/or other redox-active centers. Novel photochemical molecular devices (PMDs) may be constructed which are capable of performing useful light- and redox-induced functions—including artificial photosynthesis and photoinduced energy- and electron-transfer processes in light-harvesting "antenna" systems.[1−3] Metallosupramolecular assemblies have also been designed to mimic the photoinduced charge separation function in photosynthetic organisms, in an attempt to elucidate the complex electron- and energy-transfer mechanisms which occur in natural systems.[1,4−8] The possibility of multiple electron transfer—by absorption of several photons by linked chromophores, or the design of systems which generate more than one electron upon absorption of one photon—has significant implications in catalytic schemes, as well as understanding long-range electron transfer in biological systems, and the conductivity of "molecular wires". In molecules involving delocalized unpaired electrons, polarizability may be present so that the species exhibit interesting nonlinear optical or magnetic properties.

Polypyridyl complexes of the d^6 metals Fe^{II}, Ru^{II}, and Os^{II} have attracted particular attention as the basis of these assemblies due to a combination of favorable photophysical and redox characteristics, the longevity of their excited states, and their chemical inertness in a variety of oxidation states.[9] An important feature of these complexes is the capability of systematic variation of the ground- and excited-state properties by the judicious choice of the coordinating ligands.[10−12]

The realization of multicomponent species comprising two or more metal-based components, the elucidation of their fundamental redox, photochemical, and spectral characteristics, and their ultimate application are critically dependent on (1) the availability of synthetic strategies for the construction of structurally unambiguous polynuclear complexes; (2) a knowledge of the electron-transfer properties of the individual components; and (3) an understanding of the extent to which the properties of each component are influenced upon their inclusion into larger assemblies.

While a number of comprehensive reviews over the past decade have addressed the design of and synthetic routes to trinuclear, tetranuclear, and higher nuclearity complexes possessing a range of architectural motifs,[13−20] the fundamental electron-transfer characteristics of such systems have received significantly less attention,[1,21,22] despite their crucial importance. The review by Balzani *et al.*[1] addressed intercomponent electron- and energy-transfer processes in predominantly dinuclear luminescent and redox-active complexes, but the discussion of higher nuclearity species was restricted to a few paradigmatic examples only. The electrochemical aspects of metallosupramolecular systems have also been the subject of a number of reviews.[21,23−25] The

* E-mail: Richard.Keene@jcu.edu.au. Phone: +61-(0)7-4781 4433. Fax: +61-(0)7-4781 6078.

10.1021/cr050010o CCC: $59.00
Published on Web 05/24/2006

Deanna D'Alessandro obtained her B.Sc. specializing in chemistry, physics, and mathematics at James Cook University, and received the University Medal in 2000 following Honors studies in chemistry. She has recently completed her Ph.D. (awarded *cum laude*), under the supervision of Professor Richard Keene, in which she studied the design and synthesis of stereochemically-unambiguous polymetallic assemblies and the elucidation of spatial effects on their electron-transfer properties. During her postgraduate studies, she has been the recipient of two awards for her research at national conferences, including a Don Stranks Award of the Royal Australian Chemical Institute in 2003.

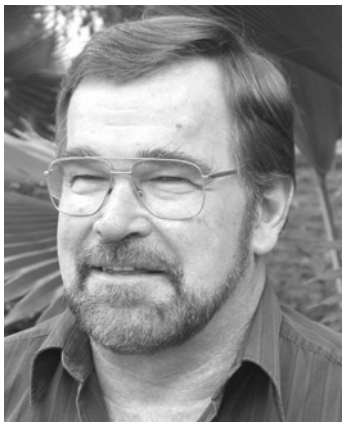

Richard Keene graduated from the University of Adelaide and subsequently undertook postdoctoral work at the Australian National University and the University of North Carolina at Chapel Hill. On his return to Australia, he was appointed to James Cook University in Townsville, where he is now the Nevitt Professor of Chemistry. He is a recipient of the Rennie Medal of the Royal Australian Chemical Institute. Richard has published in a number of areas of coordination chemistry, but his present research interests relate primarily to the stereochemistry of metallosupramolecular assemblies and its effect on their physical properties—in particular intramolecular electron transfer—and the interaction of polymetallic species with biological molecules such as DNA.

molecular architecture of the assembly, the electron-transfer properties of the components, and the bridging ligands (and their interdependence) provide the potential for control of useful processes, such as electron transfer along predetermined pathways, multielectron exchange at a predetermined potential, photoinduced charge separation, and so on.

In this context, the intervalence charge transfer (IVCT) characteristics of the mixed-valence forms of such systems provide one of the most powerful and sensitive probes of inter-metal electronic interaction. Mixed-valence compounds—which contain an element that exists in more than one formal oxidation state—have been known for centuries and possess important conductivity, magnetic, and spectral properties. In the late 1960s, Allen and Hush[26] and Robin and Day[27] published reviews of mixed-valence materials, and Hush subsequently provided a theoretical model linking their physical properties and electron-transfer processes.[28] Of particular significance was the prediction of a relationship between the maximum energy of the optically-induced IVCT band, ν_{max}, and several factors which govern the activation barrier for intramolecular electron transfer between the metal centers:

$$\nu_{max} = \lambda_i + \lambda_o + \Delta E + \Delta E' \quad (1)$$

where the Franck−Condon contributions, λ_i and λ_o, correspond to the reorganizational energies within the inner and outer spheres (respectively); the redox asymmetry, ΔE, is the difference in energy between the vibrationally-relaxed initial and final states in the hypothetical absence of electronic coupling; and $\Delta E'$ reflects any additional energy contributions due to spin−orbit coupling and ligand field asymmetry.[28,29] According to the classical Marcus−Hush theory,[28−31] for weakly-coupled symmetrical mixed-valence systems, the energy barrier for thermal electron transfer, E_{th}, is directly related to the optical process through eq 2, and the predicted bandwidth at half-height of the IVCT band, $\Delta\nu_{1/2}°$, is given by eq 3, where R is the gas constant, T is the temperature (in kelvin), and the term $16RT$ ln 2 takes the value 2310 cm^{-1} at 298 K.

$$\nu_{max} = 4E_{th} \quad (2)$$

$$\Delta\nu_{1/2}° = [16RT \ln 2(\nu_{max})]^{1/2} \quad (3)$$

A crucial issue in the analysis of mixed-valence complexes is the extent of electronic delocalization between the metal centers—which is governed by competition between the electronic coupling parameter (H_{ab}) and the sum of the factors on the right-hand side of eq 1.[28,29] For Gaussian-shaped IVCT bands, H_{ab} is given by

$$H_{ab} = 2.06 \times 10^{-2}(\epsilon_{max}\nu_{max}\Delta\nu_{1/2})^{1/2}/(br) \quad (4)$$

where ϵ_{max} and b denote the maximum molar absorption coefficient of the IVCT band and the degeneracy of the transition, respectively, and r is the distance between the metal centers in the limit of zero electronic coupling. Alternatively, the parameter α^2 has also been introduced as a diagnostic for the extent of electronic delocalization:

$$\alpha^2 = 4.2 \times 10^{-4}\epsilon_{max}\Delta\nu_{1/2}/(b\nu_{max}r^2) \quad (5)$$

According to the Robin and Day classification scheme,[27] three classes of mixed-valence systems are distinguished on the basis of the relative magnitudes of the reorganizational energy ($\lambda = \lambda_i + \lambda_o$) and $2H_{ab}$. Class I systems are characterized by noninteracting centers, "localized" Class II systems by weakly-coupled centers ($2H_{ab} \ll \lambda$), and "delocalized" class III systems by strongly-coupled centers ($2H_{ab} \gg \lambda$). Electronic delocalization is promoted by mixing between the donor (M^{II}) and acceptor (M^{III}) wave functions, and in the limit of strong overlap, delocalization is complete and the metal centers possess identical valences. In this case $E_{th} = 0$, and the process involves a transition within the molecular orbital manifold of the species. For symmetrical Class III[27] systems, the energy of the transition provides a direct measure of H_{ab} since $H_{ab} = {}^1/_2\nu_{max}$.[28,29] While the terms "IVCT transition" and "mixed-valence" are retained, the

transitions do not involve net charge transfer and the systems are more accurately defined as "average valence".

In the early 1970s, specifically designed mixed-valence compounds were synthesized—notably the Creutz−Taube ion $[(NH_3)_5Ru(\mu\text{-pyz})Ru(NH_3)_5]^{5+}$ (pyz = pyrazine)[32] and the cyclopentadienyl-linked biferrocene cation $[(C_5H_5)Fe(\mu\text{-}C_5H_4{-}C_5H_4)Fe(C_5H_5)]^+$.[33] The Marcus−Hush theory[28−31] has provided the preferred method of analysis for such mixed-valence complexes due to the facility of its application, and the validity of the model for the determination of the relative contributions of the fundamental parameters expressed in eq 1 has been extensively tested and reviewed.[34−44] Experimentally, these contributions have been probed by the dependence of the IVCT characteristics on structural and substitutional changes in the mixed-valence systems. These include the distance between the metal centers,[34] the ability of the bridging ligand to delocalize the electronic charge,[45] and the coordination environments of the metal centers[35−38,40−42,44] which can be controlled through variations in the metal centers and the bridging or terminal ligands. The characteristics of the external medium, such as the identity of the solvent[43,46−59] and anions,[60−66] also constitute critical contributions to the electron-transfer barrier. In the former case, the λ_o contribution is generally treated by the classical spherical cavity dielectric continuum model given in eq 6, in which the solvent is treated as a structureless dielectric continuum and has no specific interactions with itself or with the redox sites.[28,29] The metal centers of a symmetrical dinuclear complex are assumed to be centrally located in two noninterpenetrating spheres ($d \gg 2a$) embedded in the dielectric. The parameters a and d define the molecular radii and distance between the donor and acceptor, and D_s and D_{op} are the static and optical dielectric constants of the solvent, respectively.

$$\lambda_o = e^2\left(\frac{1}{a} - \frac{1}{d}\right)\left(\frac{1}{D_{op}} - \frac{1}{D_s}\right) \tag{6}$$

In accordance with eqs 1 and 6, ν_{max} should vary linearly with the solvent dielectric function $(1/D_{op} - 1/D_s)$, with slope $e^2(1/a - 1/d)$ and intercept $\lambda_i + \Delta E'$. The validity of the dielectric continuum model has typically been assessed experimentally through IVCT solvatochromism measurements on dinuclear systems.[28,29,35,37,38,40] Experimentally, the classification of dinuclear mixed-valence complexes is generally based upon the solvent dependence and the observed bandwidth at half-height.[28,29] In localized systems, the IVCT transitions are of low intensity, Gaussian-shaped, and broad ($\epsilon_{max} \leq 5000\ M^{-1}\ cm^{-1}$, $\Delta\nu_{1/2} \geq 2000\ cm^{-1}$) due to coupling with solvent. In delocalized species, the bands arise from transitions within the molecular orbital manifold of the systems and the bands are intense, narrow ($\epsilon_{max} \geq 5000\ M^{-1}\ cm^{-1}$, $\Delta\nu_{1/2} \leq 2000\ cm^{-1}$), and solvent independent. For systems near the transition between the localized and delocalized regimes ($\nu_{max} \approx 2H_{ab}$), the IVCT bands are frequently asymmetrically-shaped and intense.[40,45,67]

While clear examples of localized and delocalized systems have been reported in several comprehensive surveys of dinuclear mixed-valence complexes of Fe, Ru, and Os,[35−39,41−44] in many cases the classification based upon the abovementioned criteria has proven somewhat difficult. In reality, the transitions between regimes are not abrupt, and experimental studies have revealed a gradation in behavior between the fully localized and fully delocalized limits which is governed by the relative time scales for intramolecular electron transfer—and multiple nuclear and solvent vibrations which are coupled to the electron transfer.[40] A recent seminal review by Meyer and co-workers[40] addressed these issues from a semiclassical perspective, by defining an intermediate regime, "Class II-III", in which the systems literally exhibit *both* localized and delocalized behavior. This scenario arises when the time scale for reorganization of the solvent modes is faster than that for the inner-sphere vibrations, giving rise to solvent averaging and electronic localization.

The development of theoretical models to describe the transition between the localized and delocalized regimes in dinuclear systems represents a long-standing issue in mixed-valence chemistry.[34−44] Three- and four-state classical models have been proposed[67] in which the bridging ligand is explicitly included as an additional electronic state. Semiclassical models[67−72] combine a classical treatment of the solvent reorganizational contributions with a quantum mechanical description of inner-sphere modes. The localized-to-delocalized transition has also been treated through quantum mechanical vibronic coupling formalisms, such as the "PKS model",[73−76] and the computational approaches of Reimers and Hush.[77]

While the classification of mixed-valence systems is not straightforward and relies on observations from several experimental techniques with widely different time scales,[40] the appearance of IVCT bands and their solvent dependence provide the most useful experimental criterion for distinguishing between Classes II (broad, solvent-dependent, localized oxidation states) and II-III (narrow, solvent-independent, localized oxidation states). Due to the limited number of experimental studies in which the factors which influence the localized-to-delocalized transition have been systematically explored, there is currently extensive interest in the preparation of dinuclear systems which exhibit Class II-III behavior.[39,40,44,45,67,77] Likewise, the examination of the factors which govern the extent of electronic coupling between the metal centers and hence the shift between localization and delocalization in higher nuclearity species is of significant interest. While the mixed-valence properties of dinuclear complexes of Fe, Ru, and Os have been detailed in a number of reviews,[27,39,40,67,69] comparable discussions for higher nuclearity species are scarce, despite the potential of these studies to provide powerful and sensitive probes to elucidate aspects of intercomponent electron transfer. An additional level of complexity is introduced in IVCT studies on such systems due to electronic coupling of the multiple metal centers: the IVCT properties are not expected to be simply a superposition of the characteristics of the component metal-based chromophores, which may give rise to IVCT characteristics which are markedly different from those of their dinuclear counterparts.

It must be noted that the band-shape analyses of dinuclear mixed-valence systems are often challenged experimentally by a number of factors. These include (i) multiple through-bridge interactions {due to the effects of low symmetry and spin−orbit coupling at low-spin $M^{III}(d\pi^5)$ centers, which lead to multiple overlapping IVCT and interconfigurational (IC) bands in the mixed-valence spectra[40,43,78,79] which, if not separately resolved, also contribute to the bandwidth}; (ii) multiple nuclear and solvent vibrations coupled to the electron transfer which may have different time scales;[40] and (iii) contributions from environmental effects such as specific solvation and ion pairing which are not explicitly included in theoretical treatments for IVCT and which invalidate the

assumptions of the dielectric continuum model in eq 6.[43] The determination of the "Class" of a mixed-valence system based on the abovementioned criteria is also complicated by the inability to accurately determine H_{ab}. While r is typically equated with the through-space geometrical distance between the metal centers, the actual charge-transfer distance which should be employed in eq 4 may be shorter due to electronic delocalization, self-polarization, and other effects[80−84] so that the equation provides a lower limit only for H_{ab}. These considerations will likewise be of significance for higher nuclearity systems, although such aspects appear not to have been generally appreciated to date.

The present review seeks to draw attention to the current experimental and theoretical challenges in the area by addressing the fundamental electron-transfer properties of trinuclear and tetranuclear complexes through the analysis of their IVCT absorption characteristics. Of particular interest are the multiplicity of the IVCT bands, and the appearance of appreciable second-order interactions (as demonstrated by the appearance of remote IVCT transitions). Attention is also focused on the influence of the molecular shape of the assemblies on the nature of the IVCT.

Three major factors are crucial to clarify the IVCT properties of such systems: first, the effect of increasing the number of electronically-coupled metal centers on the IVCT transitions (specifically their energy, intensity, and bandwidth); second, the effect of the relative distances and orientations of the centers; and third, their stereochemical relationship.[85,86] Given the diverse range of metallosupramolecular architectures, these factors underlie the need for a systematic understanding of how the geometry of such systems influences their electron-transfer properties.

While a range of transition metal ions have been successfully incorporated into trinuclear, tetranuclear, and higher nuclearity assemblies, the present review is restricted solely to homo- or hetereonuclear species comprising the members of the "iron triad"—iron, ruthenium, and osmium. Multicomponent systems which incorporate ruthenium- and osmium-based fragments are arguably more prevalent than those of iron for studies of electron-transfer phenomena, although there has been an interest in trinuclear and tetranuclear iron complexes due to their suitability as model systems for metalloenzymic activity in biological systems.

An additional level of complexity is introduced into such systems by the potential chirality of the constituent metal centers and the nonsymmetrical nature of the bridging ligands. The present review also addresses the stereochemical complexities which are inherent in the majority of species incorporating polypyridyl ligands. The stereochemical influences on the physical properties of such systems have only recently been acknowledged.[85,86]

Studies of IVCT characteristics in trinuclear and tetranuclear complexes provide the means of bridging the gap between the interpretation of electron transfer in simple chemical reactions and that in large multicomponent systems. An understanding of the process in the larger arrays is ultimately essential if their technological potential in innovative practical devices is to be realized.

2. Cyano-Bridged Trinuclear and Tetranuclear Complexes

Cyano-bridged polynuclear complexes are among the earliest and most extensively studied mixed-valence systems,[87,88] originating in the 18th century with the discovery of Prussian Blue, an infinite three-dimensional cubic array of alternate Fe^{II} and Fe^{III} centers linked by bridging cyanide (CN^-) groups.[26,27] The recognition of the mixed-valence nature of such polymeric cyanometalates provided, for the first time, an explanation for the extraordinary colors displayed by many transition metal-containing minerals. The diverse potential applications of cyanometalates, and the suitability of $M_x(CN)_y$ building blocks for self-assembly processes have motivated the synthesis and investigation of discrete cyano-bridged complexes.[89] These systems exhibit intriguing physicochemical properties, including superparamagnetism and photoinduced magnetic ordering phenomena, as demonstrated for the molecular squares of Oshio *et al.*;[90,91] they exhibit multielectron catalytic properties in cyano-ferrocene complexes;[92] and they have been cited as photosensitizers in photovoltaic cells.[9]

Several reviews[1,5,93,94] have highlighted a range of architectural motifs for the cyanometalates of iron, ruthenium, and osmium, including square,[90,91] cube,[95,96] ring,[97,98] and star[99,100] structures, in addition to the well-established variations on the Prussian Blue structure.[101,102] The wide range of architectures are based on linear or angular arrangements of two or more M−CN−M′ rods, linked together at M and/or M′ (M, M′ = Fe, Ru, Os). For trinuclear species of the form M(μ-CN)M′(μ-CN)M, geometric isomers may be realized through the *cis* or *trans* disposition of the bridging cyanide units coordinated to the central M′ unit. The ambidentate nature of cyanide—i.e., its ability to bridge two metal centers simultaneously via C or N as the donor atom—also gives rise to linkage isomers. A nonsymmetric electronic distribution in the bridge may thus be exploited to effect vectorial energy and electron transfer in polynuclear complexes. The bonding characteristics of cyanide are clearly differentiated at its C and N termini: C-bonded *cyanide* displays an affinity for electron-rich metals such as M^{II} (M = Fe, Ru, or Os) and, hence, exhibits favorable π-acceptor properties characteristic of strong-field ligands, while N-bonded *isocyanide* has an affinity for relatively electron-deficient metals such as M^{III}, displaying predominantly σ-donor properties characteristic of medium-field ligands.

The development of synthetic strategies to control the linkage of the cyanide bridge has provided a versatile family of trinuclear cyano-bridged complexes of Fe, Ru, and Os. Indeed, this is the most comprehensively studied class of trinuclear mixed-valence systems in terms of their IVCT properties.[103] A discussion of a number of aspects of metal−metal charge transfer across cyanide bridges and in oligonuclear species has been presented by Vahrenkamp *et al.*[93]

While preliminary reviews concerning the IVCT properties of cyano-bridged trinuclear and tetranuclear systems have appeared,[37,104] a number of recent studies have provided important new insights into these properties. The influences of the following factors on the IVCT properties are of particular interest: (i) the *cis* or *trans* arrangement of the cyanide bridges at the central metal which give rise to "linear" or "round-the-corner" electronic communication between the peripheral metal centers; (ii) the cyanide−isocyanide isomerism of the ambidentate bridge; (iii) the identity of the peripheral ligands; (iv) the identity and coordination environments of the central and peripheral metal centers; and (v) the presence of specific solvent interactions at the peripheral (as opposed to bridging) cyanide units. Early attempts to elucidate the bulk structural, magnetic, and spectral properties of Prussian Blue some 25 years ago[105]

have provided the stimulus for the design and study of many of these fundamental aspects in dinuclear and trinuclear cyanometalates.

2.1. Molecular Chains and Wires Based on (Polypyridyl)ruthenium(II) Chromophores

The $Ru(bpy)_2(CN)_2$ (bpy = 2,2′-bipyridine) motif is an attractive basis for polymetallic assemblies, as the cyanide ligands offer two potential binding sites for incorporation into larger assemblies comprising other transition metal chromophores which serve as electron donors or acceptors. In studies extending the pioneering work of von Kameke and Taube[106] and Powers and Meyer[107] on trinuclear pyrazine-brided chains (section 3), Bignozzi and co-workers[104,108−115] have investigated the related cyano-bridged systems $[(NH_3)_5Ru-NC-M(bpy)_2-CN-Ru(NH_3)_5]^{4+}$ (M = Ru, Os)[104,108−110] and the analogues $[(py)(NH_3)_4Ru-NC-Ru(bpy)_2-CN-Ru(NH_3)_4(X)]^{4+}$ {X = NH_3 or py (pyridine)}.[104,110] The bridging cyano units are angularly disposed by virtue of the central *cis*-$Ru(bpy)_2$ chromophore. By comparison with the cases of the related monomeric species,[104,108−110] the metal-based oxidation processes for $[(NH_3)_5Ru-NC-Ru(bpy)_2-CN-Ru(NH_3)_5]^{4+}$ (represented by [2,2,2] to denote the valencies of the metal centers) were assigned to two sequential one-electron processes corresponding to oxidation of the terminal $Ru(NH)_3$ moieties (**I** and **II**; Figure 1), followed by one-electron oxidation of the central $Ru(bpy)_2$ unit (**III**).

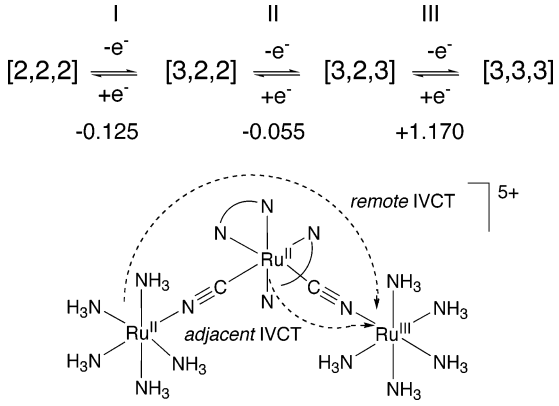

Figure 1. Structure of $[(NH_3)_5Ru-NC-Ru(bpy)_2-CN-Ru(NH_3)_5]^{n+}$ ($n = 4-7$),[108] demonstrating the adjacent and remote IVCT transitions. Potentials were recorded in aqueous solution and are quoted in volts (vs SCE).

The partially-oxidized forms of the trinuclear complexes [3,2,2] and [3,2,3] are mixed-valence species, and they exhibited a rich combination of electronic transitions in their UV/visible and near-infrared (NIR) absorption spectra, which were ascribed to transitions of both metal-to-ligand charge transfer (MLCT) and IVCT origin. In a (CN^-)-bridged trinuclear system comprising the M(μ-CN)M′(μ-CN)M″ core, two forms of IVCT may be envisaged: one that involves *adjacent* metal centers (M ↔ M′ and M′ ↔ M″), and one involving *remote* metal centers (M ↔ M″). In the present [3,2,2] mixed-valence system, the transitions were assigned as (i) $Ru_c^{II} \rightarrow$ bpy MLCT originating from the $Ru^{II}(bpy)_2$ moiety (Ru_c denotes the central ruthenium atom) and (ii) $Ru_c^{II} \rightarrow Ru_t^{III}$ IVCT between *adjacent* cyano-bridged units (Ru_t denotes the terminal ruthenium center), in addition to the intriguing observation of two types of *remote* transitions, attributed to (iii) $Ru_t^{II} \rightarrow$ bpy MLCT originating from the $Ru(NH_3)_5$ moieties, and (iv) $Ru_t^{II} \rightarrow Ru_t^{III}$ IVCT between the remote metal centers of the $Ru(NH_3)_5$ units. The latter transitions of type (iv) had been observed only once previously by von Kameke and Taube[106] in the spectrum of *trans*-$[(NH_3)_5Ru(\mu\text{-pyz})Ru(NH_3)_4(\mu\text{-pyz})Ru(NH_3)_5]^{7+}$ (see section 3), while transitions of type (iii), which were observed in the unoxidized [2,2,2] and mixed-valence [3,2,2] and [3,2,3] forms, had not been previously reported.

Analysis of the [3,2,3] spectrum for $[(NH_3)_5Ru-NC-Ru(bpy)_2-CN-Ru(NH_3)_5]^{6+}$ [104,108−110] revealed an IVCT band at 15 200 cm^{-1} {(658 nm); ϵ_{max} = 5700 M^{-1} cm^{-1}, $\Delta\nu_{1/2}$ = 4400 cm^{-1}} attributable to $Ru_c^{II} \rightarrow Ru_t^{III}$, from which the pertinent delocalization parameters, H_{ab} and α^2, were determined as 1800 cm^{-1} and 0.14, respectively, from eqs 4 and 5. A similar *remote* IVCT transition was absent in the related pyrazine-bridged mixed-valence complex,[107] although such a transition was observed in the spectrum of *trans*-$[(NH_3)_5Ru(\mu\text{-pyz})Ru(NH_3)_4(\mu\text{-pyz})Ru(NH_3)_5]^{7+}$.[106] The difference between the cyano-bridged [2,3,2] ion and the analogous pyrazine-bridged system[107] was attributed to the stronger electronic interaction mediated by the cyanide bridge. The magnitudes of the parameters, however, are sufficiently small to warrant a localized Class II description[27] for both species. The short bridge length, or the cylindrical nature of cyanide, which does not possess any steric requirements for π-overlap, was proposed to account for the higher electronic coupling in this system compared with the pyrazine-bridged species.[109]

An *adjacent* IVCT transition ($Ru_c^{II} \rightarrow Ru_t^{III}$) was also evident for the [3,2,2] mixed-valence species at 14 600 cm^{-1} (685 nm) where the band maximum was red-shifted relative to its position in the [3,2,3] system due to the lower electron-withdrawing influence of the $Ru^{II}(NH_3)_5$ moiety on the central metal. A new transition of *remote* origin (i.e. $Ru_t^{II} \rightarrow Ru_t^{III}$) was observed at 9500 cm^{-1} (1053 nm), which was observed as a long-wavelength tail on the *adjacent* IVCT band (Figure 2). Due to the correlation between the intensities of the *remote* IVCT transitions and the related *adjacent* IVCT transitions for the trinuclear cyano-bridged complexes, it was suggested that *remote* IVCT bands engage in an "intensity stealing" mechanism from the predominant *adjacent* IVCT bands (and remote MLCT bands), which is dependent on the electronic characteristics of the mediating bridging ligands.[104]

Katz and co-workers[117] investigated the related 4-cyanopyridine-bridged species $[Ru(bpy)_2\{(\mu\text{-4-CNpy})Ru(NH_3)_5\}_2]^{6+}$, where the central *cis*-$Ru(bpy)_2$ moiety is nitrile-bound to the bridging ligand (Figure 3). One-electron oxidation generated the +7 mixed-valence species which was formulated as [2,2,3], where the terminal $Ru(NH_3)_5$ moieties undergo sequential one-electron oxidation processes prior to the central ruthenium. This was accompanied by the appearance of two new bands (determined by Gaussian deconvolution) at 16 000 cm^{-1} {(625 nm); ϵ_{max} = 400 M^{-1} cm^{-1}; CH_3CN} and 9174 cm^{-1} {(1090 nm); ϵ_{max} = 20 M^{-1} cm^{-1}}, which were assigned as *adjacent* $Ru^{II} \rightarrow Ru_t^{III}$ IVCT transitions. The doubly-oxidized mixed-valence [3,2,3] species was characterized by an IVCT absorption at 15 405 cm^{-1} {(645 nm); ϵ_{max} = 700 M^{-1} cm^{-1}} which was attributed to a 2-fold degenerate $Ru^{II} \rightarrow Ru_t^{III}$ IVCT transition.[117] The comparatively lower intensities of the IVCT bands relative to those of the above-mentioned cyano-bridged systems were ascribed to the larger metal−metal separation in the 4-cyanopyridine bridged species: 9.3 vs 5 Å and 18.6 vs 10 Å

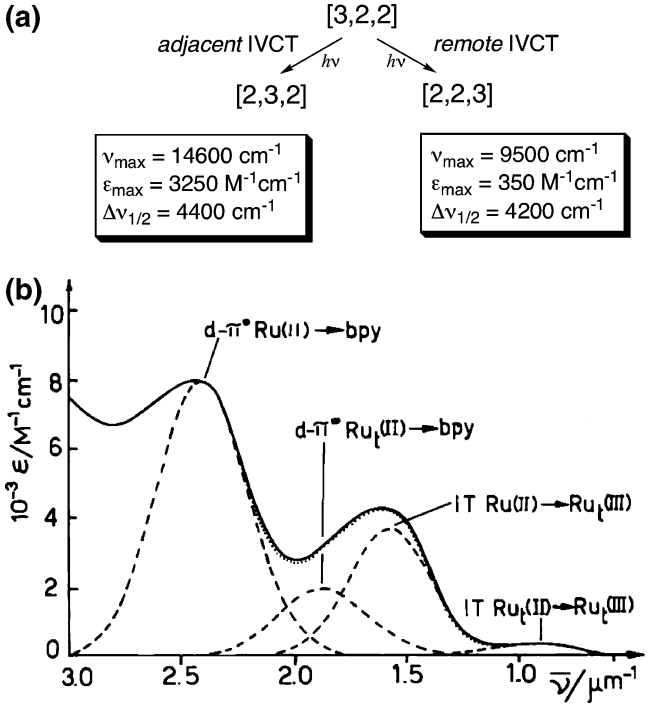

Figure 2. (a) IVCT band parameters for the adjacent and remote IVCT transitions in $[(NH_3)_5Ru-NC-Ru(bpy)_2-CN-Ru(NH_3)_5]^{5+}$.[104,108−110] (b) Absorption spectrum of the [3,2,2] ion in DMF solution.[116] The dashed lines represent an approximate Gaussian analysis of the spectrum. The dotted line represents the sum of the bands obtained by Gaussian analysis. Ru indicates the ruthenium atom of the central $Ru(bpy)_2^{2+}$ unit; Ru_t indicates the ruthenium atom of a terminal $Ru(NH_3)_5^{2+/3+}$ unit.[108]

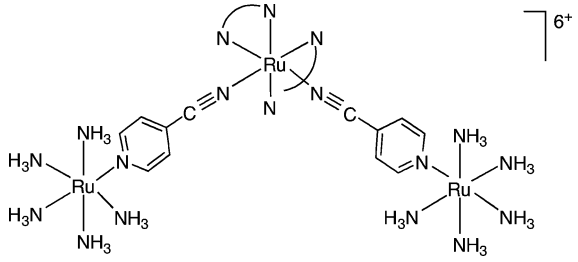

Figure 3. $[Ru(bpy)_2\{(\mu\text{-}4\text{-}CNpy)Ru(NH_3)_5\}]^{6+}$.[117]

between adjacent and remote metal centers for the 4-cyanopyridine and cyano-bridged species, respectively. The absence of remote IVCT transitions in the analogous species $[Ru(bpy)_2\{(\mu\text{-BL})Ru(NH_3)_5\}_2]^{6+}$ (BL = pyz, 4,4′-bpy = 4,4′-bipyridine[107]) was ascribed to steric effects, as the *cis* pyrazine or pyridine groups adopt an orientation that restricts appreciable π-interactions through the central ruthenium.[117]

The IVCT properties for the trinuclear [3,2,3] species $[Ru(bpy)_2\{(\mu\text{-L})Ru(NH_3)_5\}_2]^{n+}$ (n = 6, 8; BL = CN^-, pyz, 4-CNpy, 4,4′-bpy)[117] revealed a strong solvent dependence due to specific solvent interactions with the terminal pentaammineruthenium moieties.[57,63,118−120] The lesser solvent dependencies for the trinuclear systems relative to those of their dinuclear congeners were ascribed to the relatively larger molecular (solvent-excluded) volumes of the former.

In the related systems $[(py)(NH_3)_4Ru-NC-Ru(bpy)_2-CN-Ru(NH_3)_4(X)]^{4+}$ (X = NH_3 or py),[104,110] denoted [2′,2,2] and [2′,2,2′], respectively,[110] the doubly-oxidized [3′,2,3] mixed-valence species exhibited *adjacent* IVCT bands associated with a twofold degenerate $Ru^{II} \rightarrow Ru^{III}_{t'}$ transition at 13 600 cm^{-1} (635 nm) {$Ru_{t'}$ denotes the terminal $Ru(NH_3)_4(py)$ units}. The [3′,2,2′] species exhibited two distinct IVCT transitions associated with $Ru^{II} \rightarrow Ru^{III}_t$ {15 200 cm^{-1} (658 nm)} and $Ru^{II} \rightarrow Ru^{III}_{t'}$ {13 600 cm^{-1} (735 nm)} transitions (Table 1). The mono-oxidized mixed-valence species [2′,2,3] (the formulation reflects the fact that the pentaammine moiety is oxidized first) and [2′,2,3′] displayed both *adjacent* and *remote* IVCT transitions.

Interestingly, a *remote* IVCT transition was also described for the mixed-valence *trans*-$[(NH_3)_5Ru^{III}(\mu\text{-pyz})Ru^{II}(NH_3)_4(\mu\text{-pyz})Ru^{II}(NH_3)_5]^{7+}$ species reported by von Kameke and Taube;[106] however, the transition was observed at considerably lower energy {ν_{max} = 5900 cm^{-1} (1695 nm)} than the transitions of similar origin reported by Bignozzi and coworkers[104,108−110] for *cis*-configured complexes. The difference was ascribed to a greater solvent reorganizational contribution to ν_{max} due to the closer proximity of solvent molecules in the intersite region in the *cis*- relative to *trans*-configured trinuclear species.[110]

In the trinuclear system $[NC-Ru^{II}(bpy)_2-CN-Ru^{II}(bpy)_2-NC-Ru^{II}(bpy)_2-CN]^{2+}$,[111] the central $Ru(bpy)_2$ chromophore (i.e. N-bound to bridging cyanide) underwent a more facile oxidation (0.66 V vs SCE; CH_3CN) relative to the C-bound peripheral $Ru^{II}(bpy)(CN)$ moieties (1.19, 1.14 V). The chromophoric units are structurally related, with the only differences arising from the cyanide units (i.e. bridging vs terminal, and C-bound vs N-bound).[104] On the basis of structural considerations, an *all-cis* configuration involving coplanar bridging and terminal cyanides was preferred on the basis of hindrance to rotation about the bridging cyanide units.[111] The system will also exhibit stereoisomerism by virtue of the potential chirality of the three constituent metal centers. On the basis of shifts in the MLCT bands, the contribution from the redox asymmetry of the metal centers (due to the nonsymmetric nature of the bridging cyanide ligands) was estimated as 0.2−0.3 V. This was insufficient to account for the observed potential separations,[37,111] and the potential separations were instead attributed to significant electron delocalization through the system. The mixed-valence [2,3,2] species was characterized by an absorption in the region 15 000−4500 cm^{-1} (670−2220 nm) and centered at ∼7250 cm^{-1} (1380 nm)[104,108−110] which was assigned as an IVCT transition from the peripheral Ru^{II} centers to the central Ru^{III} moiety.[111] Due to the twofold degeneracy of the transition, a band with double the intensity observed for its dinuclear congener[104] might have been predicted. However, the IVCT for this trinuclear system was split into two bands of comparable intensity separated by ∼3000 cm^{-1}, which could not be attributed to spin−orbit coupling components.[111] The delocalization parameters for dinuclear $[NC-Ru^{II}(bpy)_2-CN-Ru^{III}(bpy)_2-CN]^{2+}$ {H_{ab} = 2000 cm^{-1}, α^2 = 0.07; eqs 4 and 5}[111] suggested that a valence-localized Class II description was also appropriate for the trinuclear mixed-valence system. The splitting of the IVCT band was ascribed to a non-negligible coupling between the *remote* metal centers, and the potential energy surfaces were constructed to account for the observed spectral splitting.[104] In Figure 4, two IVCT transitions arise from optical excitation between the adiabatic potential surfaces.

The electrochemical and photophysical studies on the polymetallic complexes incorporating the $M(bpy)_2$ chromophore during the 1980s provided important and timely extensions of the pioneering work of the late 1970s.[106,107] However, the ability to address fundamental aspects regarding geometrical influences on the IVCT was limited by the invariably *cis*-

Table 1. IVCT Properties of Cyano-Bridged Trinuclear and Tetranuclear Complexes

complex	*n*	mixed-valence state	origin of IVCT[a]	ν_{max}[c] (cm^{-1})	ϵ_{max} ($M^{-1}\,cm^{-1}$)	$\Delta\nu_{1/2}$ (cm^{-1})	H_{ab} (cm^{-1})	α^2	solvent	ref
$[(NH_3)_5Ru-NC-Ru(bpy)_2-CN-Ru(NH_3)_5]^{n+}$	5	[3,2,2]	$Ru^{II} \rightarrow Ru_t^{III}$	14600	3250	4400			H_2O	104, 108−110
			$Ru_t^{II} \rightarrow Ru_t^{III}$	9500	350	4200	340			
	6	[3,2,3]	$Ru^{II} \rightarrow Ru_t^{III}$	15200	5700	4400	1800[b]	0.14[b]		
$[(NH_3)_5Ru-NC-Os(bpy)_2-CN-Ru(NH_3)_5]^{n+}$	5	[3,2,2]	$Ru^{II} \rightarrow Ru_t^{III}$	7000						104
			$Ru_t^{II} \rightarrow Ru_t^{III}$	1000						
$[(py)(NH_3)_4Ru-NC-Ru(bpy)_2-CN-Ru(NH_3)_4(py)]^{n+}$	5	[2′,2,3′]	$Ru^{II} \rightarrow Ru_{t'}^{III}$	13300	2900	4700				110
			$Ru_{t'}^{II} \rightarrow Ru_{t'}^{III}$	8200	350	4200				
	6	[3′,2,3′]	$Ru^{II} \rightarrow Ru_{t'}^{III}$	13600	3000	4400				
$[(py)(NH_3)_4Ru-NC-Ru(bpy)_2-CN-Ru(NH_3)_5]^{n+}$	5	[2′,2,3]	$Ru^{II} \rightarrow Ru_t^{III}$	14700	3100	4600				110
			$Ru_{t'}^{II} \rightarrow Ru_t^{III}$	10000	370	4200				
	6	[3′,2,3]	$Ru^{II} \rightarrow Ru_t^{III}$	15200	2900	4400				
			$Ru^{II} \rightarrow Ru_{t'}^{III}$	13600	3000	4400				
$[(NC)(bpy)_2Ru-CN-Ru(bpy)_2-NC-Ru(bpy)_2(CN)]^{n+}$	3	[2,3,2]	$Ru^{II} \rightarrow Ru_t^{III}$	5700[d]			2000	0.07	D_2O	104, 111, 112
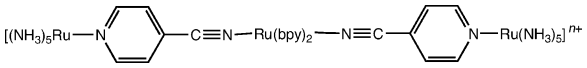	7	[3,2,2]	$Ru^{II} \rightarrow Ru_t^{III}$	16000	400				CH_3CN	117
			$Ru_t^{II} \rightarrow Ru_t^{III}$	9170	20					
	8	[3,2,3]	$Ru^{II} \rightarrow Ru_t^{III}$	15500	700	5000				
$[(NC)(bpy)_2Ru-CN-Ru(dcbpy)_2-NC-Ru(bpy)_2(CN)]^{n+}$	5	[2,3,2]	$Ru_t^{II} \rightarrow Ru^{III}$	7800	4660	3070	1370	0.031	CH_3CN	126
$[(NC)(bpy)_2Ru-CN-Ru(H_2dcbpy)_2-NC-Ru(bpy)_2(CN)]^{n+}$	1	[2,3,2]	$Ru_t^{II} \rightarrow Ru^{III}$	7810	4600	3480	1450	0.035	CH_3CN	
$[(H_2O)(bpy)_2Ru-CN-Ru(dcbpy)_2-NC-Ru(bpy)_2(H_2O)]^{n+}$	6	[2,2,3]	$Ru^{II} \rightarrow Ru_t^{III}$	9050	2830	3140	1160	0.017	CH_3CN	
$[(OH)(bpy)_2Ru-CN-Ru(H_2dcbpy)_2-NC-Ru(bpy)_2(OH)]^{n+}$	0	[2,2,3]	$Ru^{II} \rightarrow Ru_t^{III}$	11170	1900	3280	1080	0.01	CH_3CN	

[a] Ru, Ru_t, and $Ru_{t'}$ denote central $Ru(bpy)_2$, terminal $Ru(NH_3)_5$, and terminal $Ru(NH_3)_4(py)$ units, respectively. [b] Accounting for the twofold degeneracy of the IVCT band. [c] Band maxima obtained from Gaussian analysis of the band manifold. [d] The IVCT band appears as two overlapping transitions with a maximum at 5700 cm^{-1} and side band at ~7250 cm^{-1}, although spectral deconvolution of the manifold was not performed.

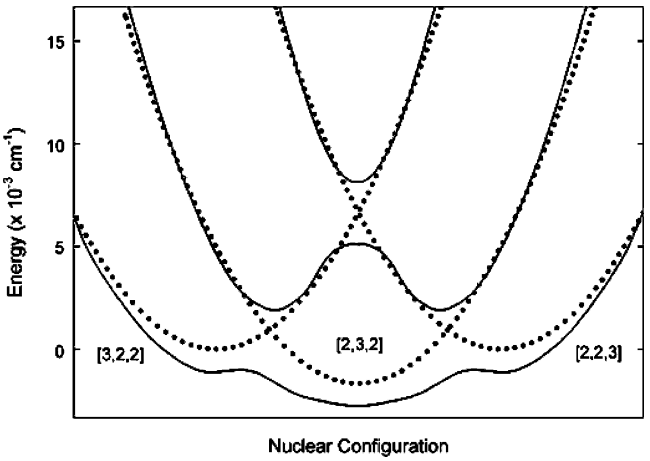

Figure 4. Schematic representation of the diabatic (dotted) and adiabatic (solid) potential energy surfaces for the trinuclear system $[NC-Ru^{II}(bpy)_2-CN-Ru^{III}(bpy)_2-NC-Ru^{II}(bpy)_2-CN]^{3+}$, where electronic couplings of 2000 and 1000 cm^{-1} are assumed between the adjacent and terminal metal centers, respectively.[104]

configured central metal, and the comparison of *adjacent* and *remote* interactions received limited attention. It was envisaged that the efficiency of long-range (*remote*) interactions was facilitated through a polynuclear backbone in which the metals and intervening bridging ligands provided a linear (rather than angular) conduit for intra-metal electron transfer. Indeed, these expectations were supported through electrochemical studies by Meyer and co-workers[121] on *trans*-$[(py)_4Ru\{NC-Ru(py)_4Cl\}_2]^{2+}$. This enabled a comparison of the effect of the overall linear or angular disposition of the terminal metal centers on the intramolecular electron-transfer characteristics with related *cis*-configured complexes such as $[(bpy)_2Ru\{NC-Ru(bpy)_2CN\}_2]^{2+}$.[111,114] Electrochemically, a 0.28 V splitting was observed between the redox potentials of the terminal Ru centers in the *trans*-configured complex,[121] compared with the 0.08 V difference for the *cis*-configured complex,[111,114] in support of the assertion that long-range interactions are facilitated through a linear, rather than an angular, assembly. Unfortunately, the consequences on the IVCT properties of the mixed-valence form of *trans*-$[(py)_4Ru\{NC-Ru(py)_4Cl\}_2]^{2+}$ were not pursued.[121] The effects of the relative orientations of the bridging and/or terminal cyanide units, and the stereochemical ambiguities that are inherent in polypyridyl-based complexes, were also largely ignored.

The observation of efficient, vectorial electron-transfer processes mediated by cyanide bridges prompted investigations of the intramolecular energy transfer properties of related trinuclear complexes based on the central $Ru^{II}(pp)_2$ chromophore {where pp is bpy, dcbpy = 4,4′-bpy$(COO)_2^{2-}$, or H_2dcbpy = 4,4′-bpy$(COOH)_2$}. These have potential applications as sensitizer units in artificial light-harvesting devices which mimic the "antenna effect" of natural systems.[122,123] Notable examples include chromophore−luminophore complexes such as $[Ru^{II}(bpy)_2\{(\mu\text{-NC})Cr^{III}(CN)_5\}_2]^{4-}$ [113] and $[Ru^{II}(bpy)_2\{trans\text{-}(\mu\text{-NC})_2Cr^{III}(cyclam)\}_2]^{4+}$ (cyclam = 1,4,8,11-tetraazacyclotetradecane),[124,125] where selective excitation of the Ru chromophore results in emission from the Cr-luminophore.[113] While the photophysical aspects of these systems are beyond the scope of the present review, it is worth noting that these systems provided the first observation of excited-state intervalence charge transfer in trinuclear complexes.

By the incorporation of the central *cis*-$Ru(dcbpy)_2^{2-}$ unit which was N-bonded to bridging cyanide, trinuclear complexes of the type $[Ru^{II}(dcbpy)_2\{(\mu\text{-NC})Ru^{II}(bpy)_2(CN)\}_2]^{2+}$ [112,114,115,126,127] were developed. The COO^- functionalities facilitate adsorption onto TiO_2 semiconductor surfaces, and the light absorbed by the peripheral antenna chromophores (C-bonded to bridging and terminal cyanides) is efficiently channeled toward the central sensitizer unit. The photochemical behavior of these systems has been extensively investigated, particularly through transient measurements of their excited-state IVCT spectra. Application of Hush theory[28,29,34] to the results of ground-state IVCT measurements yielded delocalization parameters (H_{ab} and α^2; eqns 4 and 5) which were consistent with a Class II classification for the mixed-valence [2,3,2] species.[112]

In an interesting extension of this work, Matsui and co-workers[126] investigated the singly-oxidized forms of $[(CN)(bpy)_2Ru^{II}-CN-Ru^{II}(H_2dcbpy)_2-NC-Ru^{II}(bpy)_2(CN)]^{2+}$ and

$[(CN)(bpy)_2Ru^{II}-CN-Ru^{II}(dcbpy)_2-NC-Ru^{II}(bpy)_2(CN)]^{2-}$ (**Ia**/**Ib**), as well as $[(H_2O)(bpy)_2Ru^{II}-NC-Ru^{II}(H_2dcbpy)_2-CN-Ru^{II}(bpy)_2(H_2O)]^{4+}$ and $[(OH^-)(bpy)_2Ru^{II}-NC-Ru^{II}(dcbpy)_2-CN-Ru^{II}(bpy)_2(OH^-)]^{2-}$ (**IIa**/**IIb**), shown in Figure 5. These may be considered as "linkage isomers"

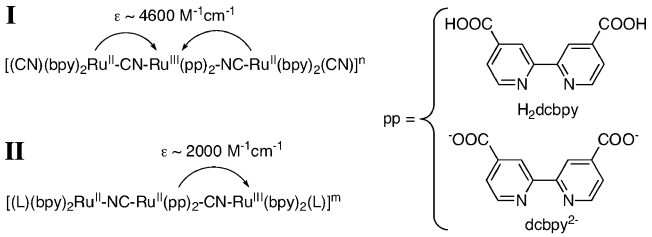

Complex	pp	L	n	m
Ia^+	H_2dcbpy	-	3+	-
Ib^+	$dcbpy^{2-}$	-	1-	-
IIa^+	H_2dcbpy	H_2O	-	5+
IIb^+	$dcbpy^{2-}$	OH^-	-	1-

Figure 5. Structures showing the direction of electron transfer in trinuclear CN^--bridged complexes. The direction of the IVCT is from terminal units to the central unit in **Ia/b** but in the opposite direction in **IIa/b**.[126]

where the central $Ru(dcbpy)_2$ chromophore is N-bound to bridging cyanide in **I** and C-bound to bridging cyanide in **II**.[126] Protonation or deprotonation of central dcbpy/H_2dcbpy ligands permitted variation in the overall charge on the complexes. Although relatively intense IVCT bands were reported in all cases, notable differences were observed in the mono-oxidized species derived from complexes **I** and **II**. The IVCT was attributed to electron transfer from the terminal to central units in **I** ($\epsilon_{max} = 4600\ M^{-1}\ cm^{-1}$), but in the opposite direction for **II** ($\epsilon_{max} = 2000\ M^{-1}\ cm^{-1}$). A red shift was observed in the IVCT band of the corresponding deprotonated mixed-valence species, and the considerably diminished intensity of the IVCT band in the latter was ascribed to the existence of two interacting donor units in **I**, as opposed to the single donor moiety in **II**. Accordingly, the α^2 values determined from Hush theory (eq 5)[28,29,34] revealed a larger degree of electron delocalization in the former; however, both species were characterized within the localized Class II regime.[27]

The orientational effect of the cyanide bridge has also been investigated for the dinuclear linkage isomers $[(H_2dcbpy)Re^I(CO)_3-(\mu\text{-BL})-Ru^{II}-(bpy)_2(CN)]^+$, where BL = CN^- or NC^- (abbreviated Re−CN−Ru or Re−NC−Ru, respectively).[128] While IVCT studies were not reported, the redox potential for the Re−CN−Ru isomer was 130 mV cathodic of the Re−NC−Ru isomer, where the first oxidation corresponds to the $Ru^{III/II}$ couple (the $Re^{II/I}$ oxidation was outside the potential window for methanol). Although not elaborated here, the marked differences between the electrochemical properties of the isomeric forms were also manifested by significant differences in their efficiencies as sensitizers anchored to TiO_2 nanocrystalline films.

For the isomeric trinuclear complexes $[Ru(bpy)_2\{(\mu\text{-BL})Re(bpy)(CO)_3\}_2]^{2+}$ (BL = CN^- or NC^-),[129] comparison of the redox potential for the first metal-based oxidation process in the isomeric pair was consistent with the general trend that the center with the more facile oxidation is bound to the cyanide nitrogen. This is 0.1−0.2 V easier to oxidize than the C-bound case. The energies of the IVCT transitions for the isomeric pair were markedly different: the Re−CN−Ru−NC−Re isomer exhibited an IVCT band at 12 280 cm^{-1} (780 nm) following one-electron oxidation, while the corresponding band in Re−NC−Ru−CN−Re appeared at 7350 cm^{-1} (1360 nm).

2.2. Other Cyano-Bridged Molecular Chains and Wires

Indelli and Scandola[130] investigated the ground- and excited-state IVCT characteristics of the heterotrinuclear complex $[\{Cr^{III}(cyclam)(CN)_2\}_2Ru^{II}(CN)_4]$ (Figure 6). The

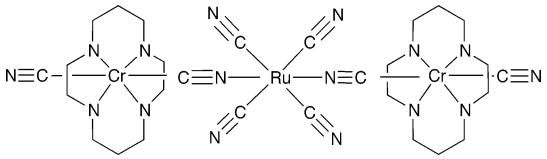

Figure 6. $[\{Cr^{III}(cyclam)(CN)_2\}_2Ru^{II}(CN)_4]$.[130]

system has the capacity to exhibit electrochromic and catalytic properties by adhesion to electrode surfaces, as the complex may be "wired" between two electrodes utilizing the terminal cyanide units.

The presence of a broad and intense absorption feature at 29 600 cm^{-1} (338 nm) in aqueous solution—which was absent from the spectra of the constituent metal-based units—was attributed to the doubly-degenerate IVCT transition from the central $Ru^{II}(CN)_4$ unit to the peripheral Cr^{III}(cyclam)(CN) moieties. On the basis of the band parameters {ϵ_{max} = 3250 $M^{-1}\ cm^{-1}$ (half the experimental intensity) and $\Delta\nu_{1/2}$ = 4000 cm^{-1}}, the results of a theoretical analysis within the framework of the Hush model[28,29,34] were consistent with a fully-localized Class II[27] system, as typically observed for cyano-bridged trinuclear complexes.

Forlano and co-workers[131] investigated a related series of complexes $[(edta)Ru^{III}-NC-M^{II}(CN)_4-CN-Ru^{III}(edta)]^{6-}$ (M = Fe^{II}, Ru^{II}, Os^{II}). The shifts in the near-infrared IVCT bands in the trinuclear complexes were indicative of Ru^{III}(edta) coordination to the exposed nitrogen atoms of the terminal cyanide ligands in the precursor dinuclear complexes. A blue shift in the IVCT band from 14 750 cm^{-1} (678 nm) in the dinuclear species to 16 260 cm^{-1} (615 nm) occurred on formation of the trinuclear species. The localized IVCT transitions were attributed to intramolecular electron transfer from the central metal to pendant Ru^{III}(edta) moieties.

Laidlaw and Denning[132] investigated the heterobi-, tri-, and tetranuclear mixed-valence complexes $[(OC)_5Cr(\mu\text{-CN})Ru(NH_3)_5]^{2+}$ (CrRu), *cis*-$[\{(OC)_5Cr(\mu\text{-CN})\}_2Ru(NH_3)_4]^+$ (Cr_2Ru), and *fac*-$[\{(OC)_5Cr(\mu\text{-CN})\}_3Ru(NH_3)_3]$ (Cr_3Ru). Electrochemically, the complexes were characterized by two redox waves corresponding to oxidation of the ruthenium center ($1e^-$), followed by oxidation of the chromium centers: the peak currents were in the ratios 1:1, 2:1, and 3:1 for CrRu, Cr_2Ru, and Cr_3Ru, respectively. A characteristic feature of the Cr_nRu set (n = 1, 2, or 3) was the virtually invariant redox potentials for both the $Ru(NH_3)_5$ and $Cr(CO)_5$ centers, which was indicative of localized intrametal interactions.

A single Gaussian-shaped absorption band was observed in each case following the initial one-electron oxidation, which was assigned as an $Cr(d^6) \rightarrow Ru(d^5)$ IVCT transition. The band parameters {e.g. in nitromethane: ν_{max} = 11 010 cm^{-1} (908 nm)/ϵ_{max} = 3640 $M^{-1}\ cm^{-1}$/$\Delta\nu_{1/2}$ = 4650 cm^{-1}

for CrRu; 10 580 (945)/5410/4840 for Cr_2Ru; and 10 525 (950)/5850/5010 for Cr_3Ru} were consistent with a localized (Class II) designation. The intensity and bandwidth increased with the number of bound Cr centers. However, a simple correlation between the band parameters and nuclearity was not apparent.

The IVCT energies exhibited a striking dependence on the solvent due to solvent−ammine hydrogen-bonding interactions. The sensitivity of the IVCT energy to solvent variation was greatest for the dinuclear complex and least for the tetranuclear complex. This was consistent with a simplistic argument in which the solvent sensitivity was directly proportional to the number of ammine ligands due to outer-sphere hydrogen bonding or, conversely, the number of solvent molecules in the immediate second solvation sphere. Such solvent−chromophore interactions are likely to predominate in the less sterically encumbered dinuclear complex. The IVCT energy was also found to depend significantly on the counterion, a trend which was more pronounced in lower donating solvents. The trends in solvation and ion pairing were consistent with a localized (Class II) assignment for the mixed-valence species.

The hetero-trinuclear complex $[(Me_2bpy)(CO)_3Re^{I}-NC-Fe^{III}(CN)_4-CN-Re^{I}(CO)_3(Me_2bpy)]^-$ (Me_2bpy = 4,4′-dimethyl-2,2′-bipyridine) was investigated by Pfennig and coworkers[133] and exhibited a single broad solvent-dependent peak in the visible region which was assigned as an IVCT transition from the terminal Re^{I} to the central $Fe^{III}(CN)_4$ unit. The trends observed in the IVCT properties of the related di- and tetranuclear species {comprising the $Fe^{III}(CN)_3$ central unit bound to three pendant $Re^{I}(CO)_3(Me_2bpy)$ moieties} were consistent with this assignment: the IVCT absorption shifted to lower energies with increasing nuclearity of the complexes: 20 120 cm^{-1} (497 nm), 18 420 (543 nm), and 17 270 cm^{-1} (579 nm) for the di-, tri-, and tetranuclear complexes, respectively. This red shift was attributed to the decrease in the energy of the M−CN π^* molecular orbital, which is induced by coordination of the lone pair of electrons on the cyanide nitrogen to one, two, or three pendant Re^{I} centers,[133] respectively. The increase in the molar absorptivities of the IVCT transitions with increasing nuclearity of the assembly was also consistent with the $Re^{I} \rightarrow Fe^{III}$ origin of the transition. In addition to the calculated delocalization parameters, application of the Hush theory yielded relatively constant values of H_{ab} over the series of complexes, which reflected the comparable internuclear distances and identical origins of the IVCT processes. As typically observed for this class of complexes, the IVCT bands exhibited a strong solvent dependence, with a linear correlation observed between the band energy and the acceptor number of the solvent.[134] The data were consistent with a Class II classification for the mixed-valence complexes.

More recently, Pfennig and co-workers[135] reported a comprehensive investigation of ten homo- and heterotrinuclear mixed-valence complexes of the form $[(NH_3)_5M-NC-Fe^{II}(CN)_4-CN-M'(NH_3)_5]^{n+}$ (M = Ru^{III}, Os^{III}, Cr^{III}, or Pt^{IV}; n = 2, 3, or 4).[135] The four symmetrical compounds (i.e. M = M′) exhibited a single broad absorption in the visible or NIR region, attributable to $Fe^{II} \rightarrow M$ IVCT, while the six unsymmetrical species (i.e. M ≠ M′) displayed two IVCT absorptions, characteristic of $Fe^{II} \rightarrow M$ and $Fe^{II} \rightarrow M'$ IVCT. While some ambiguity existed in the structural identity of the systems due to the possibility of *cis* or *trans* isomerism, comparison with the crystal structure of the related tetranuclear complex $[\{(Me_2bpy)(CO)_3Re^{I}-(\mu\text{-}NC)\}_3-Fe^{III}(CN)_3]$ suggested that a *trans* configuration was likely to predominate.[133]

The energies of the IVCT bands in the trinuclear complexes were blue-shifted relative to the case of their dinuclear analogues, while the intensities were approximately twice those observed for the related dinuclear species.[136] The IVCT bands in the symmetrical systems were assigned predominantly to transitions between the *adjacent* metal centers. The possibility of electronic coupling between *remote* metal centers was proposed to explain the observation of two closely-spaced redox processes for the geometrically-equivalent Ru^{III} centers in the $Ru^{III}-Fe^{II}-Ru^{III}$ system. Further investigation of this hypothesis was not pursued.

While the IVCT intensities for the unsymmetrical Ru species were comparable to those in their dinuclear Fe−Ru analogues, the $Fe \rightarrow M$ (M = Cr or Pt) IVCT transitions in the Os−Fe−M species exhibited significantly enhanced Fe−M electronic coupling, as shown by their relatively large intensities and H_{ab} values. The enhanced coupling for the Os system was attributed to an intensity-stealing mechanism, which is facilitated by the larger orbital size, and the increased tendency of Os^{II} to undergo strong π-back-bonding with the cyanide bridging ligand relative to the other metals of the series. The proposed mechanism may be regarded as an example of a *remote* interaction between the terminal metal centers, where the bridging ligands mediate a mixing between the $[Os^{II}-Fe^{III}-M(ox)]^*$ and $[Os^{III}-Fe^{III}-M(red)]^*$ (ox = oxidized, red = reduced) IVCT excited states and higher-energy charge-transfer states.

The stability of the +II and +IV oxidation states of platinum has motivated the design of trinuclear systems incorporating the $Pt^{IV}(L)_4$ chromophore, which have the potential to undergo multielectron charge-transfer processes which generate more than one electron upon absorption of a single photon. The trinuclear complex $[(NC)_5Fe^{II}-CN-Pt^{IV}(NH_3)_4-NC-Fe^{II}(CN)_5]^{4-}$ [137] exhibited an $Fe^{II} \rightarrow Pt^{IV}$ IVCT band at 23 585 cm^{-1} (424 nm; ϵ_{max} = 2365 M^{-1} cm^{-1} and $\Delta\nu_{1/2}$ = 7170 cm^{-1}). A linear correlation was found between the redox potential for the Fe^{II}/Fe^{III} couple and the energy of the IVCT band. Though simplistic in its approach, the establishment of general relationships between the electrochemical and spectral properties of trinuclear assemblies is important for the design of more sophisticated polynuclear assemblies.[93] The delocalization parameter (α = 0.03) and bandwidths ($\Delta\nu_{1/2}$ = 7380 cm^{-1}) were consistent with a Class II designation. The ΔE and λ ($\lambda = \lambda_i + \lambda_o$) values for the redox reaction $Fe^{II}-Pt^{IV}-Fe^{II} \rightarrow Fe^{III}-Pt^{III}-Fe^{II}$ are given in Table 2. The significant magnitude of λ in relation to symmetrical species such as $[(NC)_5Fe^{II}-CN-Fe^{III}(CN)_5]^{6-}$ was ascribed to (i) the large reorganization of the bond lengths for the Pt^{IV}/Pt^{III} couple and (ii) the large solvent reorganizational energy which

Table 2. IVCT Parameters for $[L(NC)_4Fe-CN-Pt(NH_3)_4-NC-Fe(CN)_4L]^{2-}$ Analogues[137]

L	ν_{max} ($\times 10^{-3}$ cm^{-1} (nm))	λ ($\times 10^{-3}$ cm^{-1})	ΔE ($\times 10^{-3}$ cm^{-1})
4,4′-bpy	23.6 (424)	15.97	10.84
pyz	23.9 (418)	15.89	11.21
4-CN-py	24.0 (416)	15.93	11.29
2-PCA	24.4 (410)	15.78	11.73
2-F-py	25.1 (399)	15.64	12.50
NMpyz	25.4 (393)	15.52	12.98

accompanies the process due to the different symmetries, bonding characteristics, and positions in space of the π-bonding orbital on Fe^{II} and the σ-antibonding orbital in Pt^{IV}.

Theoretical and experimental analysis of the electron-transfer processes occurring in this species[137,138] suggested that the first electron transfer occurred photochemically, while the second followed thermally from the second iron center in the high-energy $M^{III}Pt^{III}M^{II}$ intermediate (M = Fe or Ru). The mechanism of the photoinduced $M^{II} \rightarrow Pt^{IV}$ IVCT process involved the generation of the one-electron-transfer intermediate $M^{III}-Pt^{III}-M^{II}$, followed by decay of the intermediate either through back-electron transfer to yield the $M^{II}-Pt^{IV}-M^{II}$ starting material, or by thermal IVCT from the remaining M^{II} center to the Pt^{III} center to yield 2 equiv of $[M^{III}(CN)_6]^{3-}$ and 1 equiv of $[Pt^{II}(NH_3)_4]^{2+}$.

Accordingly, three potential energy surfaces were invoked to describe the available electronic configurations $M^{II}-Pt^{IV}-M^{II}$, $M^{III}-Pt^{III}-M^{II}$, and $M^{III}-Pt^{II}-M^{III}$. The potential energy diagram (Figure 7) is depicted for the Class

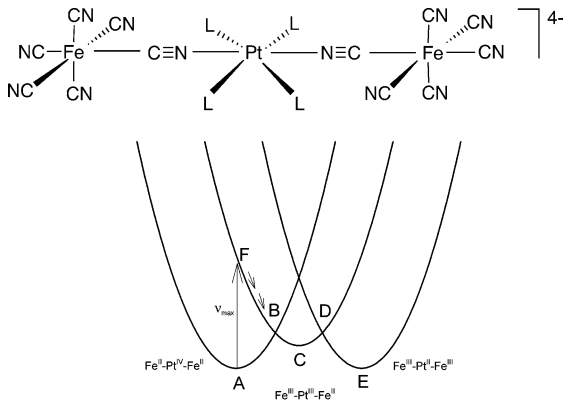

Figure 7. Schematic diagram of the potential energy surfaces for a trinuclear system of the type $[(CN)_5Fe^{II}-CN-Pt^{IV}(L)_2-NC-Fe^{II}(CN)_5]^{4-}$ {L = ethylenediamine, 2(NH_3)}.[137]

II complex. Thermal electron transfer between the metal centers occurs along the lower pathway connecting A−B−C−D−E, where B and D are the transition states for the $Fe^{II}/Pt^{IV} \rightarrow Fe^{III}/Pt^{III}$ and $Pt^{III}/Fe^{II} \rightarrow Pt^{II}/Fe^{III}$ electron-transfer processes, respectively, and C is the $Fe^{III}-Pt^{III}-Fe^{II}$ intermediate. B and D differ only in the position of the transferring electron and possess equivalent metal−ligand bond distances and solvation spheres around each metal center. An alternative charge-transfer path is the optical excitation A → F, which is not thermally accessible. Optical excitation directly transfers the electron to an excited vibronic transition state F, which, after relaxation to C, is then followed by the thermal electron transfer (C−D−E) or the back reaction (C−B−A). Theoretical analysis of the IVCT band {ν_{max} = 23 585 cm^{-1} (424 nm)} in addition to time-dependent resonance Raman experiments[139] were consistent with a one-electron $Fe^{II} \rightarrow Pt^{IV}$ transition as the primary step in the net two-electron charge transfer. The $Fe^{II} \rightarrow Pt^{IV}$ IVCT band experienced a red shift with increasing mole fraction of DMSO in a series of water/DMSO solvent mixtures,[137,138] and a decrease in intensity due to a lesser proportion of the mixed-valence species at higher DMSO fractions.

Bocarsly and co-workers[140] have investigated the femtosecond pump−probe spectroscopy of the mixed-valence complex $[(CN)_5Fe^{II}-CN-Pt^{IV}(NH_3)_4-NC-Fe^{II}(CN)_5]^{4-}$ and the related complex $[(CN)_5Ru^{II}-CN-Pt^{IV}(NH_3)_4-NC-Ru^{II}(CN)_5]^{4-}$. The energy of the IVCT band decreased linearly with increasing DMSO fraction for both complexes, whereas the absorption bandwidth remained the same. This was consistent with the linear shift of the $M^{II}-Pt^{IV}-M^{II}$ potential energy surfaces to higher energy with increasing DMSO mole fraction. The solvent dependence of the $Fe^{II} \rightarrow Pt^{IV}$ IVCT in $[(CN)_5Fe^{II}-CN-Pt^{IV}(NH_3)_4-NC-Fe^{II}(CN)_5]^{4-}$ allowed control of the activation barrier and driving force for the forward and back electron-transfer processes. The origin of the effect was ascribed to specific hydrogen-bonding interactions with the Fe^{II} moieties: the iron centers became more difficult to oxidize as the proportion of water increased. Water molecules engage in stronger interactions with the cyanide nitrogen atoms, thus lowering the energy of the CN^- π^* molecular orbitals and facilitating M−CN back-bonding. By contrast, the redox potential of the Pt^{IV} unit is relatively unaffected by the solvent, as the electron lone pairs are unavailable to interact with the second coordination sphere.

Pfennig and co-workers[137] investigated two series of trinuclear complexes in which the internal redox potentials of the terminal metallic units were varied to interrogate the properties of the homologous series of compounds: (i) $[L(NC)_4Fe-CN-Pt(NH_3)_4-NC-Fe(CN)_4L]^{2-}$, where the sixth coordination sites on the terminal iron units are varied using six different substituted pyridine or pyrazine ligands, L, shown in Figure 8; and (ii) $[Pt(NH_3)_4]_2[(NC)_5M-CN-Pt(NH_3)_4-NC-M(CN)_5]$, where M = Fe, Ru, or Os.

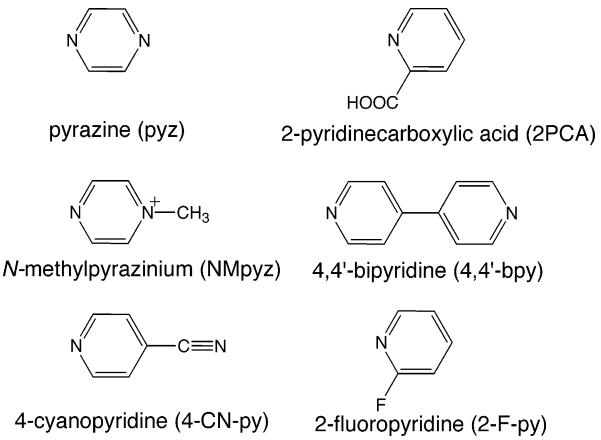

Figure 8. Structures and abbreviations of the ligands, L.[137]

Within the $[L(NC)_4Fe-CN-Pt(NH_3)_4-NC-Fe(CN)_4L]^{2-}$ series, the redox potential of the iron site was varied by substitution of the terminal site L with minor effects only on λ, as shown in Table 2. In accordance with eq 1, a linear correlation was found between ν_{max} and ΔE, given the near constancy of λ for the series.

For the $[Pt(NH_3)_4]_2[(NC)_5M-CN-Pt(NH_3)_4-NC-Fe(CN)_5]$ series, the molar absorptivities and intensities of the IVCT bands for M = Ru and Os were less than those for the Fe analogue (Table 3). The bandwidths were in reasonable agreement with those predicted on the basis of Hush theory, implying a localized description for the complex. A linear variation was again found between ν_{max} and ΔE for the series, in accordance with eq 1.

Bocarsly and co-workers[138] investigated the systems $[(CN)_5Fe^{II}-CN-Pt^{IV}(L)_2-NC-Fe^{II}(CN)_5]^{4-}$ {L = ethylenediamine, 2(NH_3)}. The lowest energy optical absorption was assigned as a one-electron-transfer $Fe^{II} \rightarrow Pt^{IV}$ IVCT transition, which was consistent with electrochemical mea-

Table 3. IVCT Parameters for $[Pt(NH_3)_4]_2[(NC)_5M-CN-Pt(NH_3)_4-NC-Fe(CN)_5]$ Analogues[137]

M	ν_{max} ($\times 10^{-3}$ cm^{-1} (nm))	ϵ_{max} (M^{-1} cm^{-1})	$\Delta\nu_{1/2}$ (cm^{-1})	λ ($\times 10^{-3}$ cm^{-1})	ΔE ($\times 10^{-3}$ cm^{-1})	α
Fe	23.6 (424)	2365	7200	16.33	10.60	0.03
Ru	28.2 (354)	760	8200	16.67	14.90	0.02
Os	26.3 (380)	1700	7100	17.03	12.65	0.02

surements which revealed a single redox event assigned to simultaneous oxidation of the two noninteracting Fe centers. The one-electron nature of the IVCT process was later confirmed by Lewis and co-workers,[141] who reported the first application of pressure-tuning spectroscopy (PTS) to the determination of the one- or two-electron multiplicity of an IVCT transition. In agreement with the report of Bocarsly and co-workers,[138] analysis of the IVCT band indicated the formation of the intermediate $[Fe^{II}-Pt^{III}-Fe^{II}]$ species, as opposed to a species arising from a simultaneous two-electron-transfer reaction.[141] No further reports on the application of PTS to the analysis of IVCT in higher nuclearity complexes have appeared.

As demonstrated previously for related dinuclear cyano-bridged complexes,[93] systematic modulation of the IVCT properties of the trinuclear assemblies is achievable by varying the solvation environment of the complex. A correlation was observed between the IVCT energy and the semiempirical Gutmann acceptor number (AN) for $[(CN)_5Fe^{II}-CN-Pt^{IV}(en)_2-NC-Fe^{II}(CN)_5]^{4-}$.[134,138] The solvent dependence was attributed to changes in ΔE (eq 1) due to specific hydrogen-bonding interactions between the solvent molecules and lone pairs of electrons on the cyanide moieties.

Pfennig and co-workers[137] constructed potential energy surfaces for trinuclear complexes,[138,141] and the Hush model was also found to be appropriate for the theoretical treatment of IVCT in trinuclear systems which exhibit weak electronic coupling between the chromophoric units.

Attempts to exploit the multiphoton capabilities of these compounds have afforded the ligand-bridged hexanuclear complexes consisting of two cyano-bridged triads $[(NC)_5Fe^{II}-CN-Pt^{IV}(NH_3)_3L-NC-Fe^{II}(CN)_5]^{4-}$, where the bridging ligand L is 4,4′-bpy, **I**, or 3,3′-dimethyl-4,4′-bipyridine, **II** (Figure 9).[142]

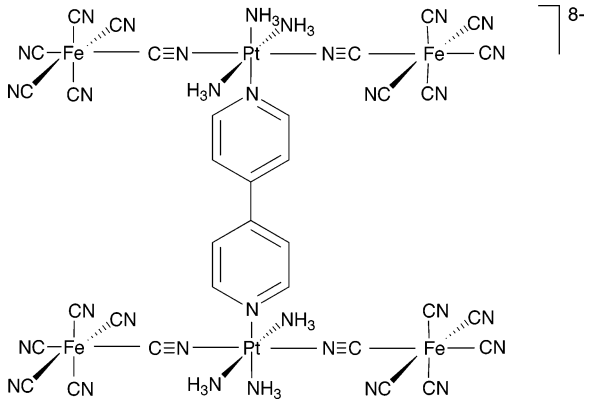

Figure 9. Proposed structure of complex **I**. Complex **II** contains methyl groups in the 3,3′-positions of the bridging ligand.[142]

Both complexes were characterized by a broad $Fe^{II} \rightarrow Pt^{IV}$ IVCT band at 23 755 cm^{-1} (421 nm; $\epsilon_{max} = 4230$ M^{-1} cm^{-1} and $\Delta\nu_{1/2} = 7400$ cm^{-1} for L = 4,4′-bpy, and $\epsilon_{max} = 4240$ M^{-1} cm^{-1} and $\Delta\nu_{1/2} = 7600$ cm^{-1} for L = 3,3′-dimethyl-4,4′-bipyridine). The integrated intensities of the IVCT manifolds were approximately twice those for the trinuclear congener $[(NC)_5Fe^{II}-CN-Pt^{IV}(NH_3)_4-NC-Fe^{II}(CN)_5]^{4-}$ {which exhibited an IVCT maximum at 23 585 cm^{-1} (424 nm; $\epsilon_{max} = 2360$ M^{-1} cm^{-1} and $\Delta\nu_{1/2} = 7200$ cm^{-1})}, which was suggestive of the additive strength of the $Fe^{II}-Pt^{IV}$ oscillator in these complexes. Since the ligand field strengths and internuclear separations of the two bridges are comparable, the different electrochemical and spectroscopic properties between the two mixed-valence complexes were attributed to different degrees of electronic coupling due to the bridging ligands. The steric hindrance of the methyl groups precludes the 3,3′-dimethyl-4,4′-bipyridine bridge from achieving a coplanar arrangement of the pyridyl rings: accordingly, the electronic interaction of the Pt^{IV} centers is comparatively weaker than that in the unsubstituted analogue, where the pyridyl rings may rotate freely and π-conjugation across the bridge is facilitated as the torsional angle approaches zero. Resonance Raman and femtosecond pump−probe experiments supported a longer excited-state lifetime of **I** versus **II**.

Electrochemically, **I** and **II** are characterized by a single redox couple corresponding to the Fe unit at 0.53 and 0.55 V vs SCE for **I** and **II**, respectively (the trinuclear complex itself exhibits a redox process at 0.55 V). A $Pt^{IV/II}$ redox couple was not observed since the electron transfer is kinetically slow due to the large reorganizational energy barrier associated with the change in geometry from square planar to octahedral accompanying the oxidation. For **I**, the cathodic redox potential is rationalized on the basis that the Pt^{IV} species is withdrawing slightly less electron density than is the case in **II** due to electronic communication across the bridge. For **II**, the Fe potentials in the tri- and hexanuclear complexes are identical due to the lack of electron coupling across the 4,4′-bpy ligands.

2.3. Molecular Chains and Wires Based on the 1,1′-Dicyanoferrocene Ligand

The weak electronic interaction between the central ferrocene moiety and the terminal ruthenium atoms resulted in comparable electrochemical and IVCT properties of the mixed-valence species derived from the trinuclear complex $[(NH_3)_5Ru-NC-Fc-CN-Ru(NH_3)_5]^{4+}$ (Fc = ferrocene; Figure 10) with those of its dinuclear congener $[(NH_3)_5Ru-NC-Fc-CN]^{2+}$.[92]

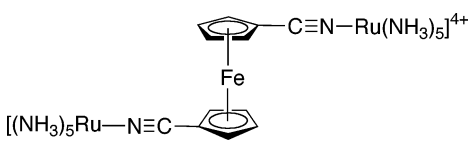

Figure 10. $[(NH_3)_5Ru-NC-Fc\text{-}CN-Ru(NH_3)_5]^{4+}$.[92]

The energy and bandwidth of the IVCT transition for the doubly-oxidized trinuclear ion $[(NH_3)_5Ru^{III}-NC-Fc-CN-Ru^{III}(NH_3)_5]^{6+}$ {12 220 cm^{-1} (818 nm), $\Delta\nu_{1/2} = 6500$ cm^{-1} in CH_3CN} were comparable with those of the analogous dinuclear species {11 900 cm^{-1} (840 nm), $\Delta\nu_{1/2} \approx 6500$ cm^{-1}}, while the intensity of the IVCT band in the trinuclear species was approximately double that of the dinuclear complex. However, the analysis was severely com-

plicated by the comproportionation equilibrium, and approximations only for the IVCT parameters were obtained. A doubly-degenerate IVCT transition was inferred for the trinuclear species, corresponding to the two equivalent IVCT transitions:

$$[(NH_3)_5Ru^{III}-NC-Fc-CN-Ru^{III}(NH_3)_5]^{6+} \xrightarrow{h\nu} [(NH_3)_5Ru^{II}-NC-Fc^{+}-CN-Ru^{III}(NH_3)_5]^{6+*}$$

$$[(NH_3)_5Ru^{III}-NC-Fc-CN-Ru^{III}(NH_3)_5]^{6+} \xrightarrow{h\nu} [(NH_3)_5Ru^{III}-NC-Fc^{+}-CN-Ru^{II}(NH_3)_5]^{6+*}$$

Electrochemical measurements revealed the presence of two closely-spaced redox processes which were attributed to oxidation of the terminal ruthenium atoms. A comproportionation constant, K_c, of 10 was thus determined, which was close to the statistical value of 4 [143] and indicative of the negligible contribution of electronic delocalization to the redox potential difference, ΔE_{ox}, between the metal centers.[144] No evidence was found for end-to-end interaction in the mono-oxidized mixed-valence species.

2.4. Consequences of Geometric and Linkage Isomerism on the IVCT Properties of [M(μ-CN)M′(μ-CN)M] Chains

Cyano-bridged coordination complexes comprising linear arrays of $(M-CN)_n$ have attracted considerable attention as systematic probes for the factors which govern long-range (i.e. *remote*) metal−metal interactions.[93] IVCT studies have focused predominantly on symmetrical trinuclear complexes of the types $M(CN-M')_2$ or $M(NC-M')_2$, as the lability of many cyanide-containing complexes has hindered attempts to prepare and unambiguously characterize tetranuclear and higher nuclearity assemblies.[93] Two notable exceptions are the crystallographically-characterized tetranuclear complexes $[Cp(dppe)Fe-CN\{Fe_2(salen)_2\}NC-Fe(dppe)Cp]^{2+}$ [149] {H_2salen = *N*,*N*′-bis(salicylidene)ethane-1,2-diamine; Cp = cyclopentadienyl anion; dppe = 1,2-bis(diphenylphosphine)-ethane} and a nearly linear tetranuclear complex comprising the [Cp(dppe)Fe−CN−MnPc−O−PcMn−NC−Fe(dppe)Cp] backbone (Pc^{2-} = phthalocyaninato anion).[150]

Despite the rarity of examples of tetranuclear complexes in which IVCT has been probed, comparisons between trinuclear species and their dinuclear M−CN−M′ analogues have furnished extensive information on several fundamental aspects regarding intermetallic coupling in cyano-bridged species. This includes the influence of bridging ligand orientation (i.e. *cis* or *trans* orientation of bridging cyanide ligands), cyanide−isocyanide linkage isomerism, the identity and coordination environment of the terminal metal units, and the one- or two-electron nature of the IVCT transitions in trinuclear cyano-bridged assemblies.[93,149,151−154]

Richardson and co-workers[151] reported the first investigation of two isomeric trinuclear complexes differing only in the *cis* or *trans* arrangement of the cyanide bridges at the central metal. The effect of the relative orientation of the two terminal metal centers was addressed through complexes comprising central *cis*- and *trans*-configured platinum(II) in trinuclear arrays incorporating Fe(dppe)Cp or $Ru(PPh_3)_2Cp$ terminal units.[151] The structural integrity of the square planar platinum center was particularly attractive in this regard, as its inertness to redox changes and ligand substitution permitted an investigation of the influence of *cis*−*trans* and linkage isomerism on the IVCT properties.

Addition of 1 equiv of chemical oxidant to *trans*-$[Fe^{III}-NC-Pt(L)_2-CN-Fe^{II}]^{3+/+}$ (L = py, CN^-) and *trans*-$[Fe^{III}-NC-Pt(L)_2-CN-Ru^{II}]^{3+/+}$ yielded a single IVCT band in each case, which vanished upon further oxidation of the second terminal unit. The Pt^{II} center is inert to photoinduced oxidation by IVCT, so that the band was assigned as a *remote* $Fe^{II} \rightarrow Fe^{III}$ IVCT. An analogous band was absent in the *cis*-configured complex *cis*-[Fe−NC−Pt(bpy)−CN−Fe]$^{3+}$. Investigations of the mixed-valence forms of *trans*-$[Fe-CN-Pt(py)_2-NC-Fe]^{3+}$ and *cis*-[Fe−CN−Pt(bpy)−NC−Fe]$^{3+}$ were precluded as the visible and NIR regions were obscured by the absorption features of the chemical oxidant. Presumably, spectroelectrochemical generation of the species may be employed, but these experiments were not pursued in this case.

Evidence for *remote* IVCT transitions was provided by the splitting (60−120 mV) of the redox waves associated with oxidation of the external metal centers (separated by ca. 10 Å) in *trans*-$[Fe-CN-Pt(py)_2-NC-Fe]^{3+}$, *trans*-$[Fe-NC-Pt(L)_2-CN-Fe]^{3+/+}$ (L = py, CN^-), and *trans*-$[Ru-NC-Pt(CN)_2-CN-Ru]^+$, where the first oxidation process occurs at the terminal metal center which is N-bound to the bridging cyanide. By contrast, all *cis*-configured complexes exhibited simultaneous two-electron oxidation of the external metal centers (separated by ca. 7 Å). The small magnitudes of the delocalization parameters (α^2) for the *remote* transitions according to Hush theory (eq 5)[28,29,34] were consistent with a Class II assignment for the mixed-valence species (Table 4). IVCT solvatochromism measurements for *trans*-$[Fe-NC-Pt(CN)_2-CN-Fe]^+$ suggested that the energy of the transition was almost entirely dependent on the reorganizational energy, λ.

The important finding from the comparison of isomeric *trans*- and *cis*-configured complexes was the enhanced remote interactions in linear (as opposed to angular) arrangements of M−CN units. Indeed, the effectiveness of the *trans* arrangement of bridging cyanide moieties in promoting long-range electron transfer was further borne out through the electrochemical studies of a tetranuclear complex comprising the nearly linear [Cp(dppe)Fe−CN−MnPc−O−PcMn−NC−Fe(dppe)Cp] backbone.[150] Two distinct Fe^{II}/Fe^{III} redox couples were observed[93,150] corresponding to successive oxidation of the terminal FeCp(dppe) units. The 0.17 V separation of the waves (3:1 benzene/acetonitrile) was indicative of a moderately-strong electronic interaction between the Fe centers separated by 13.2 Å. Attempts to probe the potential Fe^{II}/Fe^{III} mixed-valence species were not pursued.

Preparative efforts were thus focused on building blocks that allow only a *trans* arrangement of cyanide bridges at the central metal center. This was achieved by the incorporation of the tetradentate ligands salen {H_2salen = *N*,*N*′-bis-(salicylidene)ethane-1,2-diamine} and its bis(methoxy)-substituted analogue valen (Figure 11), which ensure square-planar metal coordination at the central metal ions in a series of trinuclear complexes $[(L)_2Fe_2\{(\mu\text{-}NC)Fe(L')_2Cp\}_2]^{2+}$ {L = salen or valen; $(L')_2 = (CO)_2$, dppe, or $(PPh_3)_2$}.[149]

The visible spectra of the trinuclear species were dominated by intense ligand-to-metal charge transfer (LMCT) absorptions of the (salen)Fe^{III} units. For the trinuclear species comprising the $Fe(CO)_2Cp$ terminal units, discernible IVCT bands were not observed; however, their appearance was likely to be masked by the intense LMCT transitions. For

Table 4. IVCT Parameters for M(μ-CN)M′(μ-CN)M″ Chains Comprising Terminal $Fe^{II/III}$(dppe)Cp and $Ru^{II/III}(PPh_3)_2Cp$ (in CH_2Cl_2)

backbone	origin of IVCT	ν_{max} (nm)	ν_{max} (cm^{-1})	ϵ_{max} (M^{-1} cm^{-1})	$\Delta\nu_{1/2}$(obs) (cm^{-1})	$\Delta\nu_{1/2}$(calc)[d] (cm^{-1})	α^{2} [d]	λ[d] (cm^{-1})	ref
trans-Fe^{III}−CN−$Pt^{II}(py)_2$−NC−Fe^{II}	*e*								151
cis-Fe^{III}−CN−Pt^{II}(bpy)−NC−Fe^{II}	*e*								
cis-Fe^{III}−CN−Pt^{II}(phen)−NC−Fe^{II}									
trans-Fe^{III}−NC−$Pt^{II}(py)_2$−CN−Fe^{II}	$Fe^{II} \rightarrow Fe^{III}$ (1e$^-$)	1310	7620		5200	4050	0.0008	7140	
cis-Fe^{III}−NC−Pt^{II}(bpy)−CN−Fe^{II}	no IVCT								
trans-Fe^{III}−NC−$Pt^{II}(CN)_2$−CN−Fe^{II}		1560	6410		4720	3560	0.0010	5520	
trans-Ru^{III}−NC−$Pt^{II}(CN)_2$−CN−Ru^{II}									
trans-Fe^{III}−NC−$Pt^{II}(CN)_2$−CN−Ru^{II}		750	13300		*b*	4300	0.0004	8200	
trans-Fe^{III}−CN−$Pt(py)_2$−NC−Fe^{II} [a]									
$PcFe^{III}$−$(NC-Fe^{II})_2$	$Fe^{II} \rightarrow Fe^{III}$ (2e$^-$)	1290	7730	5370	3190	1910	0.019	1570	152
Fe^{II}−CN−Fe^{III}Pc−CN−Fe^{II}	$Fe^{II} \rightarrow Fe^{III}$ (1e$^-$)	1300	7690						
	$Fe^{II} \rightarrow Fe^{III}$ (1e$^-$)	2150	4650						
$PcFe^{III}$−$(CN-Fe)_2$	$Fe^{II} \rightarrow Fe^{III}$ (2e$^-$)	2250	4440	8030	2780	1760	0.043	1350	
$PcFe^{III}$−$(NC-Ru^{II})_2$	$Ru^{II} \rightarrow Fe^{III}$ (2e$^-$)	880[c]	11360[c]	4430					
Ru^{II}−CN−Fe^{III}Pc−CN−Ru^{II}	$Ru^{II} \rightarrow Fe^{III}$ (1e$^-$)	930	10750	2150					
	$Ru^{II} \rightarrow Fe^{III}$ (1e$^-$)	1116	8960	2660					
Fe^{II}−CN−Fe^{III}Pc−CN−Ru^{II}	coincident $Ru^{II} \rightarrow Fe^{III}$ (1e$^-$) and $Fe^{II} \rightarrow Fe^{III}$ (1e$^-$)	1320	7560	3260					
Ru^{II}−CN−Fe^{III}Pc−CN−Fe^{II}	$Ru^{II} \rightarrow Fe^{III}$ (1e$^-$)	890[c]	11240[c]	1330, 6710					
	$Fe^{II} \rightarrow Fe^{III}$ (1e$^-$)	2200	4550						
(salen)Fe^{III}−$(NC-Fe^{II})$ [f]	$Fe^{II} \rightarrow Fe^{III}$ (2e$^-$)	630		3950					152, 154
trans-Fe^{III}−NC−$Ru^{II}(CN)_2(L)_2$−CN−Fe^{II} [f]	$Fe_t^{II} \rightarrow Fe_t^{III}$ (1e$^-$)	980		2600	~6500		~0.008		
L = pyridine									
L = 4-methylpyridine		990		2800					
L = 4-ethylpyridine		970		3600					

[a] Terminal metal units are $Fe^{II/III}(CN)_5$. [b] Unaccessible, as the IVCT band appeared as a shoulder only on a higher energy absorption. [c] Shoulder. [d] $\Delta\nu_{1/2}$(obs) is the observed bandwidth, and $\Delta\nu_{1/2}$(calc) is the bandwidth calculated from eq 3. The delocalization parameter (α^2) was calculated using $r = 5$ and 10 Å for Fe^{III}Pc- and Pt^{II}-centered species, respectively. [e] Investigation precluded due to interference with the absorption features of the chemical oxidant. [f] Terminal metal units are $Fe^{II/III}$Cp(dppe).

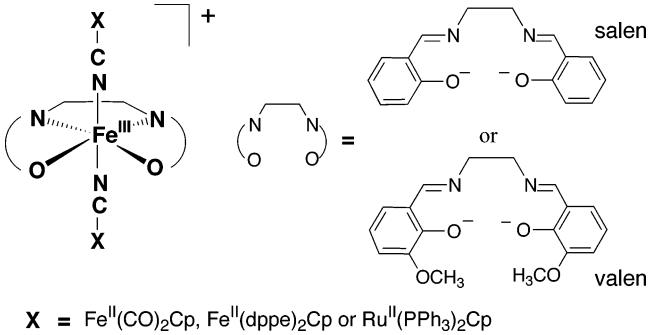

X = $Fe^{II}(CO)_2Cp$, $Fe^{II}(dppe)_2Cp$ or $Ru^{II}(PPh_3)_2Cp$

Figure 11. Schematic diagram of the trinuclear complexes $[(L)_2Fe_2\{(\mu\text{-NC})Fe(L')_2Cp\}_2]^{2+}$ {L = salen or valen; $(L')_2 = (CO)_2$, dppe, or $(PPh_3)_2$}.[149]

the complexes incorporating $Fe(dppe)_2Cp$ and $Ru(PPh_3)_2Cp$ units, weak shoulders extending into the NIR region and overlapped with the intense LMCT transitions in the visible region were assigned as two-electron IVCT transitions from the terminal Fe^{II} or Ru^{II} centers to the central Fe^{III}. The band parameters were only determinable for the dppe-containing complex {ν_{max} = 15 870 cm^{-1} (630 nm); ϵ_{max} = 3950 M^{-1} cm^{-1}}. Spectral deconvolution—which may have aided in the determination of the band parameters—was not pursued. The energy of the IVCT band for the trinuclear $Fe(dppe)_2Cp$ complex was higher than that of its dinuclear counterpart $[(salen)Fe(\mu\text{-NC})Fe(dppe)_2Cp]^{2+}$. Electrochemical characterization of the trinuclear complexes revealed a significant splitting of the redox processes for the two terminal centers: for example, the trinuclear $Fe(dppe)_2Cp$-containing complex exhibited three redox processes which were assigned to the $Fe^{III/II}$ reduction at −0.35 V, followed by the successive oxidation of the terminal $Fe^{III/II}$ centers at 0.46 and 0.86 V {CH_2Cl_2 vs Ag/AgCl}. The splitting of the latter redox processes was indicative of remote electronic interactions between the two outer organometallic units, separated by ca.10 Å. The preparation of the mono-oxidized mixed-valence species remained elusive, and attempts to observe the IVCT due to the remote IVCT interaction were unsuccessful.

Geiss and co-workers[152,153] subsequently reported a comprehensive systematic study of trinuclear $[M(\mu\text{-CN})FePc(\mu\text{-CN})M'']^{0/+}$ arrays comprising central Fe(II) or Fe(III) phthalocyaninato (Pc^{2-}) units with electron-rich external Fe(dppe)Cp or $Ru(PPh_3)_2Cp$ fragments: $[M'-C\equiv N-FePc-N\equiv C-M'']^{0/+}$ {M′,M″ = Cp(dppe)Fe or $Cp(PPh_3)_2Ru$}, $[M'-C\equiv N-FePc-C\equiv N-M'']^{0/+}$ {M′,M″ = Cp(dppe)Fe or $Cp(PPh_3)_2Ru$}, $[M'-N\equiv C-FePc-C\equiv N-M]^{0/+}$ {M′,M″ = Cp(dppe)Fe}, $[Cp(dppe)Fe-C\equiv N-FePc-C\equiv N-Ru(PPh_3)_2Cp]^{0/+}$, and $[Cp(PPh_3)_2Ru-C\equiv N-FePc-C\equiv N-Fe(dppe)Cp]^{0/+}$. In view of the negligible electronic interaction between the peripheral metal centers observed by Richardson and co-workers in the analogous *cis*-Pt^{II}(L)-centered arrays {L = bpy, phen (1,10-phenanthroline)},[151] the central FePc unit was selected to afford a *trans* orientation of the bridging cyanide ligands, so that the peripheral metal centers were linearly disposed. Structural isomers containing all three possible orientations of the bridging ligands for the external Fe(dppe)Cp fragments, and two possible orientations for the external $Cp(PPh_3)_2Ru$ fragments, were obtained from the synthetic procedures, while the stability of the central FePc unit in both the Fe(II) and Fe(III) oxidation states permitted the preparation of the oxidation-state isomers (i.e. mixed-valence species). The results offered a comprehensive insight into the influence of (i) CN/NC linkage isomerism, (ii) peripheral ligand identity, (iii) the oxidation state of the central Fe moiety, and (iv) metal sequence isomerism (as demonstrated for the unsymmetrical species) on the electronic communication between the external metal centers. Each trinuclear complex exhibited a redox process corresponding to oxidation of the central Fe^{II} to Fe^{III}, followed by two redox

waves attributable to the external organometallic units. The latter suggested the presence of long-range electronic interactions between the external centers (which are ~10 Å apart). However, the chemical instability of the doubly-oxidized species containing the central and terminal metal centers in the +III oxidation states precluded the experimental verification of such *remote* interactions.

In addition to the intense Q-bands and LMCT transitions observed in the UV/visible region, species containing central $Fe^{III}Pc$ units exhibited NIR bands which were assigned to short-range IVCT transitions from the external metals to Fe^{III} (Table 4). As demonstrated previously for the cyano-bridged systems of this type,[151] the energies of the IVCT bands for the external Fe(dppe)Cp or $Ru(PPh_3)_2Cp$ moieties correlate in a semiquantitative fashion with the redox properties: the $Ru(PPh_3)_2Cp$ units are more difficult to oxidize than the Fe(dppe)Cp units. Accordingly, the IVCT bands for the latter were observed in the NIR region and were more readily apparent than those for the $Ru(PPh_3)_2Cp$-containing systems, which appeared as shoulders in the visible region.

The influence of linkage isomerism on the IVCT properties was consistent with that found previously for isomeric cyanometalates:[129] for example, the IVCT band is shifted from 7730 cm^{-1} (1290 nm) in $[Fe^{II}-CN-Fe^{III}Pc-NC-Fe^{II}]^+$ to 4440 cm^{-1} (2250 nm) in $[Fe^{II}-NC-Fe^{III}Pc-CN-Fe^{II}]^+$. The IVCT process occurs at relatively lower energy in the latter case since the external Fe^{II} centers are relatively electron deficient in the configuration in which they are bound to the cyanide-C atoms rather than the cyanide-N atoms (Table 4).

The lability of the CN^- bridge and the thermodynamic preference for the isomers containing the cyanide N-bound to the central FePc units were demonstrated during the syntheses of the trinuclear complexes. The preparation of all three linkage isomers of $[(Pc)Fe\{(\mu\text{-}BL)Fe(dppe)Cp\}_2]^+$ (BL = CN^- and/or NC^-) was achieved *in situ* as their markedly different IVCT energies and intensities in their NIR spectra were recorded (Table 4). The $[(Pc)Fe\{(\mu\text{-}NC)Fe(dppe)Cp\}_2]^+$ form was the most thermodynamically preferred.[153]

Geiss and co-workers[153] have elucidated a number of subtle aspects regarding the isomerism in the cyanometalates. The unsymmetrical species $[Fe^{II}-CN-Fe^{III}Pc-CN-Fe^{II}]^+$ and $[Ru^{II}-CN-Fe^{III}Pc-CN-Ru^{II}]^+$ exhibit two IVCT bands corresponding to C-bound and N-bound external units. The CN/NC isomerism results in a coincidence of the IVCT bands for $[Fe^{II}-CN-Fe^{III}Pc-CN-Ru^{II}]^+$ when the identities of the terminal units differ, while two bands were evident for $[Ru^{II}-CN-Fe^{III}Pc-CN-Fe^{II}]^+$. Application of the Hush analysis[28,29,34] to the IVCT bands revealed a Class II classification for the species (Table 4). Interestingly, the deeply blue-colored complex $[Fe^{II}-CN-Fe^{III}Pc-NC-Fe^{II}]^+$, which represented the most thermodynamically stable of its three isomers,[153] was described as an authentic molecular representation of Prussian Blue where the IVCT band corresponds to an exchange of the oxidation states between Fe^{II} and Fe^{III}.

Subsequent efforts to probe remote IVCT transitions focused on the preparation of complexes involving a *trans*-arrangement of the bridging cyanide units at the central metal. By virtue of the inertness of the Ru^{II} octahedral coordination center, the trinuclear species *trans*-$[(py)_4Ru\{(\mu\text{-}CN)Fe(dppe)Cp\}_2]^{2+}$ [154] was prepared utilizing the central *trans*-$[Ru(CN)_2(py)_4]$ (py = pyridine, 4-methylpyridine, or 4-ethylpyridine) fragment. In each case, two redox processes were observed for the terminal Cp(dppe)Fe units, which were indicative of remote metal−metal interactions. The ~110 mV separation between the two processes was sufficient to enable the preparation and solid-state isolation of the stable mixed-valence complex $[Cp(dppe)Fe-NC-Ru(py)_4-CN-Fe(dppe)Cp]^{3+}$ (using chemical oxidation with 1 equiv of ferrocinium hexafluorophosphate). This rare example of the solid-state stability of a mixed-valence species contrasts the more frequent situation where *in situ* spectroscopic techniques are required for the generation and observation of such species.

A broad NIR band which appeared at higher energy than those observed previously in the related $Pt^{II}(L)_2$- [151] and FePc-centered[152,153] complexes was assigned to a long-range $Fe^{II} \rightarrow Fe^{III}$ IVCT transition. Application of the Hush formalism[28,29,34] utilizing approximate estimates for the band parameters $\{\nu_{max} = 10\,000\ cm^{-1}$ (1000 nm), $\Delta\nu_{1/2} = 6500\ cm^{-1}$, and the values of ϵ_{max} provided in Table 4$\}$ yielded $H_{ab} \approx 900\ cm^{-1}$ and an electron delocalization parameter (α) on the order of 1%, suggesting a Class II assignment.[27] These values are considerably smaller than those for related dinuclear complexes in which the metal−metal interaction occurs between adjacent metal centers, but they exceed those for the trinuclear species comprising the $Fe^{II}-NC-Pt^{II}-CN-Fe^{III}$ backbone.[151] Long-range interactions are thus enhanced when an intervening low-spin central metal (Ru^{II} in this case) possesses filled d-orbitals which can facilitate them.

2.5. Molecular Squares and Clusters

Tetranuclear cluster systems of the type $[(\mu_4,\eta^4\text{-TCNQ})\{Os(PPr^i_3)_2(CO)(H)Cl\}_4]$ {designated $[(TCNQ)(Os)_4]$, where "Os" represents terminal $[Os^{II}(PPr^i_3)_2(CO)(H)Cl]$ (PPr^i = isopropyl) fragments coordinated via pendant cyanide moieties; Figure 12} have been investigated with regard to their unusual magnetic ordering phenomena.[155]

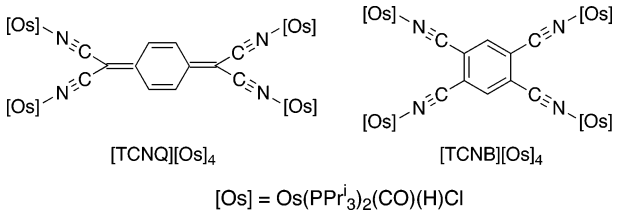

Figure 12. $[(TCNQ)(Os)_4]$ and $[(TCNB)(Os)_4]$.[155]

The electrochemistry of $[(TCNQ)(Os)_4]$ revealed a single two-electron oxidation wave corresponding to the formation of the mixed-valence dication, which was characterized by an intense IVCT transition at 8032 cm^{-1} (1245 nm; ϵ_{max} = 50 000 $M^{-1}\ cm^{-1}$) and formulated as $[(TCNQ^0)(Os^{2.5})_4]^{2+}$. The two-electron nature of the IVCT process was rationalized in terms of the existence of two electronically-uncoupled, isolated bridged $Os^{III}-Os^{II}$ subunits separated by the 2,2′-(cyclohexa-2,5-diene-1,4-diylidene) bridge.

A new class of self-assembled metallosupramolecular architectures comprising macrocyclic tetranuclear cores has emerged in recent years. These "molecular squares" are the subject of intense current interest, motivated by their potential application in nanoscale devices and molecular machinery.[156−158] However, only two reports concerning the oxidative IVCT properties of such systems have appeared: Oshio and co-workers[90,91] investigated the mixed-valence forms of the cyanide-bridged cluster molecules $[Fe^{II}_2M^{II}_2(\mu\text{-}CN)_4-$

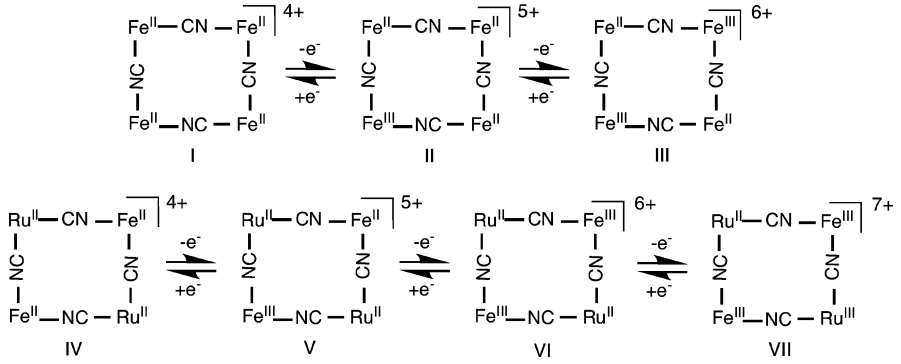

Figure 13. Schematic diagram of the mixed-valence molecular squares $[Fe_2M_2(\mu\text{-}CN)_4(bpy)_8]^{n+}$ (M = Fe, Ru).[90,91]

$(bpy)_8]^{4+}$ (M = Fe, Ru), where the cyanide moieties bridge four *cis*-configured metal centers, giving rise to chiral squares (which have been characterized crystallographically) possessing either ΛΛΛΛ or ΔΔΔΔ configurations.

$[Fe^{II}_4(\mu\text{-}CN)_4(bpy)_8]^{4+}$ {abbreviated [Fe(CN)Fe(NC)Fe(CN)Fe(NC)]$^{n+}$} exhibited two quasi-reversible one-electron redox processes corresponding to oxidation of the N-bound Fe^{II} centers (0.67 and 0.86 V vs SSCE/CH_3CN) followed by an irreversible process (1.37 V) corresponding to oxidation of a C-bound center, according to the sequence shown in **I**/**II**/**III** in Figure 13. The d orbitals of the N-bound Fe^{II} ions are destabilized, while the C-bound ions are stabilized by π-back-donation, so that the former undergo more facile oxidation. Formation of the mono-oxidized +5 mixed-valence species (**I**) was manifested by the appearance of a new band in the NIR region, which gained intensity following a further electron oxidation to the +6 mixed-valence state (**II**). The band {7246 cm^{-1} (1380 nm), ϵ_{max} = 8600 M^{-1} cm^{-1}; −35 °C, CH_3CN} was assigned as an IVCT transition from the C-bound Fe^{II} units to the *adjacent* N-bound Fe^{III} units. The pertinent delocalization parameters were obtained from Hush theory,[28,29,34] based on ϵ_{max} = 4300 M^{-1} cm^{-1} (two chromophores), ν_{max} = 7250 cm^{-1} (1380 nm), and $\Delta\nu_{1/2}$ = 1450 cm^{-1}, which yielded H_{ab} = 870 cm^{-1} and α^2 = 0.014 (or H_{ab} = 1230 cm^{-1} and α^2 = 0.028 by disregarding the double degeneracy of the transition), consistent with the Class II classification of the mixed-valence system. Presumably, investigations on subsequent mixed-valence states were precluded on the basis of the irreversibility of the associated electrochemical processes.

The above studies were subsequently elaborated by investigation of the heteronuclear molecular square, $[Ru^{II}_2Fe^{II}_2(\mu\text{-}CN)_4(bpy)_8]^{4+}$ {abbreviated $[Ru^{II}_2Fe^{II}_2]^{n+}$, where the Fe^{II} and Ru^{II} centers are N-bound and C-bound, respectively, to the bridging cyanide units}.[90,91] All four accessible oxidation states of the square were realized electrochemically (0.69, 0.94, 1.42, and 1.70 V vs SSCE; CH_3CN), which permitted an investigation of two of the three mixed-valence states (**IV** and **V** in Figure 13). One-electron electrochemical oxidation to the mixed-valence species $[Ru^{II}_2Fe^{II}Fe^{III}]^{5+}$ (**V**) was accompanied by the appearance of a new band in the NIR region {4255 cm^{-1} (2350 nm), ϵ_{max} = 5500 M^{-1} cm^{-1}; −35 °C, CH_3CN}, while complete two-electron oxidation to $[Ru^{II}_2Fe^{III}_2]^{6+}$ (**VI**) resulted in the formation of a new band at 7246 cm^{-1} (1380 nm; ϵ_{max} = 8600 M^{-1} cm^{-1}). The bands were subsequently assigned as IVCT transitions originating from the Fe^{II} to Fe^{III} site in **V**, and from the Ru^{II} to Fe^{III} sites in **VI**. Analysis of the IVCT transitions according to the Hush model[28,29,34] yielded H_{ab} and α^2 values of 1090 cm^{-1} and 0.065 for **V**, and 1990 cm^{-1} and 0.096 for **VI**. While the magnitude of delocalization in the heteronuclear mixed-valence squares **V** and **VI** is greater than that in their homonuclear analogues (**I** and **II**), the parameters are similarly indicative of a Class II assignment for the mixed-valence species.[27]

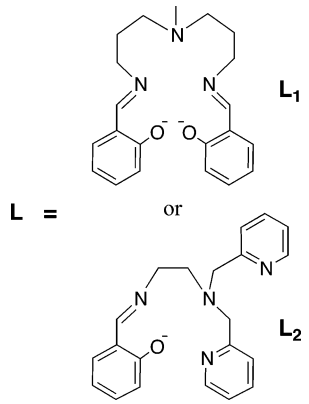

Figure 14. Peripheral ligands employed by Rogez *et al.*[159]

2.6. Prussian Blue Mimics

Prussian Blue is generally represented by the formulation $Fe^{II}Fe^{III}(CN)_6.xH_2O$, and it contains cyanide C-bonded to Fe^{II} and N-bonded to Fe^{III}.[93] It exhibits an IVCT transition at 14 700 cm^{-1} (680 nm). Attempts to prepare structural models and mimics for Prussian Blue have focused on the preparation of mixed-valence complexes comprising Fe^{II} and Fe^{III}. While organic ligands are generally considered to play an innocent role in such polynuclear complexes, Rogez and coworkers[159] demonstrated the ability to tune the energy of the Fe^{II} to Fe^{III} charge-transfer excited state through variation in the peripheral ligand (L_1 or L_2, Figure 14) in the cyanide-bridged polynuclear complexes $[Fe^{II}(CNFe^{III}L)_6]^{n+}$. The bands for the heptanuclear complexes were almost identical to those for their mononuclear analogues, with the appearance of an additional band in the region 10 000−22 000 cm^{-1} (1000−455 nm) which was assigned as an IVCT transition from the central low-spin Fe^{II} to the peripheral high-spin Fe^{III} ions. The band occurs at lower energy when the Fe^{III} chelating ligand is L_2, consistent with the more easily reducible nature of this complex. An additional low-energy band was not observed in the spectrum of the mixed-valence tetranuclear complex $[Co^{III}\{CNFe^{III}(L_1)\}_3]^{3+}$, where Fe^{II} was replaced by isoelectronic low-spin Co^{III}. This was considered indirect confirmation that the additional transitions in the spectra of the homonuclear iron complexes are indeed due to $Fe^{II} \rightarrow Fe^{III}$ IVCT.

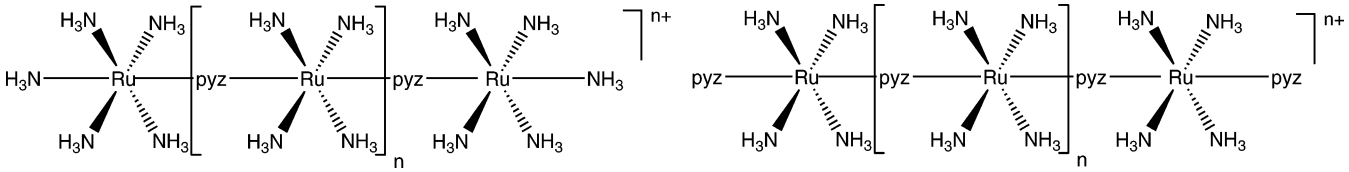

Figure 15. Pyrazine-bridged species based on *trans*-tetraammineruthenium as the linking metal unit, used in the studies by von Kameke, Tom and Taube.[106]

3. Pyrazine-Bridged Species

In early work, Meyer *et al.*[107] investigated a series of trinuclear complexes $[(NH_3)_5Ru(L)Ru(bpy)_2(L)Ru(NH_3)_5]^{6+}$ (designated [2,2,2]; L = pyrazine, 4,4′-bipyridine, or other dibasic N-heterocyclic ligand bridges) and their redox properties. In the mixed-valence 8+ ion, the sites of oxidation were isolated on the pentaammine termini ([3,2,3]). The IVCT bands were similar in energy and intensity for the +7 and +8 species, which indicated there was no long-range interaction between the terminal pentaammine centers in the +7 case. The mixed-valence species appear localized in nature, and the properties of the IVCT bands were treated in terms of the Hush analysis.[28,29,34] The dependence of ν_{max} on the identity of the bridge in the series indicates that ν_{max} is distance dependent. The authors recognized the possibility of oxidation isomerism {i.e. [3,3,2] as distinct from [3,2,3]} in these species, but there was no evidence for two transitions.

Another early study by von Kameke, Tom, and Taube[106] investigated two series of pyazine-bridged complexes with *trans*-tetraammineruthenium as the linking metal unit: in the first, NH_3 occupied the terminal *trans* positions ($n = 1-4$) while, in the other series, the terminal *trans* ligand was pyrazine ($n = 0-2$; Figure 15). For the NH_3-terminal species, the terminal Ru center was oxidized first. Only in the trinuclear case ($n = 1$) was there NIR evidence for end-to-end electron transfer in the one-electron oxidized species, where a comproportionation constant of 70—considerably above the statistical value of 4—was measured for the equilibrium [3,2,3] + [2,2,2] ⇌ 2[3,3,3]. For the 7+ form of this trinuclear species, the IVCT was unsymmetrical and was sensitive to solvent, implying it was a composite band. The IVCT band for the 8+ form was symmetrical.

The situation in the pyz-capped complexes was complicated by protonation of the pyz ligands, but IVCT was observed in the partially-oxidized species.

A study of the trinuclear complex *trans*-$[\{Ru(NH_3)_5(pyz)\}_2Ru(NH_3)_4]^{m+}$ ($m = 6-9$) was undertaken by Denti *et al.*[103] Electrochemistry showed three distinct oxidations: chemical oxidation (using Ce^{4+}) in combination with spectral measurements showed the appearance of an IVCT absorption at 5646 cm^{-1} (1770 nm) for the 7+ ion, which disappeared with the appearance of a new peak at 9680 cm^{-1} (1033 nm) for the 8+ ion.

4. Polyferrocences

High molecular weight polymers ($M_n > 10\,000$) consisting of a backbone of conjugated ferrocenyl {Fc = (η^5-$C_5H_4^-$)-Fe(η^5-$C_5H_4^-$)} units have been the subject of extensive research efforts since the 1960s through attempts to exploit their attractive electronic and magnetic features. A recent (2001) review of the electrochemical and IVCT properties of di-, tri-, and tetranuclear and higher nuclearity polyferrocenes by Nishihara[160] has provided an excellent and detailed account of the IVCT trends among series of linear polyferrocenes, and we therefore refer the reader to this article. Accordingly, our present discussion is restricted to reports on tri- and tetranuclearity polyferrocenes that have appeared since 2001, as well as selected pertinent examples of prior work which were not addressed in that earlier review.

4.1. Linear Polyferrocenes

Work by Meyer *et al.*[161] investigated bi-, 1,1′-tri-, and 1,1′-tetraferrocenes (Figure 16) using electrochemical techniques.

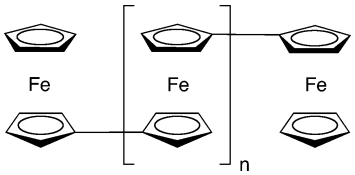

Figure 16. 1,1′-Polyferrocene ions studied by Brown *et al.*[161]

In all cases, the ferrocene groups were oxidizable to ferricinium at distinct potentials, implying localized Fe^{II} and Fe^{III} centers. Partial oxidation of the trinuclear and tetranuclear species gave discrete mixed-valence ions which exhibit IVCT transitions in the NIR region of the spectrum 5882−5000 cm^{-1} (~1700−2000 nm). The increase in the nuclearity of the dinuclear, trinuclear, and tetranuclear complexes was apparent in the relative energies and intensities of the IVCT transitions. The trinuclear species exhibits two mixed-valence states for the one- and two-electron oxidized systems, where ν_{max} and ϵ_{max} are 5020 cm^{-1} (1990 nm) and 1560 M^{-1} cm^{-1} in the former case, and 5990 cm^{-1} (1670 nm) and 1080 M^{-1} cm^{-1} in the latter. The similar IVCT energies for the mono-oxidized trinuclear species with its dinuclear congener {ν_{max} and ϵ_{max} are 5260 cm^{-1} (1900 nm) and 760 M^{-1} cm^{-1}} support a localized classification for the trinuclear system, where the presence of two donor Ru^{II} centers and a single Ru^{III} center is reflected in the intensity enhancement of a factor of two in the IVCT manifold over the dinuclear case. For the doubly-oxidized trinuclear system, an additional ΔE_0 component must be accounted for in the IVCT energy, as the product of the light-induced electron transfer is an energetically-unfavorable oxidation state isomer, i.e., $Fc^+-Fc-Fc^+ \rightarrow (Fc^+-Fc^+-Fc)^*$. The transition energy is blue-shifted as a result and of lower intensity relative to that of the mono-oxidized state due to the presence of a single Ru^{II} donor. In the tetranuclear case, only the two-electron oxidized mixed-valence state was characterized {ν_{max} and ϵ_{max} are 5590 cm^{-1} (1790 nm) and 1720 M^{-1} cm^{-1}}. The energy of the transition was intermediate between that for the two-electron-oxidized trinuclear system and that for the dinuclear species, and the relative intensity of the IVCT manifold was again indicative of a localized classification.

Plenio *et al.*[162] have reported studies on ferroceneacetylene oligomers, including the trinuclear complexes shown in

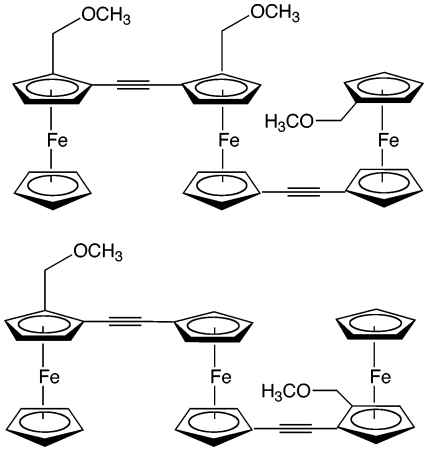

Figure 17. Symmetrical trinuclear ferrocenes, used in the study by Plenio *et al.*[162]

Figure 17: IVCT transitions were observed {7520−9524 cm^{-1} (1330−1050 nm)}, but there was no consideration of oxidation state isomers.

Nishihara *et al.*[163−165] reported a systematic investigation of the IVCT bands for the mixed-valence states for the series of oligo(1,1′-dihexylferrocene-1,1′-diyl)s (Figure 18), where

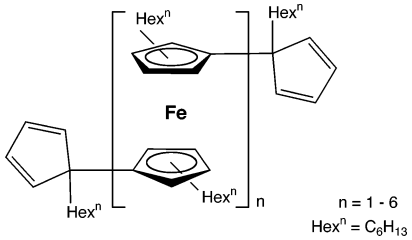

Figure 18. Oligo(1,1′-dihexylferrocene-1,1′-diyl)s.[163−165]

$n = 2-6$, generated by quantitative electrochemical or chemical oxidation (1,1′-dichloroferrocenium hexafluorophosphate in CH_2Cl_2/acetone). A broad IVCT band was observed in the NIR region {4300−6300 cm^{-1} (2325−1587 nm)} for the mixed-valence species of each oligomer from dinuclear to hexanuclear. While the possibility of multiple IVCT bands for each mixed-valence state was deemed, their experimental observation was considered unlikely due to the broadness of the NIR absorption bands, which typically extended into the mid-IR region, beyond the limit of detection. The IVCT bands were thus simulated as a single Gaussian-shaped curve for analysis. The general trend was a shift in ν_{max} to higher energy and a shift in ϵ_{max} to lower intensity with increasing oxidation state of the assembly, while ν_{max} for the first mixed-valence state (monocationic form) shifted to lower energy with an increase in the number of ferrocene units. The bandwidths of 3300−4000 cm^{-1} were comparable to those calculated from Hush theory[28] (3200−3800 cm^{-1}), consistent with a localized Class II classification for the polyferrocenes.

The shift in ν_{max} of the IVCT bands was analyzed on the basis of a "neighboring-site interaction model" in which the mixed-valence states are assumed to represent linear combinations of reduced and oxidized nuclei. The shift in ν_{max} of the IVCT band to higher energy with increasing oxidation state for a given oligomer was qualified by the consideration of the increase in energy required for the optical electron-transfer process. Accordingly, if R and O denote the unoxidized and oxidized centers, respectively, the R−O combination is attractive while the O−O combination is repulsive and thus requires greater energy for the metal−metal interaction (assuming the internuclear distance remains constant).

The product $\nu_{max}\epsilon_{max}\Delta\nu_{1/2}$ (which is proportional to H_{ab} and α) was also observed to decrease monotonically with an increase in the oxidation number for each oligomer and was higher for even-numbered, compared with odd-numbered, oligomers; however, no rationale was provided for these observations. While the simple neighboring-site interaction model afforded a qualitatively sound rationalization for the trends in the IVCT properties for the linear polyferrocenes, the concept was unable to account for the observed properties of the mixed-valence states of the oligoferrocenes, as potentially important effects on the electronic distribution such as long-range interactions and solvation effects are neglected. Nevertheless, the theoretical concept has provided a valuable "first-principles" insight into the origins of the internuclear electronic interactions in linear polymetallic assemblies.

Rulkens *et al.*[166] observed a similar shift of the IVCT band to higher energy with increasing oxidation state in their systematic investigation of three series of oligo(ferrocenyldimethylsilane)s. Spectroelectrochemical experiments on the series shown in Figure 19 revealed an IVCT absorption

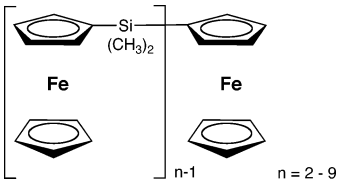

Figure 19. Oligo(ferrocenyldimethylsilane)s.[166]

in the range 9090−7410 cm^{-1} (1100−1350 nm; $\epsilon_{max} \leq 150$ M^{-1} cm^{-1}) for the partially-oxidized complexes, typical for Class II mixed-valence complexes.

Nishihara *et al.*[167] investigated the IVCT characteristics of the symmetrical and unsymmetrical linear azo-bridged ferrocene trimers, Fc—Fc′—N=N—Fc and Fc—N=N—Fc′—N=N—Fc, where Fc and Fc′ are (η^5-C_5H_5)Fe(η^5-$C_5H_4^-$) and Fe(η^5-$C_5H_4^-$)$_2$, respectively (Figure 20). The unsymmetrical

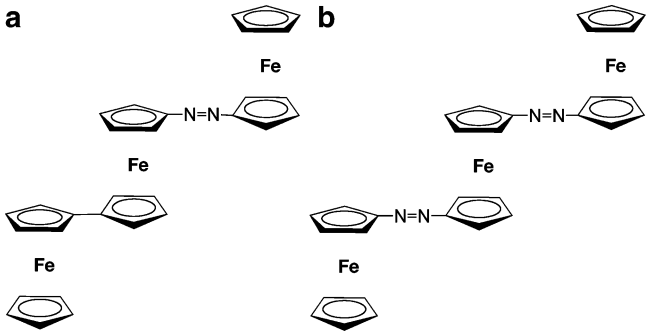

Figure 20. (a) Unsymmetrical and (b) symmetrical ferrocene trimers [Fc—Fc′—N=N—Fc] and Fc—N=N—Fc′—N=N—Fc], where Fc and Fc′ are (η^5-C_5H_5)Fe(η^5-$C_5H_4^-$) and Fe(η^5-$C_5H_4^-$)$_2$, respectively.[167]

complex exhibited three one-electron redox waves, giving rise to two mixed-valence states in which the charge distributions are approximately formulated as Fc^+—Fc′—N=N—Fc and Fc^+—Fc′—N=N—Fc^+. A single IVCT band was observed at 5625 and 7465 cm^{-1} (1778 and 1340 nm, respectively) for the mono- and dicationic mixed-valence

states, which compares with the IVCT band at 4910 cm^{-1} (2036 nm) for the dinuclear analogue.

The symmetrical complex exhibited a reversible two-electron redox process corresponding to nearly simultaneous oxidation of the terminal Fe units, followed by a one-electron process associated with the central metal. The two mixed-valence states were observed at 4905 and 6870 cm^{-1} (2039 and 1456 nm, respectively) for the mono- and dioxidized forms. The IVCT process was rationalized by a hole-transfer mechanism to explain the shift to higher energy of both the IVCT and LMCT bands in more donating solvents.

Aoki and Chen[168] proposed a theoretical method for the prediction of the redox response of linear trinuclear, tetranuclear and higher nuclearity assemblies. The authors explicitly recognized that the different redox isomers possessed various kinds of interaction energy depending on configurational arrangements. For linear trinuclear complexes, four redox states can exist when all redox sites are equivalent, as shown in Figure 21, where R and O denote a

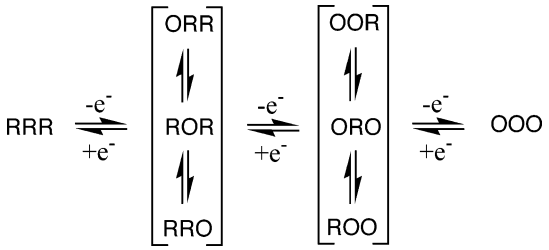

Figure 21. Chemical and electrochemical equilibrium reactions for a linear trinuclear complex, where R and O denote the reduced (unoxidized) and oxidized metal centers, respectively.

general reduced (unoxidized) and oxidized metal center, respectively. The approach was based on the treatment of the interaction between neighboring redox sites, such that the redox properties arise from combinations of the interaction energies for OR, OO, and RR.[168] The so-called "additive pair model" predicted the appearance of three redox waves for a system comprising an odd number of redox nuclei, and the appearance of four redox waves for a system comprising an even number of redox nuclei, with the number of waves converging to two as the number of nuclei approached infinity. The appearance of fewer peaks than redox centers (when $n \geq 5$) was ascribed to energetically-degenerate mixed-valence states.

The linear polyferrocenes have provided an important experimental basis to test and verify these theoretical predictions. The electrochemical properties of the series of bi-, 1,1′-tri-, and 1,1′-tetraferrocenes investigated by Meyer *et al.*[161] were consistent with the prediction that the number of voltammetric waves was equivalent to the number of redox centers. However, for linear pentanuclear and higher nuclearity polyferrocenes—as well as more general trinuclear, tetranuclear and higher nuclearity species comprising ring and starburst architectures—the treatment of nearest-neighbor interactions only was shown to be invalid where delocalization was present (i.e., when the delocalization of the electron was not restricted to the pair but spread to other redox centers).

4.2. Cyclic and Starburst Polyferrocenes

Weyland and co-workers[169] have studied the systems shown in Figure 22. For the dinuclear species, the crystal structure of the one-electron oxidation product showed the

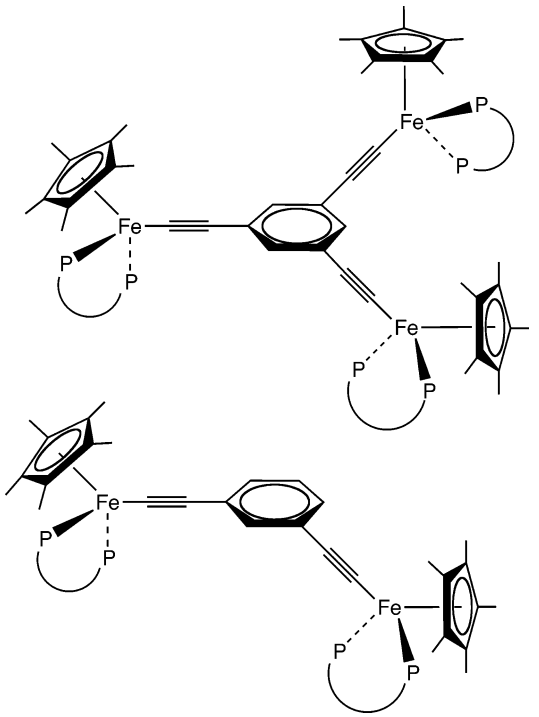

Figure 22. Two- and three-center cyclopentadienyliron complexes with *meta* connections around a phenylene ring.[169]

two Fe centers were not equivalent, a result supported by IR, Mössbauer, ESR, and UV/visible spectroscopy which also showed localization in the mixed-valence species (Class II). An IVCT absorption was observed {5290 cm^{-1} (1890 nm)} which was weakly coupled ($H_{ab} = 161$ cm^{-1}). In both cases, $\Delta\nu_{1/2}$ was close to that derived by the Hush equation,[28,29,34] assuming a symmetrical complex. For the one-electron-oxidized trinuclear species, $\nu_{max} = 5460$ cm^{-1} (1832 nm) and $H_{ab} = 143$ cm^{-1}. For the two-electron-oxidized trinuclear species, two IVCT bands were observed, which were attributed to energetically distinct transitions for the singlet and triplet states of the mixed-valence compound arising from the alternate antiparallel and parallel arrangements of the two unpaired electrons at the formally Ru^{III} sites, respectively (Figure 23). This was the first observation of

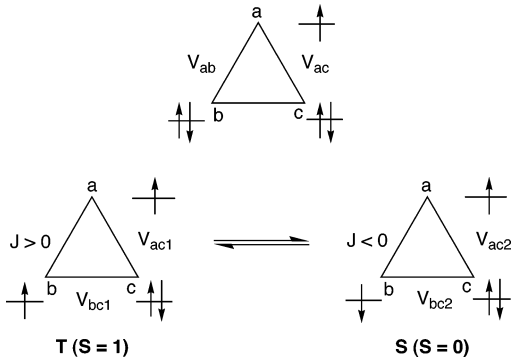

Figure 23. Spin combinations in a three-center complex.[169]

such a phenomenon in a synthetic mixed-valence system. ESR spectroscopy indicated the singlet/triplet population ratio is 25/75. In all cases, IVCT bands were obtained by deconvolution of the observed spectra to eliminate LMCT absorptions.

A recent publication has reported an electrochemical and spectral study of the series of Ru_2Fe_2 heterotetranuclear σ-acetylide complexes[170] shown in Figure 24. One-electron

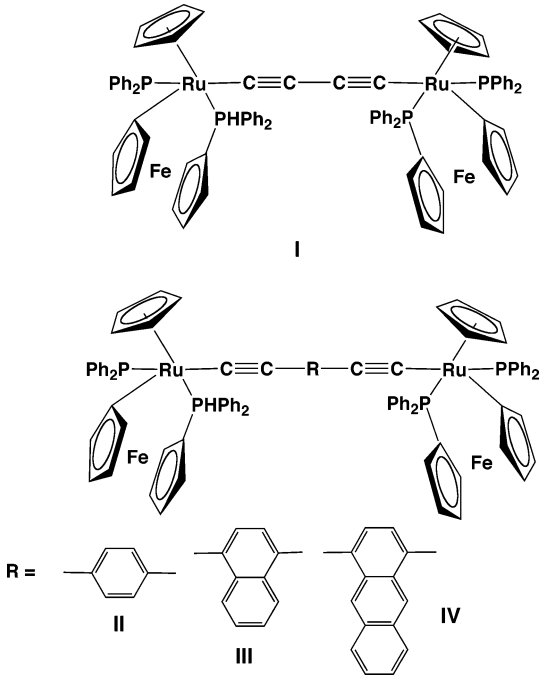

Figure 24. Ru_2Fe_2 tetranuclear σ-acetylide complexes.[170]

oxidition of **I**, **II**, and **IV** (by chemical means, using ferrocenium hexafluorophosphate) yielded $Ru^{II}Ru^{III}$ mixed-valence species. Electrochemical and visible/IR spectral studies reveal that the electronic delocalization depends on the R grouping in the bridging ligand C≡C−R−C≡C. For **I**, the comproportionation constant was $K_c = 9.74 \times 10^{10}$ (calculated from ΔE_{ox} data) and the IVCT band at 11 040 cm^{-1} (906 nm) was solvent-independent with $\epsilon_{max} = 16\,400$ M^{-1} cm^{-1}. The observed half-width of the band ($\Delta\nu_{1/2} = 3666$ cm^{-1}) was markedly narrower than that predicted (5040 cm^{-1}) on the basis of eq 3,[28,29] so this complex was assigned to the Class III regime. For compounds $\mathbf{III}^+$ and $\mathbf{IV}^+$, the IVCT bands occurred at 7622 and 9010 cm^{-1} (1312 and 1110 nm) with $\epsilon_{max} = 15\,950$ and 19 110 M^{-1} cm^{-1}, respectively, with a small solvent dependence. The measured half-widths were $\Delta\nu_{1/2} = 2786$ and 2753 cm^{-1} compared with the calculated values of 4191 and 4557 cm^{-1}, respectively. While it is clear that the coupling between these centers is still strong, they were assigned to a regime between the localized and delocalized limits.

4.3. Quantum Cellular Automata

The smallest building block of a quantum cellular automata (QCA) is a mixed-valence complex, as it consists of two "dots" containing a mobile single electron. A more versatile building block is a square containing four electronically-coupled "dots" containing two mobile electrons, and a recent paper by Jaio *et al.*[171] reports the first four-metal mixed-valence complex containing two mobile electrons in a square geometry. A schematic representation of the system [{(η^5-C_5H_5)Fe(η^5-C_5H_4)}$_4$(η^4-C_4)Co(η^5-C_5H_5)] (abbreviated **I**) is given in Figure 25. The X-ray crystal structure of the one-electron-oxidized product, $[\mathbf{I}]^+$, was determined, demonstrating the square-planar array of ferrocene moieties. An NIR IVCT band was found to be solvent-dependent, indicating Class II behavior for this mixed-valence ion. EPR confirmed the localized assignment, as did Mössbauer studies, which showed two doublets (ratio 1:3). IR ring deformations also showed a ferrocenium/ferrocene ratio of 1:3.

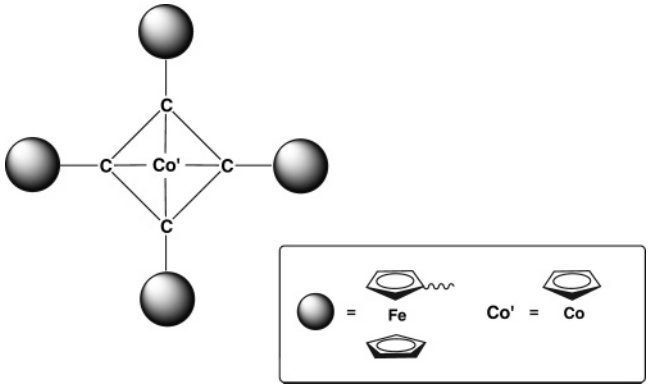

Figure 25. Schematic representation of **I**.[171]

For the two-electron-oxidized analogue ($[\mathbf{I}]^{2+}$), the IVCT transition shifted to a higher energy than that observed for $[\mathbf{I}]^+$ (solvent-independent, Class II−III), and Mössbauer (two doublets with an area ratio of 1:1), IR (ring deformations for ferrocenium/ferrocene 1:1), and magnetic susceptibility measurements (consistent with the spins of two uncoupled electrons) indicate that $[\mathbf{I}]^{2+}$ is a two-electron, two-hole mixed-valence state. There are two possible oxidation isomers for this species, but the *trans* geometry is likely to be favored electrostatically.

5. Polypyridyl Bridges

Serroni and co-workers investigated the tetranuclear complex [(bpy)$_2$Ru$_A$(μ-bpt$^-$)Ru$_C${(μ-2,3-dpp)Ru$_B$(bpy)$_2$}$_2$]$^{7+}$ containing both electron-deficient 2,3-bis(2-pyridyl)pyrazine (2,3-dpp) and electron-rich 3,5-bis(pyridin-2-yl)-1,2,4-triazolate (bpt$^-$) bridging ligands, as shown in Figure 26.[172]

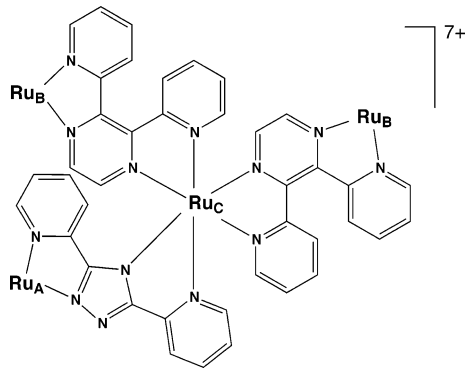

Figure 26. Tetranuclear complex [(bpy)$_2$Ru$_A$(μ-bpt)Ru$_C${(μ-2,3-dpp)Ru$_B$(bpy)$_2$}$_2$]$^{7+}$.[172]

Electrochemically, the complex exhibited two reversible redox processes at +1.09 and +1.55 V (in acetonitrile vs SCE) corresponding to a one-electron oxidation of the Ru_A center followed by two simultaneous one-electron oxidations of the Ru_B centers. Oxidation of the central Ru_C center was beyond the anodic potential window. Only the one-electron-oxidized [(bpy)$_2$Ru$_A^{III}$(μ-bpt$^-$)Ru$_C${(μ-2,3-dpp)Ru$_B$(bpy)$_2$}$_2$]$^{8+}$ mixed-valence species was characterized, and it exhibited a NIR band at 1370 nm (7300 cm^{-1}, $\epsilon_{max} = 1870$ M^{-1} cm^{-1}, $\Delta\nu_{1/2} = 3690$ cm^{-1}) which was assigned as an $Ru_C^{II} \rightarrow Ru_A^{III}$ IVCT transition. On the basis of the classical Hush analysis[28] (assuming an Ru_C-Ru_A distance of 6.18 Å), a localized classification was determined for the mixed-valence species.[172]

Haga *et al.* have synthesized the tetranuclear species [{Os(bpy)$_2$(bbbyH$_2$)}$_3$Ru]$^{6+}$,[173] where bbbyH$_2$ = 2,2′-bis-

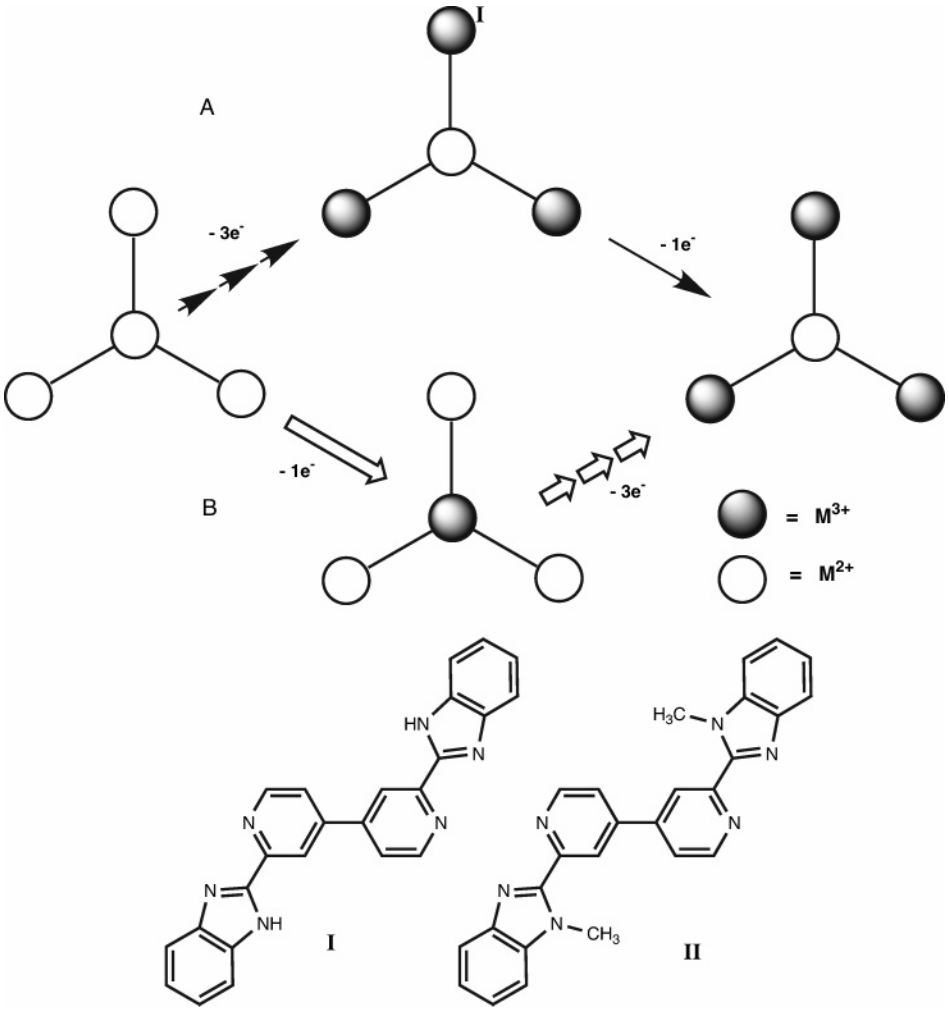

Figure 27. Bridging ligands used by Haga *et al*.,[173,174] and the two redox patterns in the ligand-bridged tetranuclear complexes.

(benzimidazol-2-yl)-4,4′-bipyridine (**I** in Figure 27), in which the oxidation pattern is dependent on whether the bridging ligand is protonated. When the bridge is deprotonated ($bbby^{2-}$), the central Ru^{II} center is oxidized first, followed by the oxidation of the three outer Os^{II} centers (pathway B in Figure 27), whereas for the nondeprotonated bridge ($bbbyH_2$), the order of oxidation is reversed (pathway A). The one-electron oxidation of the deprotonated species was achieved electrochemically, and the product showed no absorption in the NIR region. However, when the bridging ligand was protonated, three absorptions appeared in the NIR region—at 9524 cm^{-1} (1050 nm; assigned as an IVCT transition) and at 5263 and 4350 cm^{-1} (1900 and 2300 nm, respectively; assigned as $d\pi-d\pi$ transitions within the Os^{III} part of the complex). Accordingly, the Os → Ru electron-transfer reaction below can be induced by protonation of the bridging ligand:

$$[\{Os^{II}(bpy)_2(bbby)\}_3Ru^{III}]^{3+} + 6H^+ \rightarrow [\{Os^{III}(bpy)_2(bbbyH_2)\}\{Os^{II}(bpy)_2(bbbyH_2)\}_2Ru^{II}]^{9+}$$

In a subsequent publication, Haga and co-workers examined the analogous tetranuclear system with four Ru centers and with the imidazole rings methylated in the bridging ligand (**II**).[174] The oxidation sequence is consistent with pathway B in Figure 27. The electrochemical oxidation of the central Ru ion was separated from the three closely-spaced one-electron processes of the peripheral Ru ions. The latter have small differences due to electrostatic and statistical factors, although the potential separations were small and, therefore it was not possible to perform selective oxidations to form the individual mixed-valence species (which might disproportionate in any case). Instead, the authors reported a flow-through voltammetry technique which allowed the calculation of the individual redox potentials for the successive processes, from which the characteristics of the IVCT bands for the three mixed-valence species have been extracted using the respective comproportionation constants. Such calculations lead to the conclusion that the IVCT spectra for the 9+, 10+, and 11+ species occur at essentially the same energy {8390 cm^{-1} (1192 nm)} with absorption coefficients of 120, 180, and 50 M^{-1} cm^{-1}, respectively. The reason for the two-electron-oxidized species showing the highest absorption was not addressed.

Redox interactions in starburst complexes—for example, tetranuclear complexes such as those shown in Figure 28—have been treated theoretically by Aoki and co-workers.[175,176] Typically, two types of mixed-valence state are envisaged (as shown in Figure 27): a central oxidized metal with three peripheral reduced metals, or a central reduced metal with three peripheral oxidized metals. Assuming that interaction *only* occurs between neighboring redox sites (i.e., an outer site has no direct interaction with the other two outer sites and optical isomerism is ignored), eight redox and geometric isomers are envisaged. Contrary to the naive expectation that a complex with four redox sites exhibits four

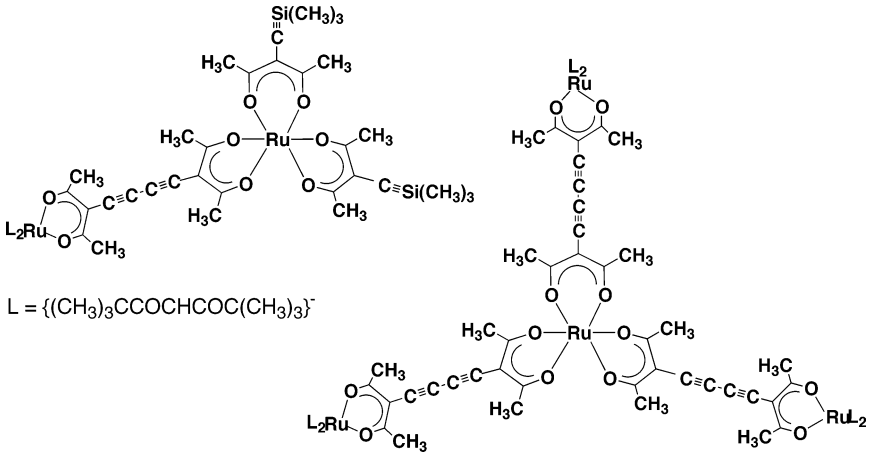

Figure 28. Diyl-linked dinuclear and tetranuclear species based on $Ru(acac)_3$ centers.[176]

redox waves, configurational mixing and the overlapping nature of the various redox isomers lead to the appearance of two waves, corresponding to pathway B in Figure 27, i.e., the appearance of a simultaneous three-electron oxidation of the peripheral metal centers, followed by one-electron oxidation of the central metal.[176]

Interestingly, the tetranuclear complex in Figure 28 exhibited a peak potential difference for the mixed-valence state which was twice that for the mixed-valence state of the corresponding dinuclear complex.[176] This suggested that configurational stabilization of the mixed-valence state was enhanced by the presence of the additional metal centers, indicating delocalization of the electron density over the whole molecule. The result could only be realized from a quantum chemical model of the redox interaction rather than an "additive pair" model.

Rillema *et al.*[177] reported studies of the di-, tri-, and tetranuclear complexes of the ligands 2,2′,3,3′-tetrakis(2-pyridyl)-6,6′-biquinoxaline. The sequence of attachment of Ru moieties is given in Figure 29, and electrochemical

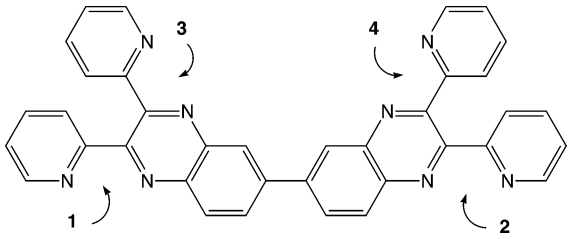

Figure 29. Bridging ligand 2,2′,3,3′-tetrakis(2-pyridyl)-6,6′-biquinoxaline, showing the positions of metal coordination.[177]

studies showed that the two "benzoquinoxaline" halves (**1**/**3** and **2**/**4**) behaved identically and that the two halves did not communicate; that is, there are two di-bidentate bridging ligands held together by a bond between two benzene groups.

The IVCT behavior was consistent with this assignment: an IVCT band {at ~5263 cm^{-1} (1900 nm)} was seen only for the partially-oxidized trinuclear and tetranuclear species, which had similar characteristics in both cases. There are also possibilities in this system for IVCT in partially-reduced species. Although there was some electrochemical evidence for interaction between the subunits in these studies, no IVCT transitions were detected.

Rillema and co-workers[178] subsequently reported studies of the tetranuclear complex $[\{Ru(bpy)_2(BiBzIm)\}_3Ru]^{n+}$ (Figure 30a). The mixed-valence $[\{Ru^{II}(bpy)_2(BiBzIm)\}_3$-

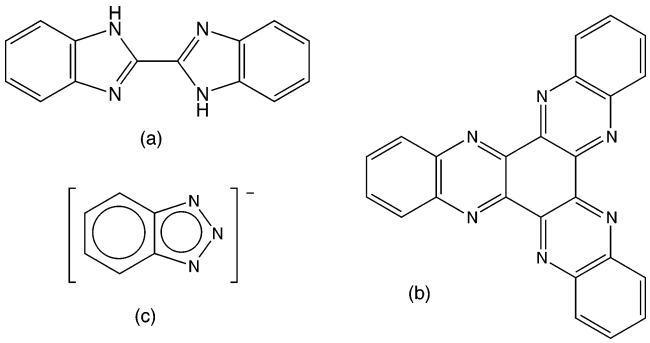

Figure 30. (a) 2,2-Bibenzimidole ($BiBzImH_2$);[178] (b) bridging ligand diquinoxaline[2,3-*a*:2′,3′-*c*]phenazine;[179] (c) benzotriazolate ion (bta^-).[180]

$Ru^{III}]^{3+}$ species showed an absorption in the NIR region {12 200 cm^{-1} (820 nm) in CH_3CN solution} which was attributed to overlapping LMCT and IVCT transitions, but this IVCT behavior was not investigated further.

Kalyanasundaram *et al.*[181] have studied the oligonuclear complexes involving the bridging 5,5′-bis(2-pyridyl)-3,3′-bi(1,2,4-triazolate) anion (BPBT) and its protonated form $BPBTH_2$ (Figure 31). In the dinuclear species $[\{Ru(bpy)_2\}_2$-

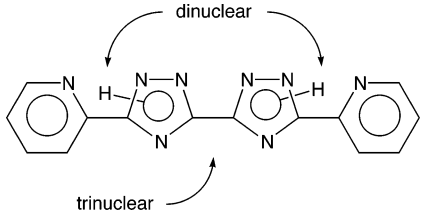

Figure 31. 5,5′-Bis(2-pyridyl)-3,3′-bi(1,2,4-triazole) {BPBT}, showing coordination positions adopted in the dinuclear and trinuclear complexes.[181]

$(\mu\text{-}BPBTH_2)]^{4+}$, the ruthenium centers are believed to attach at the two "ends", involving both terminal pyridyl groups. For the trinuclear species $[\{Ru(bpy)_2\}_3(\mu\text{-}BPBT)]^{4+}$, the additional ruthenium center attaches at the N4 and N4′ sites of the triazolate groups. There are stereoisomeric forms of both species, but the isomers were not separated in this study. In the mixed-valence dinuclear species, the IVCT would arise between two Ru centers located at the extremities of the bridge. However, in the case of the one-electron-oxidized trinuclear species, the first oxidation was claimed to occur at the central Ru center, so that IVCT would be over a shorter distance.

The mixed-valence complexes were observed by spectral studies using chemical oxidation. The dinuclear complex shows an IVCT transition at 5714 cm^{-1} (1750 nm), while, for the trinuclear complex, an IVCT band is seen at 5882 cm^{-1} (~1700 nm). In both cases, the nature of the IVCT bands indicated strong metal−metal interaction (i.e. significant delocalization). It is interesting to note the similarity of IVCT bands, despite the difference in interchromophoric distance in the two cases. No comment was made about the IVCT characteristics of the two-electron-oxidized species, for which there would be alternative pathways for IVCT behavior.

Kaim *et al.*[179] have reported studies of the $[\{(acac)_2Ru^{II}\}_3(\mu\text{-L})]$ trinuclear species {acac$^-$ = acetylacetonate anion; L = diquinoxaline[2,3-*a*:2′,3′-*c*]phenazine (shown in Figure 30b)}. In this case, although the redox potentials for the oxidation processes leading to the formation of the mixed-valence + and 2+ forms were well separated (ΔE_{ox} = 340 mV), no obvious IVCT bands were determined, suggesting weak electronic coupling.

Rocha and Toma[180] have reported electrochemical and spectroelectrochemical studies of the trinuclear complex *trans*-$[(NH_3)_4Ru\{(bta)Ru(edta)\}_2]^{n-}$ {bta$^-$ = benzotriazolate (Figure 30c), edta = ethylenediamine-*N*,*N*,*N*′,*N*′-tetraacetate; *n* = 1,2, or 4}. The electrochemical data indicate negligible communication between the peripheral Ru(edta) units, while there is significant electronic interaction between adjacent terminal and central Ru groups. The IVCT characteristics of the mixed-valence $Ru^{III}-Ru^{II}-Ru^{III}$ complex are similar to those of the dinuclear species *trans*-$[(NH_3)_4Ru(bta)Ru(edta)]^-$. Using the properties of the IVCT band and a theoretical intermetallic distance, values of H_{ab} = 945 cm^{-1} and α^2 = 0.021 were obtained using the Hush model,[28,35] which reveal that the extent of electronic coupling (and therefore delocalization) is significantly enlarged in the symmetrical trinuclear system compared with the dinuclear analogue (H_{ab} = 870 cm^{-1} and α^2 = 0.017).

In a recent paper, Thomas *et al.*[182] reported a trinuclear ruthenium metallomacrocyle in which three Ru([9]-ane-S_3) moieties are linked by 9-methyladenine bridges (Figure 32).

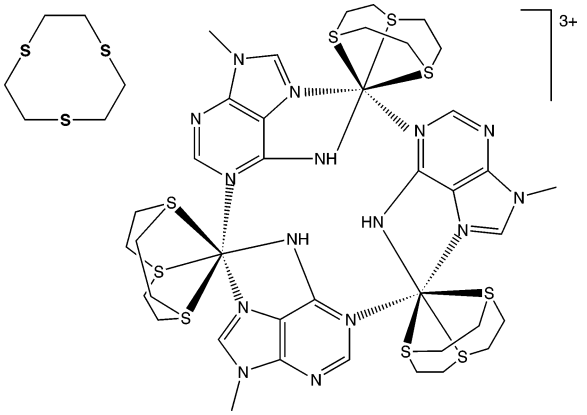

Figure 32. Macrocyclic ligand 1,4,7-trithiacyclononane, and the triruthenium complex formed with each ruthenium center coordinated to one macrocyclic ligand and bridged by 9-methyladenine.[182]

Electrochemical studies revealed three reversible metal-based oxidation processes, where ΔE_{ox} values for the successive redox couples are 175 and 380 mV.

Accordingly, the comproportionation constants for the 4+ and 5+ species are 760 and 2.8 × 10^6, respectively. Such a variation is unusual in triangular complexes where the three metal centers are identical: it implies that there is significantly greater delocalization in the more highly-charged mixed-valence form. Not unexpectedly, the two mixed-valence species exhibit significantly different IVCT characteristics. In the NIR region, the 4+ state shows a structured, low-intensity broad band—characteristic of a valence-localized system—which appears to be comprised of several overlapping transitions. For the 5+ analogue, the NIR absorption is intense (ϵ_{max} = 8500 M^{-1} cm^{-1}) and consists of at least three overlapping transitions: the sharpness and intensity of the bands indicates a valence-delocalized system. The application of Hush theory[28,29] to these two systems reveals $\Delta\nu_{1/2} \sim$ 3500 cm^{-1} (compared with the calculated value of 4100 cm^{-1}) for the 4+ species, whereas $\Delta\nu_{1/2}$ = 900 cm^{-1} (calculated value 3325 cm^{-1}) for the 5+ analogue. The results imply the complexes were in the Class II and Class III regimes,[27] respectively.

Studies by Belser *et al.*[183] have investigated a series of trinuclear species in which $Os(bpy)_2$ and/or $Ru(bpy)_2$ moieties are bridged by the series of ligands shown in Figure 33. In these cases, the electrochemical oxidation of each Ru

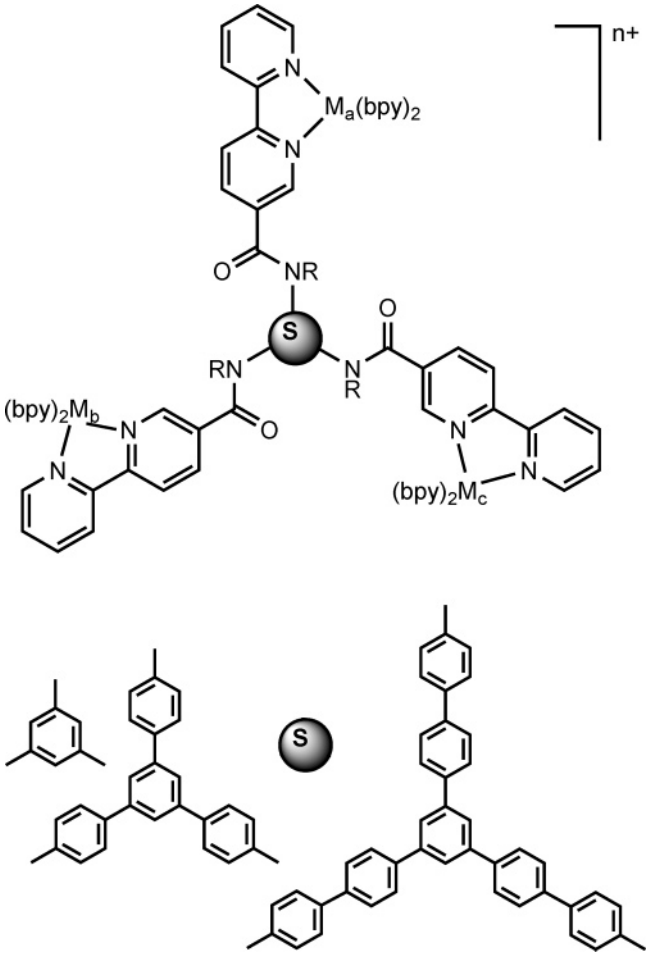

Figure 33. Bridging ligands generating trinuclear complexes, reported by Belser *et al.*[183]

or Os center always occurs near the same potential regardless of the tripod, and no IVCT bands were observed in the NIR region.

6. Stereochemical Influences on IVCT

The vast majority of studies concerning the physical characteristics of tri- and tetranuclear assemblies containing

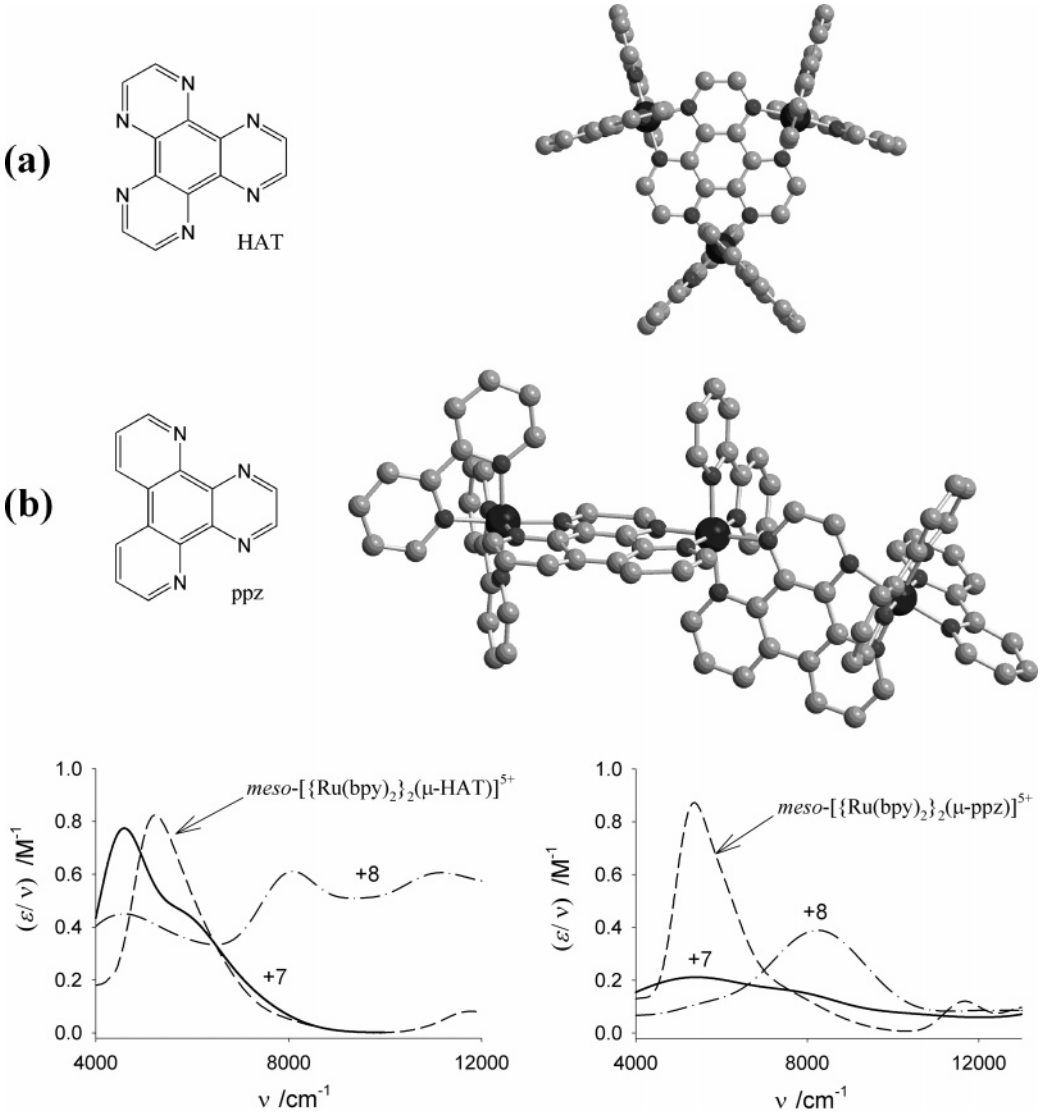

Figure 34. Bridging ligands HAT and ppz, and comparison of the IVCT transitions for the di- and trinuclear mixed-valence systems (a) *homochiral*-[{Ru(bpy)$_2$}$_3$(μ-HAT)]$^{n+}$ (n = 7, 8) and *meso*-[{Ru(bpy)$_2$}$_2$(μ-HAT)]$^{5+}$; and (b) $\Delta\Delta^t\Delta$-[{Ru(bpy)$_2$}$_2${Ru(bpy)(μ-ppz)$_2$}]$^{n+}$ (n = 7, 8) and *meso*-[{Ru(bpy)$_2$}$_2$(μ-ppz)]$^{5+}$. The spectra are reported as (ϵ/ν) vs ν.

polypyridyl ligands have been conducted on systems which may be comprised of many stereoisomeric forms, although this stereochemical complexity has been avoided in a number of cases by virtue of their design.[17,184−196] While the presence of many isomeric forms has often been acknowledged, the influence of the inherent stereochemistry of such species on their spectral, electrochemical, and photophysical properties has only recently been reported.[22,85,86,197−200] Keene and coworkers[85,86,200] were the first to reveal differences in the characteristics of the IVCT bands between diastereoisomeric forms of the same complex and reported the first systematic study on the IVCT properties of the stereochemically-unambiguous trinuclear systems which are "cluster-like" *homochiral* (Δ_3/Λ_3)- and *heterochiral* ($\Delta_2\Lambda/\Lambda_2\Delta$)-[{Ru(bpy)$_2$}$_3$($\mu$-HAT)]$^{6+}$ [201] and "chainlike" $\Delta\Delta^t\Delta$-[{Ru(bpy)$_2$}$_2${Ru(bpy)(μ-ppz)$_2$}]$^{6+}$, shown in Figure 34 (where the superscript t denotes the *trans* arrangement of the ppz ligands at the central metal).[202] The bridging ligands HAT (1,4,5,8,9,12-hexaazatriphenylene) and ppz (4,7-phenanthrolino-5,6:5′,6′-pyrazine) are closely related electronically and structurally, and the planarity of the ligands overcomes the problem of conformational lability in complexes incorporating 2,3-dpp,[86] which have been utilized extensively in the construction of tri- and tetranuclear and higher nuclearity assemblies.[1,203,204]

Cyclic and differential pulse voltammetry studies of the [{Ru(bpy)$_2$}$_3$(μ-HAT)]$^{6+}$ systems revealed three reversible one-electron redox processes, corresponding to successive oxidation of the metal centers. For example, the potential differences between the three oxidation processes in the trinuclear stereoisomer $\Delta_2\Lambda/\Lambda_2\Delta$-[{Ru(bpy)$_2$}$_3$($\mu$-HAT)]$^{6+}$ ($\Delta E_{ox(2-1)}$ = 220 and $\Delta E_{ox(3-2)}$ = 244 mV, for the first and second oxidations, respectively, 0.1 M [(n-C$_4$H$_9$)$_4$]PF$_6$/CH$_3$CN) were indicative of a significant degree of electronic delocalization within the assembly.[201] By comparison, $\Delta\Delta^t\Delta$-[{Ru(bpy)$_2$}$_2${Ru(bpy)(μ-ppz)$_2$}]$^{6+}$ exhibited two closely-spaced one-electron redox processes (E_{ox1} ~1137 mV, $\Delta E_{ox(2-1)}$ < 100 mV) corresponding to oxidation of the terminal Ru^{II} centers to Ru^{III}, followed by one-electron oxidation of the central Ru^{II}.[202] The results indicate that the terminal centers are not significantly electronically-coupled through the chainlike framework.

The IVCT characteristics of the trinuclear mixed-valence assemblies are consistent with the electrochemical studies,

vary significantly depending on the extent of oxidation and the overall geometry of the assembly, and differ markedly from the IVCT properties of their dinuclear counterparts. As shown in Figure 34, $[\{Ru(bpy)_2\}_2(\mu\text{-HAT})]^{5+}$ [201] and $[\{Ru(bpy)_2\}_2(\mu\text{-ppz})]^{5+}$ [202] exhibit asymmetrically-shaped IVCT bands which are consistent with a borderline localized-to-delocalized classification. Each trinuclear system exhibits two mixed-valence states which were generated upon one- and two-electron oxidation of the +6 species at −15 °C.

For the $[\{Ru(bpy)_2\}_3(\mu\text{-HAT})]^{6+}$ system, spectroelectrochemical generation of the +7 mixed-valence species was accompanied by the appearance of a new absorption feature in the range 3500−9000 cm^{-1} (2850−1110 nm) (Figure 34a). Spectral deconvolution revealed the presence of three underlying transitions, separated by 1305 and 1340 cm^{-1} (*heterochiral*) and 1275 and 1430 cm^{-1} (*homochiral*). The overall integrated intensity of the IVCT manifold for the *heterochiral* form is slightly greater than that for the *homochiral* form, and the intensities are approximately twice those for the related dinuclear complexes. The difference may be rationalized on the basis of the doubly-degenerate nature of the optically-induced transition from the two formally Ru^{II} centers to the hole at the formally Ru^{III} center in the trinuclear species. The bands were assigned as separate optically-induced transitions between energy levels within the molecular orbital manifold of the trinuclear complexes which are split predominantly by spin−orbit coupling of the metal centers.

The +8 mixed-valence species exhibited IVCT bands at ~8000 and 11 500 cm^{-1} (1250 and 870 nm, respectively). The transitions in the region at higher energies than 13 000 cm^{-1} (770 nm) were assigned to LMCT and MLCT absorptions by comparison with the related dinuclear species and by their behavior on oxidation to the +9 species.[133] The possibility exists that the multiple IVCT transitions originate from optically-induced electron transfer between different "exciton" states. The doubly-oxidized (+8) species comprises two formally Ru^{III} centers and one formally Ru^{II} center and therefore possesses two unpaired electrons. These may be aligned in a parallel or antiparallel fashion, giving rise to an overall singlet or triplet state for the trinuclear complex. The energy required for optical excitation to these two different "exciton" states will differ, in which case the two new transitions observed in the NIR region for the +8 species may be rationalized in terms of transitions to singlet and triplet exciton states in a valence-localized trinuclear mixed-valence species. The interpretation is not without precedence: Weyland *et al.*[169] proposed a similar argument to account for the observation of multiple IVCT transitions in other trinuclear complexes (section 4.2; Figure 23).

The IVCT characteristics of the mixed-valence forms of $\Delta\Delta^t\Delta$-$[\{Ru(bpy)_2\}_2\{Ru(bpy)(\mu\text{-ppz})_2\}]^{6+}$ [202] exhibit localized behavior and are markedly different from those of the corresponding mixed-valence forms of $[\{Ru(bpy)_2\}_3(\mu\text{-HAT})]^{6+}$.[157] One-electron oxidation of a terminal Ru center in $\Delta\Delta^t\Delta$-$[\{Ru(bpy)_2\}_2\{Ru(bpy)(\mu\text{-ppz})_2\}]^{6+}$ gave rise to a broad, low intensity IVCT band for the +7 mixed-valence species which was composed of two underlying Gaussian-shaped bands (Figure 34b). The transitions were identified as *adjacent* and *remote* IVCT transitions, with the former dominating the intensity of the IVCT manifold. The +8 mixed-valence species exhibits a single dominant IVCT band arising from the equivalent IVCT transitions from the central Ru^{II} to peripheral Ru^{III} centers. As shown in Figure 34a, the three Ru centers in $[\{Ru(bpy)_2\}_3(\mu\text{-HAT})]^{6+}$ are equivalently disposed and share in the available electron density. By comparison, a "chainlike" arrangement of the three metal centers in $\Delta\Delta^t\Delta$-$[\{Ru(bpy)_2\}_2\{Ru(bpy)(\mu\text{-ppz})_2\}]^{6+}$ (Figure 34b) gives rise to a decreased coupling through the central metal. As a result, the $[\{Ru(bpy)_2\}_3(\mu\text{-HAT})]^{6+}$ complex exhibits a comparable degree of electronic coupling to its dinuclear analogue, while the degree of electronic coupling in $\Delta\Delta^t\Delta$-$[\{Ru(bpy)_2\}_2\{Ru(bpy)(\mu\text{-ppz})_2\}]^{6+}$ is reduced relative to that in its dinuclear counterpart.

Theoretically, the assumption of a two-state model and classical analysis was adequate for the IVCT transitions in the predominantly localized $\Delta\Delta^t\Delta$-$[\{Ru(bpy)_2\}_2\{Ru(bpy)(\mu\text{-ppz})_2\}]^{n+}$ (n = 7, 8) mixed-valence complex. However, for the dinuclear $[\{Ru(bpy)_2\}_2(\mu\text{-ppz})]^{5+}$ and $[\{Ru(bpy)_2\}_2(\mu\text{-HAT})]^{5+}$ complexes, as well as the trinuclear $[\{Ru(bpy)_2\}_3(\mu\text{-HAT})]^{n+}$ (n = 7, 8) complexes where delocalization is more extensive, a molecular orbital approach which includes vibronic coupling is required. The treatment of these issues represents a challenging problem which will require focused computational efforts in the future.

7. Trinuclear Oxo-Centered Iron Carboxylates

Mixed-valence trinuclear oxo-centered carboxylate complexes with coexisting Fe^{II} and Fe^{III} centers have received extensive interest due to the recognition of the role of such complexes in biological systems and their potential medicinal properties.[205] Recently, the incorporation of sulfur-containing ligands such as mercaptocarboxylic acids (HSR′COOH) has been reported for the first time,[205,206] and we mention them briefly here in light of the potential interest in these variants on the more generally recognized carboxylates due to their incorporation of both "soft" sulfur and "hard" oxygen donor atoms.

Pandey[205] investigated the class of trinuclear oxo-centered iron carboxylate complexes, $[Fe^{II}Fe^{III}_2O(OOCR)_3(OOCR'SH)_3(L)_3]$ {where R = $C_{13}H_{27}$ or $C_{15}H_{31}$; R′ = CH_2 or C_6H_4; and L = pyridine (Figure 35a)}, which are characterized by a

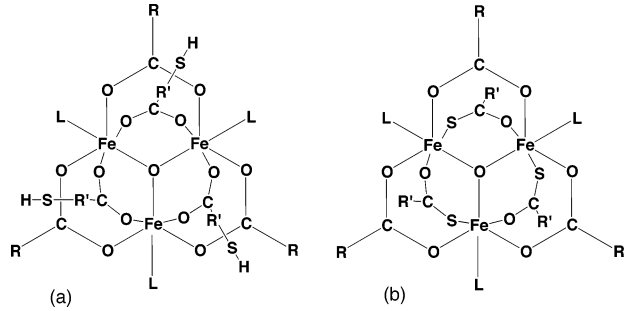

Figure 35. Structures of the trinuclear mixed-valence iron carboxylates: (a) $[Fe_3O(OOCR)_3(OOCR'SH)_3(L)_3]$, where R = $C_{13}H_{27}$ or $C_{15}H_{31}$, R′ = CH_2 or C_6H_4, and L = pyridine,[205] and (b) $[Fe_3O(SOCR')_3(OOCR)_3(L)_3]$, where R = $C_{13}H_{27}$, $C_{15}H_{31}$, or $C_{17}H_{35}$, R′ = CH_3 or C_6H_5, and L = CH_3OH.[206]

broad absorption in the region 13 680−13 860 cm^{-1} (730−720 nm) assigned as an IVCT band. Analysis of the absorption band manifold was not pursued; however, the valence-localized classification for the species was confirmed by Mössbauer spectroscopic studies up to 295 K, which indicated coexisting Fe^{II} and Fe^{III} centers.

The incorporation of thiocarboxylic acids and straight-chain fatty acids has also been demonstrated by the realization of trinuclear complexes with the general formulas

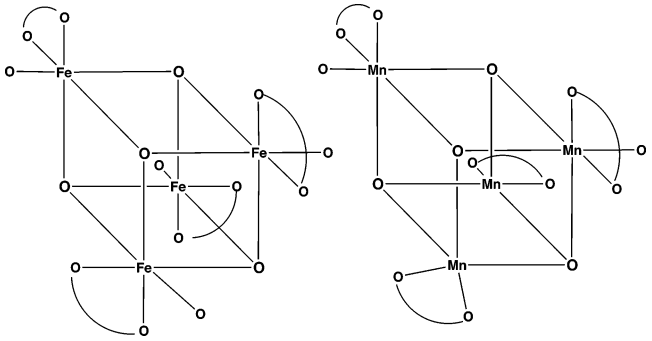

Figure 36. Schematic structures of $[M_4(OR)_4]^{4+}$ cubes.[211]

$[Fe^{II}Fe^{III}{}_2O(SOCR')_6(H_2O)_3]$ and $[Fe^{II}Fe^{III}{}_2O(SOCR')_3(OOCR)_3(CH_3OH)_3]$ {where R = $C_{13}H_{27}$, $C_{15}H_{31}$, or $C_{17}H_{35}$ and R′ = CH_3 or C_6H_5 (Figure 35b)}.[206] The broad absorption in the region 13785−13862 cm^{-1} (725−720 nm) was of IVCT origin, and the presence of localized Fe^{II} and Fe^{III} centers was confirmed by Mössbauer measurements up to 315 K.

A particularly interesting feature of the more general class of neutral trinuclear iron carboxylates, $[Fe^{II}Fe^{III}{}_2O(OOCR)_6(L)_3]$ {where R = CH_3 or $C(CH_3)_3$ and L = H_2O, pyridine, or NC_5H_5} was the presence of phase transitions. Below 35 K, Mössbauer spectra reveal the existence of discrete Fe^{III} (sites 1 and 2) and Fe^{II} (site 3) states in the expected 2:1 ratio, therefore establishing localized (Class II) behavior. The complexes undergo temperature-dependent phase transitions, and at room temperature, the Fe−(μ^3-O) bond lengths reveal two Fe^{II} sites (1 and 2) and one Fe^{III} site (3).[207] Since the intramolecular electron-transfer process involves sites 2 and 3 only, with site 1 being valence-trapped at all temperatures, the room-temperature data were consistent with a delocalized description for the mixed-valence species. The theoretical treatment for the mixed-valence trinuclear iron carboxylates has been considered by a number of groups[207−210] and involves the generalization of the adiabatic potential energy surfaces developed for the two-site model[28,29] to the three-site case. The underlying assumptions were identical to those employed in the two-site treatment: i.e., the harmonic nature of the framework vibrations, a single vibrational mode (of appropriate symmetry type) coupled to electron transfer, the involvement of one orbital from each metal atom only, and the applicability of a first-order perturbation treatment. The model was employed to rationalize the localized nature of the mixed-valence states.[208]

8. Iron and Manganese Alkoxide Cubes

Taft *et al.*[211] have investigated a series of cubic structures in which there are four metal ions and four bridges at alternating corners of a cube (Figure 36): Fe_4S_4 clusters of this type are used as models for active sites of iron−sulfur proteins, and there is a proposal of a similar cubic arrangement of manganese and bridging ligands for the oxygen-evolving center of photosystem II.[212]

The cubic core $[Fe^{III}Fe^{II}{}_3(OMe)_5(MeOH)_3(OBz)_4]$ was prepared by slow oxidation of $FeCl_2$ in the presence of methoxide and benzoate anions. The complex has C_1 symmetry, and X-ray structural studies (at −85 °C) indicated that the Fe^{III} center was valence-localized—a result corroborated by Mössbauer studies which indicate there is no delocalization up to 250 K. The iron atoms are antiferromagnetically exchange-coupled.

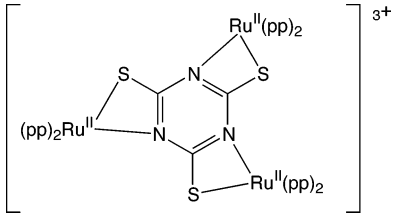

Figure 37. Triruthenium complex based on the bridging ligand 1,3,5-triazine-2,4,6-trithiol.[213]

The species shows an IVCT absorption at 10 810 cm^{-1} {925 nm; CD_2Cl_2/CD_3OD (1:1); ϵ_{max} = 295 M^{-1} cm^{-1}} which is solvent-dependent. The value of $\Delta\nu_{1/2}$ = 7600 cm^{-1} (obtained from deconvolution of the IVCT and the spin-allowed transition) compares with a theoretical value of 5000 cm^{-1} obtained from the Hush analysis:[28,29,34] it was considered that the large experimental value may be due to other transitions within the envelope. The value of ν_{max} is generally observed to be high in Fe complexes containing Fe−O bonds, although the reason for this phenomenon is uncertain.

9. Tri-bidentate Bridges

Kar *et al.*[213] have studied the triruthenium complex shown in Figure 37 (where pp = bpy or phen). The electrochemistry showed three quasi-reversible oxidations separated by ∼200 mV. EPR studies showed that, in the 4+ ($Ru^{II}Ru^{II}Ru^{III}$) and 5+ ($Ru^{II}Ru^{III}Ru^{III}$) mixed-valence ions, the unpaired electron(s) were primarily located on the metal center. In both mixed-valence ions, the IVCT band was seen at 5263 cm^{-1} (∼1900 nm), with the width being consistent with Class II behavior. In each case H_{ab} = 560 cm^{-1} (assuming a Ru···Ru separation of 5.9 Å), implying there are equivalent routes for $Ru^{II} \rightarrow Ru^{III}$ transfer in the two cases.

In the diradical 5+ ($Ru^{II}Ru^{III}Ru^{III}$) mixed-valence case, two IVCT transitions are possible due to magnetic exchange between the formally Ru^{III} centers which may give rise to energetically-distinct singlet and triplet states, as observed previously by Weyland *et al.*[169] While the presence of two energetically-distinct IVCT transitions should lead to a broader envelope, no significant difference was detected between the IVCT bands in the 4+ and +5 mixed-valence species.

10. Dimers of Trimers

Complexes of the type $[\{Ru^{III}{}_2Ru^{II}(\mu_3\text{-}O)(\mu\text{-}CH_3CO_2)_6(abco)\}_2(\mu\text{-}pyz)]$ {abco = 1-azobicyclo[2,2,2]octane; pyz = pyrazine}[214] and related species of the general type $[\{(Ru_3O)(OAc)_6(CO)(L)\}_2(\mu\text{-}pyz)]$ (L = pyridine derivatives containing electron-donating or electron-withdrawing substituents)[215−217] are hexanuclear species but are more akin to the dinuclear mixed-valence species in their behavior and are not discussed in any detail here. However, a recent study is noted involving a cluster of the type $[\{(Ru_3O)(OAc)_6(CO)(py)\}(\mu\text{-Mepyz})\{(Ru_3O)(OAc)_6(^{13}C^{18}O)(py)\}]$ (Mepyz = 2-methylpyrazine), in which there are two isomers arising from the position of the methyl group in the unsymmetrical bridging ligand relative to the trinuclear cluster containing the labeled carbonyl ligand.[218] Electrochemical studies of the one-electron-reduced species revealed that the mixed-valence isomers are observed as discrete chemical species.

11. Conclusions and Future Perspectives

The field of mixed-valence chemistry has a long and rich history which has been characterized by a strong interplay

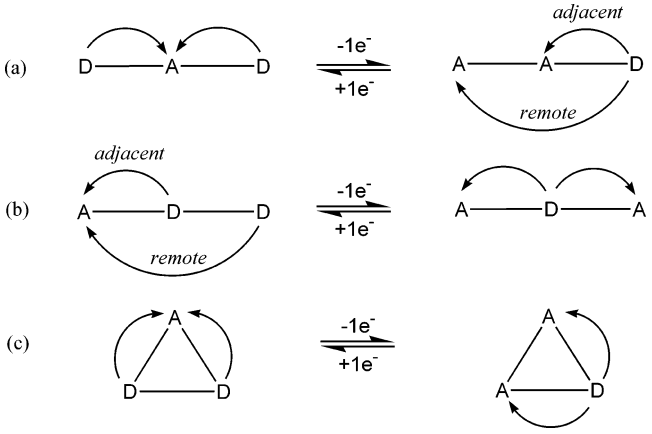

Figure 38. Schematic representation of the two mixed-valence states of trinuclear complexes with chainlike (a and b) or "triangular" (c) architectures. The arrows depict the possible interactions between the oxidized electron-acceptor (A) and unoxidized electron-donor (D) metal centers.

of experimental, theoretical, and computational studies. The analysis of IVCT transitions has provided a powerful window to the elucidation of fundamental factors which govern the activation barrier to electron transfer, such as the Franck−Condon factors and the extent of electronic delocalization. While these studies have focused predominantly on dinuclear mixed-valence complexes, the present review has sought to address the IVCT properties of trinuclear and tetranuclear complexes of Fe, Ru, and Os, which provide the link between the understanding of electron transfer in dinuclear systems and electron transfer in extended arrays and supramolecular systems. For the experimental chemist, it is also evident that characterization of the redox properties of higher nuclearity complexes offers important insights into the relative energies of the metal-based components within such assemblies and may aid in the identification of the origins of the IVCT transitions.

While considerable complexity may be expected in the theoretical analysis of IVCT transitions in tri- and tetranuclear complexes due to the presence of multiple, electronically-coupled chromophores, classical models[28,29] (eqs 1−5) have been successfully applied to weakly-coupled systems. Qualitatively, the IVCT bands are reminiscent of those in the analogous dinuclear mixed-valence complexes, and the trends in the properties (energies, intensities, and bandwidths) of the transitions are readily interpreted by considering the degeneracy of the transition and the oxidation state of the assembly. More specifically, the increase in nuclearity is generally manifested by an increase in the intensity of the IVCT and a shift to higher energy with increasing oxidation state.

As the extent of electronic delocalization increases, however, the valence-localized scenario is no longer appropriate, and the IVCT characteristics of tri- and tetranuclear complexes have been shown to exhibit intriguing new properties that are distinct from those of their dinuclear counterparts. As an illustrative example, two mixed-valence states may arise from the two successive one-electron oxidation processes in a linear trinuclear complex, where the initial site of oxidation occurs at the central (a) or peripheral (b) metal centers, as shown in Figure 38. A trinuclear system in which the metal centers are disposed in a "triangular" fashion is depicted in Figure 38c.

Oxidation of the central metal (prior to the terminal units) gives rise to the scenario in Figure 38a, where electron transfer occurs from the two degenerate donors (D) to the terminal acceptor (A). In this case, a doubly-degenerate IVCT transition of approximately twice the intensity of that for the related dinuclear congener is expected between the weakly- to moderately-coupled metal centers. As the extent of delocalization increases, however, the IVCT manifold has been shown to split into two transitions of similar intensity but slightly different energy.[104] The splitting has been rationalized on the basis of appreciable second-order interactions between the terminal metal centers, and the fact that the overall integrated intensity of the band manifold is approximately doubled relative to the IVCT for the related dinuclear complex is consistent with the two-electron nature of the IVCT processes. The construction of adiabatic potential energy surfaces (shown schematically in Figure 4) provides a qualitative rationalization for the appearance of two IVCT transitions.

A second scenario may be envisaged upon oxidation of one of the terminal metal chromophores (Figure 38b) and gives rise to two IVCT transitions between *adjacent* and *remote* metal centers. The situation is exemplified by the class of trinuclear cyano-bridged complexes discussed in section 2. The cyanide bridging ligand mediates a moderately strong intercomponent electronic interaction, in which a valence-localized (Class II) designation has been proposed for the majority of its tri- and tetranuclear complexes. Experimentally, the moderate metal−metal interactions result in moderately intense IVCT bands which are attributed to transitions between *adjacent* and *remote* metal centers. The latter exhibit weak intensities, reflecting the larger metal−metal separation between the peripheral (as opposed to *adjacent*) centers. Indeed, the existence of such appreciable second-order interactions suggests that cyanide bridges act as conduits for long-range vectorial electron and energy transfer. A through-bond superexchange-assisted electronic coupling mechanism can be invoked to provide a first-order semiquantitative approach for the appearance of such *remote* interactions. The valence-localized classification of the higher nuclearity cyano-bridged assemblies is consistent with their description as "supramolecular" species: they exhibit properties reminiscent of the constituent molecular components which are perturbed to a limited extent and in a predictable manner by intercomponent interactions.

For the two-electron-oxidized (diradical) mixed-valence system depicted in Figure 38c, two IVCT transitions are anticipated due to magnetic exchange interactions between the two radical centers. The [3,3,2] species possesses two energetically-distinct electronic states depending on the antiparallel or parallel alignment of the spins at the formally Ru^{III} centers. IVCT studies alone are insufficient to determine whether the dominant coupling is ferromagnetic or antiferromagnetic; however, unless the coupling is extraordinarily strong, both states will be occupied at 298 K, leading to slightly different energies for the two IVCT processes. The effect will be to broaden the IVCT manifold for the [3,3,2] versus the [3,2,2] mixed-valence system. Unfortunately, the identification of this effect has been complicated in a number of cases by the broadening of the IVCT manifold from other sources such as low symmetry, extensive orbital mixing, spin−orbit coupling of the metal $d\pi$ orbitals[40] and overlap of the IVCT with low-lying LMCT and MLCT transitions. Clearly, reliable spectral deconvolution procedures are paramount to discern the IVCT features of interest.

Conclusive evidence for the presence of singlet and triplet IVCT transitions in a diradical mixed-valence system has been reported in one case only for the diradical form of a localized trinuclear mixed-valence complex by Weyland,[169] while a tentative assignment has also been made for the stereoisomers of borderline localized-to-delocalized trinuclear polypyridyl complexes.[201]

An important difference between dinuclear and higher nuclearity systems is the possibility for additional second-order spin-dependent electronic processes due to the existence of itinerant "extra" electrons hopping over the exchange-coupled magnetic sites. Various theoretical approaches for the treatment of trinuclear mixed-valence complexes have been proposed, as three-state extensions[208,219,220] of the classical two-state model.[28,29] Early classical treatments were developed for the trinuclear iron carboxylates[208] and involved the construction of adiabatic potential energy surfaces. While the quantitative details of these analyses are beyond the scope of the present review, the application of a simple first-order perturbation treatment to the three-site case results in the prediction of two IVCT transitions, as discussed in relation to Figure 4.

A semiclassical treatment for trinuclear mixed-valence systems has also appeared[221] and was based upon the solution of the vibronic problem using a similar starting formalism to the PKS model of Pieko, Krausz, and Schatz (with the simplifying assumption of a single vibrational mode).[73] Importantly, the prediction $\nu_{max} = 4E_{th}$ (eq 2) originally formulated for dinuclear complexes was also found to be applicable to weakly-coupled trinuclear complexes. The influence of the third metal center was such that the localized-to-delocalized transition is predicted to occur earlier within the three-site classical model relative to the two-site case;[28,29] however, the effect has not been investigated experimentally.

Clearly, the understanding of the IVCT phenomena in trinuclear and higher nuclearity complexes which exhibit moderately strong to extensive electronic coupling, and the experimental design of systems with interesting new electron-transfer phenomena, would benefit enormously from the clarification of the theoretical issues. For dinuclear mixed-valence systems in the localized-to-delocalized and delocalized regimes, the importance of additional states, the consideration of the full vibronic coupling problem, and the proper treatment of the asymmetric and symmetric modes are subjects of intense current research efforts,[40,45,67] and these issues will likewise be important for higher nuclearity systems. However, since the complexity of the computational problem increases with the size of the polymetallic assembly, it would seem that the clarification of the first-order perturbation theory approach (i.e. the adiabatic problem) represents a crucial preliminary step toward a more quantitative theoretical basis for IVCT in higher nuclearity trinuclear and tetranuclear complexes.

For the experimental chemist, the challenge is to synthesize structurally and stereochemically unambiguous assemblies in which the nature of the IVCT transitions can be interrogated.

12. Acknowledgments

We thank the Australian Research Council for financial support.

13. References

(1) Balzani, V.; Juris, A.; Venturi, M.; Campagna, S.; Serroni, S. *Chem. Rev.* **1996**, *96*, 759.
(2) Belser, P.; Bernhard, S.; Blum, C.; Beyeler, A.; De Cola, L.; Balzani, V. *Coord. Chem. Rev.* **1999**, *190*−*192*, 155.
(3) Garcia, C. G.; de Lima, J. F.; Iha, N. Y. M. *Coord. Chem. Rev.* **2000**, *196*, 219.
(4) Ward, M. D. *Chem. Soc. Rev.* **1997**, *26*, 365.
(5) Barigelletti, F.; Flamigni, L. *Chem. Soc. Rev.* **2000**, *29*, 1.
(6) Gust, D.; Moore, T. A.; Moore, A. L. *Acc. Chem. Res.* **2001**, *34*, 40.
(7) Balzani, V.; Credi, A.; Raymo, F.; Stoddart, J. F. *Angew. Chem., Int. Ed.* **2000**, *39*, 3348.
(8) Dürr, H.; Bossmann, S. *Acc. Chem. Res.* **2001**, *34*, 905.
(9) Balzani, V.; De Cola, L. *Supramolecular Chemistry*; Kluwer Academic Publishers: Dordrecht, 1992.
(10) Anderson, P. A.; Deacon, G. B.; Haarmann, K. H.; Keene, F. R.; Meyer, T. J.; Reitsma, D. A.; Skelton, B. W.; Strouse, G. F.; Thomas, N. C.; Treadway, J. A.; White, A. H. *Inorg. Chem.* **1995**, *34*, 6145.
(11) Anderson, P. A.; Keene, F. R.; Meyer, T. J.; Moss, J. A.; Strouse, G. F.; Treadway, J. A. *J. Chem. Soc., Dalton Trans.* **2002**, 3820.
(12) Jandrasics, E. Z.; Keene, F. R. *J. Chem. Soc., Dalton Trans.* **1997**, 153.
(13) Balzani, V.; Credi, A.; Venturi, M. *Chem.*−*Eur. J.* **2002**, *8*, 5525.
(14) Holliday, B. J.; Mirkin, C. A. *Angew. Chem., Int. Ed.* **2001**, *40*, 2022.
(15) Steed, J. W.; Atwood, J. L. *Supramolecular Chemistry*; Wiley: Chichester, 2000.
(16) Provent, C.; Williams, A. F. In *Transition Metals in Supramolecular Chemistry*; Sauvage, J. P., Ed.; Wiley: Chirchester, 1999.
(17) MacDonnell, F. M.; Kim, M.-J.; Bodige, S. *Coord. Chem. Rev.* **1999**, *185*−*186*, 535.
(18) Zeng, F.; Zimmerman, S. C. *Chem. Rev.* **1997**, *97*, 1681.
(19) Constable, E. C. *Chem. Commun.* **1997**, 1073.
(20) Sauvage, J.-P.; Hosseini, M. W. *Comprehensive Supramolecular Chemistry*; Pergamon: New York, 1996.
(21) Boulas, P. L.; Gomez-Kaifer, M.; Echegoyen, L. *Angew. Chem., Int. Ed.* **1998**, *37*, 216.
(22) Rutherford, T. J.; Van Gijte, O.; Kirsch − De Mesmaeker, A.; Keene, F. R. *Inorg. Chem.* **1997**, *36*, 4465.
(23) Roffia, S.; Casadei, R.; Paolucci, F.; Paradisi, C.; Bignozzi, C. A.; Scandola, F. *J. Electroanal. Chem.* **1991**, *302*, 157.
(24) Marcaccio, M.; Paolucci, F.; Paradisi, C.; Roffia, S.; Fontanesi, C.; Yellowlees, L. J.; Serroni, S.; Campagna, S.; Denti, G.; Balzani, V. *J. Am. Chem. Soc.* **1999**, *121*, 10081.
(25) Venturi, M.; Credi, A.; Balzani, V. *Coord. Chem. Rev.* **1999**, *185*−*186*, 233.
(26) Allen, G. C.; Hush, N. S. *Prog. Inorg. Chem.* **1967**, *8*, 357.
(27) Robin, M. B.; Day, P. *Adv. Inorg. Chem. Radiochem.* **1967**, *10*, 247.
(28) Hush, N. S. *Prog. Inorg. Chem.* **1967**, *8*, 391.
(29) Hush, N. S. *Electrochim. Acta* **1968**, *13*, 1005.
(30) Marcus, R. A. *J. Chem. Phys.* **1957**, *26*, 867.
(31) Marcus, R. A. *J. Chem. Phys.* **1956**, *24*, 966.
(32) Creutz, C.; Taube, H. *J. Am. Chem. Soc.* **1973**, *95*, 1086.
(33) LeVanda, C.; Bechgaard, K.; Cowan, D. O.; Rausch, M. D. *J. Am. Chem. Soc.* **1977**, *99*, 2964.
(34) Hush, N. S. *Coord. Chem. Rev.* **1985**, *64*, 135.
(35) Creutz, C. *Prog. Inorg. Chem.* **1983**, *30*, 1.
(36) Crutchley, R. J. *Adv. Inorg. Chem.* **1994**, *41*, 273.
(37) Kalyanasundaram, K.; Nazeeruddin, M. K. *Inorg. Chim. Acta* **1994**, *226*, 213.
(38) Ward, M. D. *Chem. Soc. Rev.* **1995**, *24*, 121.
(39) Barbara, P. F.; Meyer, T. J.; Ratner, M. A. *J. Phys. Chem.* **1996**, *100*, 13148.
(40) Demadis, K. D.; Hartshorn, C. M.; Meyer, T. J. *Chem. Rev.* **2001**, *101*, 2655.
(41) Launay, J.-P. *Chem. Soc. Rev.* **2001**, *30*, 386.
(42) Kaim, W.; Klein, A.; Glöckle, M. *Acc. Chem. Res.* **2000**, *33*, 755.
(43) Chen, P.; Meyer, T. J. *Chem. Rev.* **1998**, *98*, 1439.
(44) D'Alessandro, D. M.; Keene, F. R. *Chem. Soc. Rev.* **2006**, *35*, 424.
(45) Nelsen, S. F. *Chem.*−*Eur. J.* **2000**, *6*, 581.
(46) Nelsen, S. F.; Trieber, D. A., II.; Ismagilov, R. F.; Teki, Y. *J. Am. Chem. Soc.* **2001**, *123*, 5684.
(47) Hupp, J. T.; Weaver, M. J. *Inorg. Chem.* **1984**, *23*, 3639.
(48) Katriel, J.; Ratner, M. A. *J. Phys. Chem.* **1989**, *93*, 5065.
(49) Drago, R. S.; Richardson, D. E.; George, J. E. *Inorg. Chem.* **1997**, *36*, 25.
(50) Barthel, E. R.; Martini, I. B.; Schwartz, B. J. *J. Phys. Chem. B* **2001**, *105*, 12230.
(51) Matyushov, D. V.; Schmid, R. *J. Phys. Chem.* **1994**, *98*, 5152.
(52) Sullivan, B. P.; Curtis, J. C.; Kober, E. M.; Meyer, T. J. *Nouv. J. Chim.* **1980**, *4*, 643.
(53) Roberts, J. A.; Hupp, J. T. *Inorg. Chem.* **1992**, *31*, 157.

(54) Blackbourn, R. L.; Hupp, J. T. *J. Phys. Chem.* **1988**, *92*, 2817.
(55) Blackbourn, R. L.; Hupp, J. T. *Inorg. Chem.* **1989**, *28*, 3786.
(56) Hupp, J. T.; Weydert, J. *Inorg. Chem.* **1987**, *26*, 2657.
(57) Ennix, K. S.; McMahon, P. T.; de la Rosa, R.; Curtis, J. C. *Inorg. Chem.* **1987**, *26*, 2660.
(58) Brunschwig, B. S.; Ehrenson, S.; Sutin, N. *J. Phys. Chem.* **1986**, *90*, 3657.
(59) D'Alessandro, D. M.; Keene, F. R. *Chem. Phys.* **2006**, *324*, 8.
(60) Nelsen, S. F.; Ismagilov, R. F. *J. Phys. Chem. A* **1999**, *103*, 5373.
(61) Marcus, R. A. *J. Phys. Chem. B* **1998**, *102*, 10071.
(62) Pereztejeda, P.; Neto-Ponce, P.; Sánchez, F. *J. Chem. Soc., Dalton Trans.* **2001**, 1686.
(63) Lau, K. W.; Hu, A. M. H.; Yen, M. H. J.; Fung, E. Y.; Grzybicki, S.; Matamoros, R.; Curtis, J. C. *Inorg. Chim. Acta* **1994**, *226*, 137.
(64) Lewis, N. A.; Obeng, Y. S.; Purcell, W. L. *Inorg. Chem.* **1989**, *28*, 3796.
(65) Lewis, N. A.; Obeng, Y. S. *J. Am. Chem. Soc.* **1988**, *110*, 2306.
(66) D'Alessandro, D. M.; Junk, P. C.; Keene, F. R. *Supramol. Chem.* **2005**, *17*, 529.
(67) Brunschwig, B. S.; Creutz, C.; Sutin, N. *Chem. Soc. Rev.* **2002**, *31*, 168.
(68) Brunschwig, B. S.; Sutin, N. *Electron Transfer in Chemistry*; Wiley-VCH Verlag GmbH: Germany, 2001.
(69) Brunschwig, B. S.; Sutin, N. *Coord. Chem. Rev.* **1999**, *187*, 233.
(70) Sutin, N. *Prog. Inorg. Chem.* **1983**, *30*, 441.
(71) Sutin, N.; Brunschwig, B. S. *ACS Symp. Ser.* **1982**, *198*, 105.
(72) Creutz, C.; Newton, M. D.; Sutin, N. *J. Photochem.* **1994**, *82*, 47.
(73) Piepho, S. B.; Krausz, E. R.; Schatz, P. N. *J. Am. Chem. Soc.* **1978**, *100*, 2996.
(74) Wong, K. Y.; Schatz, P. N. *Prog. Inorg. Chem.* **1981**, *28*, 369.
(75) Piepho, S. B. *J. Am. Chem. Soc.* **1988**, *110*, 6319.
(76) Piepho, S. B. *J. Am. Chem. Soc.* **1990**, *112*, 4197.
(77) Reimers, J. R.; Hush, N. S. *Chem. Phys.* **1996**, *208*, 177.
(78) Kober, E. M.; Goldsby, K. A.; Narayana, D. N. S.; Meyer, T. J. *J. Am. Chem. Soc.* **1983**, *105*, 4303.
(79) Powers, M. J. *J. Am. Chem. Soc.* **1980**, *102*, 1289.
(80) Bublitz, G. U.; Boxer, S. G. *Annu. Rev. Phys. Chem.* **1997**, *48*, 213.
(81) Brunschwig, B. S.; Creutz, C.; Sutin, N. *Coord. Chem. Rev.* **1998**, *177*, 61.
(82) Walters, K. A. *Compr. Coord. Chem. II* **2003**, *2*, 303.
(83) Ferretti, A. *Coord. Chem. Rev.* **2003**, *238*−*239*, 127.
(84) Vance, F. W.; Williams, R. D.; Hupp, J. T. *Int. Rev. Phys. Chem.* **1998**, *17*, 307.
(85) Keene, F. R. *Coord. Chem. Rev.* **1997**, *166*, 122.
(86) Keene, F. R. *Chem. Soc. Rev.* **1998**, *27*, 185.
(87) Glauser, R.; Hauser, U.; Herren, F.; Ludi, A.; Roder, P.; Schmidt, E.; Siegenthaler, H.; Wenk, F. *J. Am. Chem. Soc.* **1973**, *95*, 8457.
(88) Haim, A.; Wilmarth, W. K. *J. Am. Chem. Soc.* **1961**, *83*, 509.
(89) Fukita, N.; Ohba, M.; Okawa, H.; Matsuda, K.; Iwamura, H. *Inorg. Chem.* **1998**, *37*, 842.
(90) Oshio, H.; Onodera, H.; Tamada, O.; Mizutani, H.; Hikichi, T.; Ito, T. *Chem.*−*Eur. J.* **2000**, *6*, 2523.
(91) Oshio, H.; Onodera, H.; Ito, T. *Chem.*−*Eur. J.* **2003**, *9*, 3946.
(92) Dowling, N.; Henry, P. M. *Inorg. Chem.* **1982**, *21*, 4088.
(93) Vahrenkamp, H.; Gieb, A.; Richardson, G. N. *J. Chem. Soc., Dalton Trans.* **1997**, 3643.
(94) Hupp, J. T.; Williams, R. D. *Acc. Chem. Res.* **2001**, *34*, 808.
(95) Klausmeyer, K. K.; Rauchfuss, T. B.; Wilson, S. R. *Angew. Chem., Int. Ed.* **1998**, *37*, 1694.
(96) Heinrich, J. L.; Berseth, P. A.; Long, J. R. *Chem. Commun.* **1998**, 1231.
(97) Lai, S.-W.; Cheung, K.-K.; Chan, M. C.-W.; Che, C.-M. *Angew. Chem., Int. Ed.* **1998**, *37*, 182.
(98) Schinnerling, P.; Thewalt, U. *J. Organomet. Chem.* **1992**, *431*, 41.
(99) Fritz, M.; Rieder, D.; Bär, E.; Beck, G.; Fuchs, J.; Holzmann, G.; Fehlhammer, W. P. *Inorg. Chim. Acta* **1992**, *198*−*200*, 513.
(100) Parker, R. J.; Hockless, D. C. R.; Moubaraki, B.; Murray, K. S.; Spiccia, L. *Chem. Commun.* **1996**, 2789.
(101) Ferlay, S.; Mallah, T.; Ouahés, R.; Veillet, P.; Verdaguer, M. *Nature* **1995**, *378*, 701.
(102) Entley, W. R.; Girolami, G. S. *Science* **1995**, *268*, 397.
(103) Sommovigo, M.; Ferretti, A.; Venturi, M.; Ceroni, P.; Giardi, C.; Denti, G. *Inorg. Chem.* **2002**, *41*, 1263.
(104) Scandola, F.; Argazzi, R.; Bignozzi, C. A.; Chiorboli, C.; Indelli, M. T.; Rampi, M. A. *Coord. Chem. Rev.* **1993**, *125*, 283.
(105) Buser, H. J.; Schwarzenback, D.; Petter, W.; Ludi, A. *Inorg. Chem.* **1977**, *16*, 2704.
(106) von Kameke, A.; Tom, G. M.; Taube, H. *Inorg. Chem.* **1978**, *17*, 1790.
(107) Powers, M. J.; Callahan, R. W.; Salmon, D. J.; Meyer, T. J. *Inorg. Chem.* **1976**, *15*, 894.
(108) Roffia, S.; Paradisi, C.; Bignozzi, C. A. *J. Electroanal. Chem.* **1986**, *200*, 105.
(109) Bignozzi, C. A.; Roffia, S.; Scandola, F. *J. Am. Chem. Soc.* **1985**, *107*, 1644.
(110) Bignozzi, C. A.; Paradisi, C.; Roffia, S.; Scandola, F. *Inorg. Chem.* **1988**, *27*, 408.
(111) Bignozzi, C. A.; Roffia, S.; Chiorboli, C.; Davila, J.; Indelli, M. T.; Scandola, F. *Inorg. Chem.* **1989**, *28*, 4350.
(112) Bignozzi, C. A.; Argazzi, R.; Schoonover, J. R.; Gordon, K. C.; Dyer, R. B.; Scandola, F. *Inorg. Chem.* **1992**, *31*, 5260.
(113) Bignozzi, C. A.; Indelli, M. T.; Scandola, F. *J. Am. Chem. Soc.* **1989**, *111*, 5192.
(114) Bignozzi, C. A.; Argazzi, R.; Chiorboli, C.; Scandola, F.; Dyer, R. B.; Schoonover, J. R.; Meyer, T. J. *Inorg. Chem.* **1994**, *33*, 1652.
(115) Bignozzi, C. A.; Argazzi, R.; Chiorboli, C.; Roffia, S.; Scandola, F. *Coord. Chem. Rev.* **1991**, *111*, 261.
(116) Reprinted from *J. Electroanal. Chem.*, *200*, Roffia, S., Paradisi, C., Bignozzi, C. A., Electrochemical and spectroscopic behaviour of cyano-bridged bi- and trinuclear complexes of ruthenium containing 2,2′-bipyridine and ammonia as ligands. Convolutive potential sweep voltammetric study of two Nernstian waves, pp 105−118 (ref 108), Figure 4 (p 113), Copyright 1986, with permission from Elsevier.
(117) Katz, N. E.; Creutz, C.; Sutin, N. *Inorg. Chem.* **1988**, *27*, 1687.
(118) Chen, Y. J.; Kao, C.-H.; Lin, S. J.; Tai, C.-C.; Kwan, K. S. *Inorg. Chem.* **2000**, *39*, 189.
(119) Liu, T.-Y.; Chen, Y. J.; Tai, C.-C.; Kwan, K. S. *Inorg. Chem.* **1999**, *38*, 674.
(120) Hupp, J. T. *J. Am. Chem. Soc.* **1990**, *112*, 1563.
(121) Coe, B. J.; Meyer, T. J.; White, P. S. *Inorg. Chem.* **1995**, *34*, 3600.
(122) Juris, A.; Campagna, S.; Bidd, I.; Lehn, J.-M.; Ziessel, R. *Inorg. Chem.* **1988**, *27*, 4007.
(123) Meyer, T. J. *Acc. Chem. Res.* **1989**, *22*, 163.
(124) Bignozzi, C. A.; Chiorboli, C.; Indelli, M. T.; Scandola, F.; Bertolasi, V.; Gilli, G. *J. Chem. Soc., Dalton Trans.* **1994**, 2391.
(125) Bignozzi, C. A.; Bortolini, O.; Chiorboli, C.; Indelli, M. T.; Rampi, M. A.; Scandola, F. *Inorg. Chem.* **1992**, *31*, 172.
(126) Matsui, K.; Nazeeruddin, M. K.; Humphry-Baker, R.; Grätzel, M.; Kalyanasundaram, K. *J. Phys. Chem.* **1992**, *96*, 10587.
(127) Amadelli, R.; Argazzi, R.; Bignozzi, C. A.; Scandola, F. *J. Am. Chem. Soc.* **1990**, *112*, 7099.
(128) Argazzi, R.; Bignozzi, C. A.; Heimer, T. A.; Meyer, G. J. *Inorg. Chem.* **1997**, *36*, 2.
(129) Kalyanasundaram, K.; Grätzel, M.; Nazeeruddin, M. K. *Inorg. Chem.* **1992**, *31*, 5243.
(130) Indelli, M. T.; Scandola, F. *J. Phys. Chem.* **1993**, *97*, 3328.
(131) Forlano, P.; Cukiernik, F. D.; Poizat, O.; Olabe, J. A. *J. Chem. Soc., Dalton Trans.* **1997**, 1595.
(132) Laidlaw, W. M. *Inorg. Chim. Acta* **1996**, *248*, 51.
(133) Pfennig, B. W.; Cohen, J. L.; Sosnowski, I.; Novotny, N. M.; Ho, D. M. *Inorg. Chem.* **1999**, *38*, 606.
(134) Gutmann, V. *Electrochim. Acta* **1976**, *21*, 661.
(135) Pfennig, B. W.; Fritchman, V. A.; Hayman, K. A. *Inorg. Chem.* **2001**, *40*, 255.
(136) Parker, W. L.; Crosby, G. A. *Int. J. Quantum Chem.* **1991**, *39*, 299.
(137) Pfennig, B. W.; Bocarsly, A. B. *J. Phys. Chem.* **1992**, *96*, 226.
(138) Wu, Y.; Cohran, C.; Bocarsly, A. B. *Inorg. Chim. Acta* **1994**, *226*, 251.
(139) Pfennig, B. W.; Wu, Y.; Kumble, R.; Spiro, T. G.; Bocarsly, A. B. *J. Phys. Chem.* **1996**, *100*, 5745.
(140) Watson, D. F.; Tan, H. S.; Schreiber, E.; Mordas, C. J.; Bocarsly, A. B. *J. Phys. Chem. A* **2004**, *108*, 3261.
(141) Lewis, N. A.; McNeer, R. R.; Taveras, D. V. *Inorg. Chim. Acta* **1994**, *225*, 89.
(142) Pfennig, B. W.; Mordas, C. J.; McCloskey, A.; Lockard, J. V.; Salmon, P. M.; Cohen, J. L.; Watson, D. F.; Bocarsly, A. B. *Inorg. Chem.* **2002**, *41*, 4389.
(143) Goldsby, K. A.; Meyer, T. J. *Inorg. Chem.* **1984**, *23*, 3002.
(144) The comproportionation constant, K_c, expresses the thermodynamic stability of a mixed-valence species. For dinuclear complexes, the comproportionation equilibrium is

$$[2,2] + [3,3] \overset{K_c}{\rightleftharpoons} 2[3,2] \qquad K_c = \frac{[3,2]^2}{[2,2][3,3]}$$

K_c may be deduced from electrochemical measurements, since $K_c = \exp\{\Delta E_{ox}F/RT\}$, where F/RT takes the value 38.92 V^{-1} at 298 K and ΔE_{ox} is the separation between the two metal-based redox processes.[35] For trinuclear complexes, the comproportionation equilibria are

$$[2,2,2] + [3,3,2] \overset{K_{c1}}{\rightleftharpoons} 2[3,2,2] \qquad K_{c1} = \frac{[3,2,2]^2}{[2,2,2][3,3,2]}$$

$$[3,2,2] + [3,3,3] \overset{K_{c2}}{\rightleftharpoons} 2[3,3,2] \quad K_{c2} = \frac{[3,3,2]^2}{[3,2,2][3,3,3]}$$

where K_{c1} and K_{c2} are determined from electrochemical measurements,

with ΔE taken as the potential separation between the first and second, and second and third metal-based redox processes, respectively. By the conservation of masses and charges, [2,2,2] + [3,2,2] + [3,3,2] + [3,3,3] = 1, and [3,2,2] + 2[3,3,2] + 3[3,3,3] = n, where n is the number of metal centers oxidized.[145] The system of equations is solved for known K_{c1} and K_{c2} (and $n = 1, 2$) by successive iterations to obtain the proportion of the one- and two-electron oxidized (mixed-valence) species present in solution. In all cases, any comparison of K_c values derived from ΔE values needs to be treated with some caution due to the effect of the medium (anion, solvent) on such electrochemical measurements.[146−148]

(145) Bonvoisin, J.; Launay, J. P.; Verbouwe, W.; Vanderauweraer, M.; Deschryver, F. C. *J. Phys. Chem.* **1996**, *100*, 17079.
(146) D'Alessandro, D. M.; Keene, F. R. *Dalton Trans.* **2004**, 3950.
(147) Barriere, F.; Camire, N.; Geiger, W. E.; Mueller-Westerhoff, U. T.; Sanders, R. *J. Am. Chem. Soc.* **2002**, *124*, 7262.
(148) LeSuer, R.; Geiger, W. E. *Angew. Chem., Int. Ed.* **2000**, *39*, 248.
(149) Geiss, A.; Vahrenkamp, H. *Eur. J. Inorg. Chem.* **1999**, 1793.
(150) Geiss, A.; Keller, M.; Vahrenkamp, H. *J. Organomet. Chem.* **1997**, *541*, 441.
(151) Richardson, G. N.; Brand, U.; Vahrenkamp, H. *Inorg. Chem.* **1999**, *38*, 3070.
(152) Geiss, A.; Kolm, M. J.; Janiak, C.; Vahrenkamp, H. *Inorg. Chem.* **2000**, *39*, 4037.
(153) Geiss, A.; Vahrenkamp, H. *Inorg. Chem.* **2000**, *39*, 4029.
(154) Sheng, T.; Vahrenkamp, H. *Eur. J. Inorg. Chem.* **2004**, 1198.
(155) Baumann, F.; Kaim, W.; Olabe, J. A.; Parise, A. R.; Jordanov, J. *J. Chem. Soc., Dalton Trans.* **1997**, 4455.
(156) Stang, P. J.; Olenyuk, B. *Acc. Chem. Res.* **1997**, *30*, 502.
(157) Olenyuk, B.; Fechtenkötter, A.; Stang, P. J. *J. Chem. Soc., Dalton Trans.* **1998**, 1707.
(158) Leininger, S.; Olenyuk, B.; Stang, P. J. *Chem. Rev.* **2000**, *100*, 853.
(159) Rogez, G.; Riviere, É.; Mallah, T. *C. R. Chim.* **2003**, *6*, 283.
(160) Nishihara, H. *Bull. Chem. Soc. Jpn.* **2001**, *74*, 19.
(161) Brown, G. M.; Meyer, T. J.; Cowan, D. O.; LeVanda, C.; Kaufman, F.; Roling, P. V.; Rausch, M. D. *Inorg. Chem.* **1975**, *14*, 506.
(162) Plenio, H.; Hermann, J.; Sehring, A. *Chem.—Eur. J.* **2000**, *6*, 1820.
(163) Aoki, K.; Chen, J.; Nishihara, H.; Hirao, T. *J. Electroanal. Chem.* **1996**, *416*, 151.
(164) Horikoshi, T.; Kubo, K.; Nishihara, H. *J. Chem. Soc., Dalton Trans.* **1999**, 3355.
(165) Nishihara, H.; Horikoshi, T. *Synth. Met.* **1999**, *102*, 1523.
(166) Rulkens, R.; Lough, A. J.; Manners, I.; Lovelace, S. R.; Grant, C.; Geiger, W. E. *J. Am. Chem. Soc.* **1996**, *118*, 12683.
(167) Kurosawa, M.; Nankawa, T.; Matsuda, T.; Kubo, K.; Kurihara, M.; Nishihara, H. *Inorg. Chem.* **1999**, *38*, 5113.
(168) Aoki, K.; Chen, J. Y. *J. Electroanal. Chem.* **1995**, *380*, 35.
(169) Weyland, T.; Costuas, K.; Toupet, L.; Halet, J.-F.; Lapinte, C. *Organometallics* **2000**, *19*, 4228.
(170) Gao, L.-B.; Zhang, L.-Y.; Shi, L.-X.; Chen, Z.-N. *Organometallics* **2005**, *24*, 1678.
(171) Jaio, J.; Long, G. J.; Grandjean, F.; Beatty, A. M.; Fehlner, T. P. *J. Am. Chem. Soc.* **2003**, *125*, 7522.
(172) Serroni, S.; Campagna, S.; Denti, G.; Keyes, T. E.; Vos, J. G. *Inorg. Chem.* **1996**, *35*, 4513.
(173) Haga, M.-A.; Ali, M. M.; Arakawa, R. *Angew. Chem., Int. Ed. Engl.* **1996**, *35*, 76.
(174) Haga, M.; Ali, M. M.; Sato, H.; Monjushiro, H.; Nozaki, K.; Kano, K. *Inorg. Chem.* **1998**, *37*, 2320.
(175) Aoki, K.; Chen, J.; Haga, M.-A. *J. Electroanal. Chem.* **1995**, *396*, 309.
(176) Aoki, K.; Kamo, H.; Chen, J. Y.; Hoshino, Y. *J. Electroanal. Chem.* **1997**, *420*, 189.
(177) Rillema, D. P.; Callahan, R. W.; Mack, K. B. *Inorg. Chem.* **1982**, *21*, 2589.
(178) Rillema, D. P.; Sahai, R.; Matthews, P.; Edwards, A. K.; Shaver, R. J.; Morgan, L. *Inorg. Chem.* **1990**, *29*, 167.
(179) Patra, S.; Sarkar, B.; Ghumaan, S.; Fiedler, J.; Kaim, W.; Lahiri, G. K. *Dalton. Trans.* **2004**, 754.
(180) Rocha, R. C.; Toma, H. E. *Polyhedron* **2002**, *21*, 2089.
(181) Müller, E.; Nazeeruddin, M. K.; Gratzel, M.; Kalyanasundaram, K.; Prome, J. C. *New J. Chem.* **1996**, *20*, 759.
(182) Shan, N.; Vickers, S. J.; Adams, H.; Ward, M. D.; Thomas, J. A. *Angew. Chem., Int. Ed.* **2004**, *43*, 3938.
(183) Belser, P.; von Zelewsky, A.; Frank, M.; Seel, C.; Vogtle, F.; De Cola, L.; Barigelletti, F.; Balzani, V. *J. Am. Chem. Soc.* **1993**, *115*, 4076.
(184) MacDonnell, F. M.; Bodige, S. *Inorg. Chem.* **1996**, *35*, 5758.
(185) Bodige, S.; Torres, A. S.; Maloney, D. J.; Tate, D.; Kinsel, G. R.; Walker, A. K.; MacDonnell, F. M. *J. Am. Chem. Soc.* **1997**, *119*, 10364.
(186) Campagna, S.; Serroni, S.; Bodige, S.; MacDonnell, F. M. *Inorg. Chem.* **1999**, *38*, 692.
(187) Chen, J.; MacDonnell, F. M. *Chem. Commun.* **1999**, 2529.
(188) Torres, A. S.; Maloney, D. J.; Tate, D.; Saad, Y.; MacDonnell, F. M. *Inorg. Chim. Acta* **1999**, *293*, 37.
(189) MacDonnell, F. M.; Meser Ali, M. D.; Kim, M.-J. *Inorg. Chem.* **2000**, *39*, 1.
(190) Kim, M.-J.; MacDonnell, F. M.; Gimon-Kinsel, M. E.; Du Bois, T.; Asgharian, N.; Griener, J. C. *Angew. Chem., Int. Ed.* **2000**, *39*, 615.
(191) Constable, E. C.; Walker, J. V. *Polyhedron* **1998**, *17*, 3089.
(192) Constable, E. C.; Elder, S. M.; Hannon, M. J.; Martin, A.; Raithby, P. R.; Tocher, D. A. *J. Chem. Soc., Dalton Trans.* **1996**, 2423.
(193) Constable, E. C.; Thompson, A. M. W.; Cherryman, J.; Liddiment, T. *Inorg. Chim. Acta* **1995**, *235*, 165.
(194) Collin, J.-P.; Guillerez, S.; Sauvage, J.-P. *J. Chem. Soc., Chem. Commun.* **1989**, 776.
(195) Beley, M.; Collin, J.-P.; Sauvage, J.-P.; Sugihara, H.; Heisel, F.; Miehe, A. *J. Chem. Soc., Dalton Trans.* **1991**, 3157.
(196) Indelli, M. T.; Scandola, F.; Collin, J. P.; Sauvage, J. P.; Sour, A. *Inorg. Chem.* **1996**, *35*, 303.
(197) Kelso, L. S.; Reitsma, D. A.; Keene, F. R. *Inorg. Chem.* **1996**, *35*, 5144.
(198) Rutherford, T. J.; Keene, F. R. *Inorg. Chem.* **1997**, *36*, 2872.
(199) Treadway, J. A.; Chen, P.; Rutherford, T. J.; Keene, F. R.; Meyer, T. J. *J. Phys. Chem. A* **1997**, *101*, 6824.
(200) D'Alessandro, D. M.; Kelso, L. S.; Keene, F. R. *Inorg. Chem.* **2001**, *40*, 6841.
(201) D'Alessandro, D. M.; Keene, F. R. *Chem.—Eur. J.* **2005**, *11*, 3679.
(202) D'Alessandro, D. M.; Keene, F. R. *Dalton Trans.* **2006**, 1060.
(203) Balzani, V.; Juris, A. *Coord. Chem. Rev.* **2001**, *211*, 97.
(204) Serroni, S.; Campagna, S.; Puntoriero, F.; Di Pietro, C.; McClenaghan, N. D.; Loiseau, F. *Chem. Soc. Rev.* **2001**, *30*, 367.
(205) Pandey, A. K.; Gupta, T.; Baranwal, B. P. *Trans. Met. Chem.* **2004**, *28*, 370.
(206) Baranwal, B. P.; Gupta, T. *Spectrochim. Acta A* **2003**, *59*, 859.
(207) Schiøtt, B.; Overgaard, J.; Larsen, F. K.; Iversen, B. B. *Int. J. Quantum Chem.* **2004**, *96*, 23.
(208) Cannon, R. D.; Montri, L.; Brown, D. B.; Marshall, K. M.; Elliott, C. M. *J. Am. Chem. Soc.* **1984**, *106*, 2591.
(209) Kambara, T.; Hendrickson, D. N.; Sorai, M.; Oh, S. M. *J. Chem. Phys.* **1986**, *85*, 2895.
(210) Overgaard, J.; Larsen, F. K.; Schiøtt, B.; Iversen, B. B. *J. Am. Chem. Soc.* **2003**, *125*, 11089.
(211) Taft, K.; Caneschi, A.; Pence, L. E.; Delfs, C. D.; Papaefthymiou, G. C.; Lippard, S. J. *J. Am. Chem. Soc.* **1993**, *115*, 11753.
(212) Brudvig, G. W.; Thorp, H. H.; Crabtree, R. H. *Acc. Chem. Res.* **1991**, *24*, 311.
(213) Kar, S.; Miller, T. A.; Chakraborty, S.; Sarkar, B.; Pradhan, B.; Sinha, R. K.; Kundu, T.; Ward, M. D.; Lahiri, G. K. *Dalton Trans.* **2003**, 2591.
(214) Yamaguchi, T.; Imai, N.; Ito, T.; Kubiak, C. P. *Bull. Chem. Soc. Jpn.* **2000**, *73*, 1205.
(215) Londergan, C. H.; Kubiak, C. P. *J. Phys. Chem. A* **2003**, *107*, 9301.
(216) Londergan, C. H.; Rocha, R. C.; Brown, M. G.; Shreve, A. P.; Kubiak, C. P. *J. Am. Chem. Soc.* **2003**, *125*, 13912.
(217) Londergan, C. H.; Salsman, C.; Ronco, S.; Kubiak, C. P. *Inorg. Chem.* **2003**, *42*, 926.
(218) Salsman, J. C.; Kubiak, C. P.; Ito, T. *J. Am. Chem. Soc.* **2005**, *127*, 2382.
(219) Borrás-Almenar, J. J.; Coronado, E.; Palii, A. V.; Tsukerblat, B. S.; Georges, R. *Chem. Phys.* **1998**, *226*, 231.
(220) Borshch, S. A.; Kotov, I. N.; Bersuker, I. B. *Chem. Phys. Lett.* **1982**, *89*, 381.
(221) Launay, J. P.; Babonneau, F. *Chem. Phys.* **1982**, *67*, 295.

CR050010O